Study of materials using Mössbauer spectroscopy

D. Bandyopadhyay*

A comprehensive review is presented of the recent contributions Mössbauer spectroscopy has made in materials science and engineering. After a brief introduction to the basic methodology, examples of the application of ^{57}Fe and ^{119}Sn Mössbauer spectroscopy in both transmission and back-scattering mode are presented and discussed. Recent technological and software developments of this technique are also included. Coverage is further extended to recent, pertinent developments in space research and also in biological science and technology where Mössbauer techniques are very widely used. Efforts have also been made to cover applications to archaeological samples where Mössbauer spectroscopy is an important analytical tool.

Keywords: Archaeology, Biological science, Magnetic materials, Metallic glass, Minerals, Mössbauer spectroscopy, Nanomaterials, Space research, Steels

Introduction

In 1957, R.L. Mössbauer[1] discovered the phenomenon of recoilless nuclear emission and absorption of γ-radiation from an embedded radiating atom. This was named the 'Mössbauer Effect' after its discoverer who was awarded a Nobel Prize in Physics in 1961. Owing to the sharpness of the resonance, the Mössbauer effect in solids was soon recognised as a sensitive technique to study electronic, magnetic, structural, and phase identification studies of different materials having basic scientific and technological interest. Out of 91 elements in nature, about 81 show the Mössbauer effect. In particular, the use of ^{57}Fe as the Mössbauer nucleus initiated research interest in physics, chemistry, biology, material sciences, physical metallurgy, mineralogy, geochemistry and several other fields. This was possible because of the easy availability and utility of a large number of iron compounds, alloys and minerals. ^{57}Fe Mössbauer spectroscopy has been used to study binary and ternary alloys of iron, steels, metallic glasses, iron based minerals, superconductors, nano-structured materials, biological materials and several other iron containing materials. Literature and books are available on the studies of materials in different fields using this 'nondestructive' technique,[2–10] and hence no attempt will be made to go into detail here. In addition, many presentations and publications on above stated fields have been made at international conferences of ISIAME, ICAME, LACAME sponsored by the Mössbauer community, and further details on such topics are contained in their published proceedings.[11–16] However, for the sake of completeness, the basic principles of the Mössbauer effect and its methodology will briefly be outlined.

Physics Group, Birla Institute of Technology and Science, Pilani, Rajasthan 333031, India

*Email, bandy@bits-pilani.ac.in

Mössbauer effect

Recoilless emission and absorption

In nuclear resonance absorption and emission, the two main obstructions are the recoil energy shift and the thermal Doppler shift between the emitting and absorbing atom. Figure 1 shows an isolated atom in the gas phase undergoing a nuclear transition from an excited state, E_e to the ground state, E_g. The recoil energy of the free nucleus, E_R, is proportional to the mass of the nucleus, M, and the emitted γ radiation energy E_γ, and is given by

$$E_R = \frac{E_\gamma^2}{2Mc^2} \quad (1)$$

The spectral line broadening owing to the emission or absorption of the γ radiation is due to the Hinesburg uncertainty in energy and life-time of the excited state. The second cause of the broadening is the relative Doppler velocity between the source and the absorber in the experiment. It may be due to the relative velocity between the source and absorber when they are at the same temperature or may be due to the different average thermal velocities when there is a temperature difference between them. The contribution of the Doppler effect to the broadening of γ radiation owing to the first reason, when both the source and the absorber are at the same temperature, can be given by

$$\bar{E}_D = E_\gamma \sqrt{\frac{2\bar{E}_K}{Mc^2}} \quad (2)$$

where $\bar{E}_K$ is the mean kinetic energy per translational degree of freedom of a free atom, $E_D = M(\vec{V}_x, \vec{v})$. The broadening of natural line width owing to Hinesburg uncertainty is very small (10^6 times) compared to the above effect. The same is true for absorption of the γ radiation. The energy profile diagram of emitted and absorbed gamma radiation owing to all these effects is shown in Fig. 2. With reference to this figure, the

Published by Maney for the Institute and ASM International
DOI 10.1179/174328006X79490

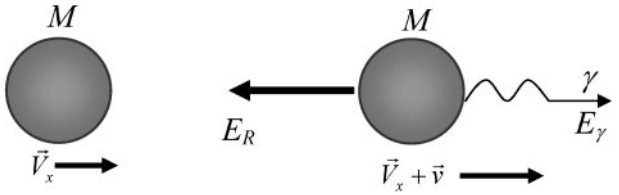

1 Free nucleus receiving recoil energy during γ radiation

resonance absorption is only possible when the factor E_R is less than the factor $\bar{E}_D$. This is possible only when the atom is well embedded in a lattice. Here, the recoil energy is now absorbed by the whole lattice instead of the single isolated nucleus. Under this condition, the mass of the nucleus in equation (2) will be replaced by the mass of the whole lattice, and as a result, the factor E_R in the lattice will be very much less than E_R in the case of free atoms, and hence much less than $\bar{E}_D$. Therefore, resonance absorption is possible as shown in Fig. 2.

Recoil free factor

Although the nucleus is bound in the lattice, it is free to vibrate, so the recoil energy can be transferred to the lattice as quantised lattice vibration. If the recoil energy is less than the lowest quantised energy, the lattice does not absorb any recoil energy, and as a result a recoil free event will occur. The probability of such a recoilless event can be expressed by the recoil-less factor, f, as follows

$$f = \exp\left(\frac{-E_\gamma^2 < x >^2}{\mathrm{h}c^2}\right) \tag{3}$$

where, $\langle x \rangle^2$ is the mean square displacement of the emitting or absorbing nucleus. It can be seen that f decreases with the energy of the γ radiation. The other dependent factor $\langle x \rangle^2$ is a function of both binding strength and temperature. The optimum f factor, and hence the best signal-to-noise ratio, is obtained for isotopes with very low lying excited states at a temperature well below the Debye temperature (θ_D). A good example is ^{57}Fe, with Mössbauer gamma ray energy of 14·4 keV and θ_D of 470 K.

Mössbauer spectroscopy

Mössbauer spectroscopy (MS) involves the γ radiation emitted from radioactive nuclei (source) embedded in a non-interactive matrix (for example, a ^{57}Co source in a Rh matrix) to probe the γ radiation in the sample to be studied. The source contains the parent nucleus of the Mössbauer isotope, embedded in a rigid matrix, to give a high recoilless factor (f). The gamma rays are absorbed by the sample and re-emited. The reemitted gamma rays carry information about the sample under study. The recorded absorption Mössbauer spectrum is a plot of normalised transmission intensity versus the relative velocity of the source. The line shape of the Mössbauer spectrum is Lorentzian. Different types of Mössbauer spectra due to different effects in the samples will be discussed in the following section.

Hyperfine interactions

When the nucleus is embedded in a lattice, it can interact with the electronic and magnetic fields produced by the

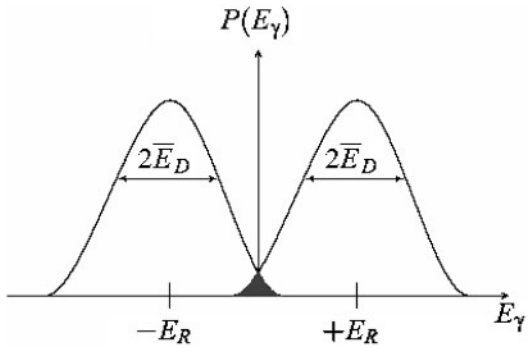

2 Energy profile diagram of emitted (left) and absorbed (right) gamma radiation; overlapping region (black) shows resonance

extra nuclear environment. These interactions, known as hyperfine interactions, are very small compared to the energy levels of the nucleus, but extreme energy resolution of the Mössbauer effect enables these interactions to be observed. The hyperfine interactions may shift or split the nuclear energy levels. All these interactions can be expressed by the interaction Hamiltonian of the nucleus as

$$H = H_0 + E_0 + M_1 + E_2 + \cdots \tag{4}$$

where H is the total Hamiltonian of the system, H_0 is the Hamiltonian without any hyperfine interaction, E_0 refers to electric quadrupole interactions, M_1 the magnetic dipole interactions and E_2 the electric quadrupole interactions. The effects of the higher order terms in the Hamiltonian are very small and can be neglected. Effects of these interactions on the Mössbauer spectrum will be discussed in terms of different Mössbauer parameters as follows.

Isomer shift or chemical shift (δ)

In sample materials from different chemical environments (extra nuclear charge and current density), the energy levels of the Mössbauer isotopes shift about their actual position because of the finite size of the nucleus and the interaction between the nuclear charge with the s-electron charge density. But the s-electron density of the Mössbauer atom is not the same in the source and in the absorber. So the shift of the nuclear energy levels in the source and absorber is also different. As a result of this shift, the difference between the excited and ground state energy levels $E_\gamma^s = \Delta E_s = E_{es} - E_{gs}$ becomes different as in the source. Therefore, for resonance absorption, the gamma radiation from the source needs more energy ($\delta = E_\gamma^a - E_\gamma^s$), and can be supplied by the Doppler velocity of the transducer where the source is mounted. So the Mössbauer spectrum shows a single dip with a shift by an amount δ mm s^{-1} in the velocity scale, and this shift is known as the isomer shift of the Mössbauer spectrum. The relation between the s-electron charge density and the nuclear size can be given by

$$\delta = \frac{2}{3}\pi Z e^2 \left(|\psi_S(0)_S|^2 - |\psi_S(0)_A|^2\right)\left(< R_e^2 > - < R_g^2 >\right) \tag{5}$$

where $\langle R_e^2 \rangle$ and $\langle R_g^2 \rangle$ are the mean square radius of the excited and the ground state of the nucleus, $|\psi_S(0)_S|^2$ and $|\psi_S(0)_A|^2$ are the s electron density of the electron in the source and absorbing nucleus. A typical Mössbauer

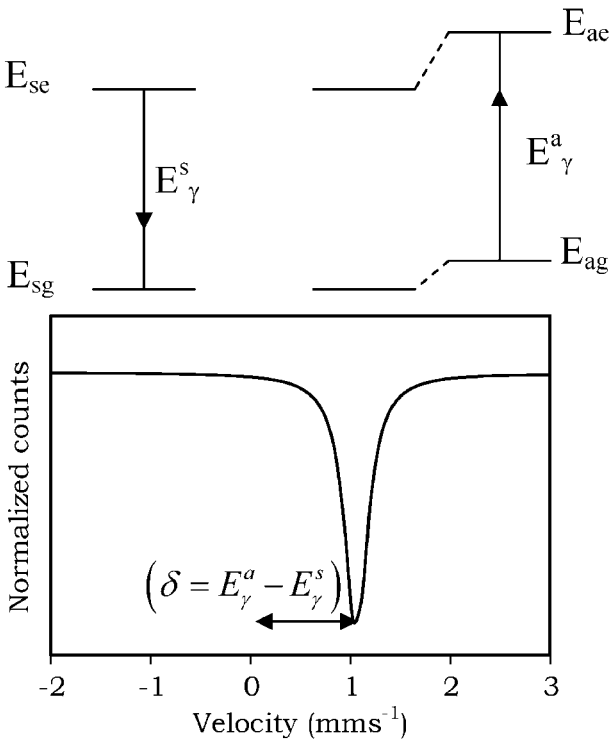

3 Mössbauer spectrum due to isomer shift effect

spectrum due to an isomer shift is shown in Fig. 3 with the source and absorber energy levels.

Second-order Doppler shift (δ_{SOD})

A second-order Doppler shift is the temperature-dependent effect on the centre shift of a Mössbauer spectrum. If the source and the absorber are in different temperature environments, then the lattice vibration is different in these two different systems. This gives some additional shift in the nuclear energy levels and hence in the shift of the Mössbauer spectrum on the velocity scale. This shift can be given by

$$\delta_{\mathrm{SOD}} = E_\gamma \frac{<v^2>}{2c^2} \tag{6}$$

Therefore, one can study the lattice dynamics and can calculate the Debye temperature of a system in a temperature dependent Mössbauer spectroscopic study.

Quadrupole splitting (E)

In the case of nuclei having nuclear spin, $I>1/2$, and nuclear charge distribution deviates from spherical symmetry, there will be an interaction between the nuclear charge distribution and the extra nuclear electric field produced at the centre of the nucleus. More precisely, the Z-component of the electric field at the nuclear site interacts with the nuclear charge distribution. As a result, the higher energy level of spin $I=3/2$ when ^{57}Fe splits into two levels of $m_{\mathrm{I}}=\pm 3/2$ and $\pm 1/2$. Following the selection rule $m_{\mathrm{I}}=\pm 1$ and 0, there will be two possible transitions of the absorbed γ radiation, and the single absorption line now splits symmetrically into two about its mean position as shown in Fig. 4 with the energy level diagram. The separation between the two lines is known as quadrupole splitting in MS. The theory of quadrupole splitting has been discussed by several authors.[2–8] In the case of the ^{57}Fe nucleus, the

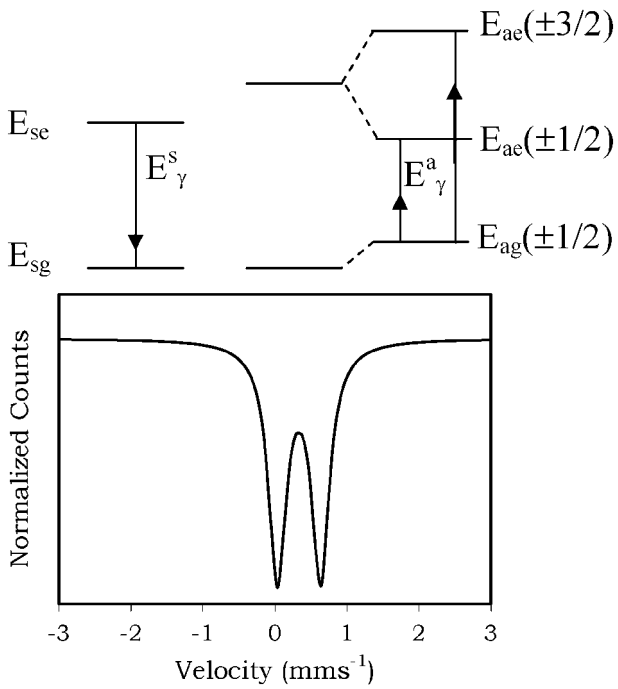

4 Mössbauer spectrum due to combined effect of isomer shift and quadrupole splitting effects

quadrupole splitting (ΔQ or QS) can be expressed as

$$\Delta E = \mathrm{QS} = \frac{1}{2}e^2qQ\left[1 + \frac{\eta^2}{3}\right]^{\frac{1}{2}} \tag{7}$$

where Q is the electric quadrupole moment of the nucleus, $eq=V_{ZZ}$=the negative Z-component of the electric field gradient (EFG), e is the protonic charge, η is the asymmetry parameter$=(V_{XX}-V_{YY})/V_{ZZ}$ and $q=(1-R)_{\mathrm{qval}}+(1-\gamma_\infty)_{\mathrm{qlat}}$.

The analysis of QS values determined from the observed Mössbauer spectra provides valuable information for studying solids.

Magnetic hyperfine interaction (H_{int})

Magnetic hyperfine splitting is caused by the dipole interaction between the nuclear spin moment and the magnetic field produced by the extra nuclear environment. The combined field experienced by the nucleus is a combined field produced by the atom itself and by the lattice when the external field is absent. Under this combined effect the energy levels with spin $I>1/2$ split into a number of components. In case of ^{57}Fe, the transition between these levels gives six different absorption lines in the Mössbauer spectrum as shown in Fig. 5. The ratio of six lines is 3:2:1:1:2:3. Introduction of Doppler velocity between the source and the absorber leads to the energy modification of the gamma-ray from E_γ to E^{D}_γ as follows

$$E^{\mathrm{D}}_\gamma = E_\gamma \pm \frac{vE_\gamma}{c} \tag{8}$$

The internal magnetic field H_{int} at the ^{57}Fe nucleus can be determined by measuring the peak positions of the resonance lines in the Mössbauer spectrum. In the case of the ^{57}Fe nucleus, the value of internal magnetic field can be shown to be

$$H_{\mathrm{int}} = 0{\cdot}843 \times 10^5 (L_5 - L_3) \times \text{(calibration const. in mm s}^{-1}\text{)} \tag{9}$$

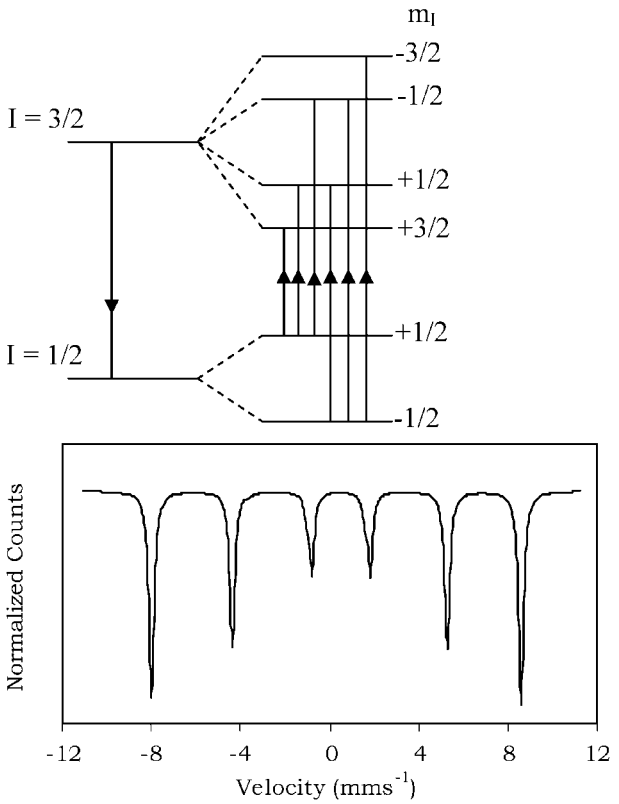

5 Mössbauer spectrum due to effect of internal magnetic field

where L_3 and L_5 are the peak positions of the third and fifth lines in the Mössbauer spectrum.

Basic Mössbauer spectrometer

Figure 6 shows a schematic diagram of a Mössbauer spectrometer at room temperature. The radioactive source is mounted in front of the electromagnetic transducer. The source velocity (Doppler velocity) and hence the velocity of the electromagnetic transducer is controlled by a function generator. The driving pulses from the function generator can produce vibrations in the transducer in constant acceleration mode. So the voltage waveform from the function generator can control the oscillation of the transducer and can improve the oscillation after receiving the feedback signal from the transducer. The detector of the γ radiation from the sample under study is a proportional counter connected by a preamplifier and finally an amplifier. The amplified signal from the amplifier is then fed first into a single channel analyser (SCA) and then finally into a multi channel analyser (MCA). The synchronisation takes place between the transducer and MCA and is actually controlled by the function generator by sending start and delay pulses to the MCA and a proper timescale voltage pulse to the transducer. This is the standard geometry of a transmission Mössbauer spectrometer, and one can study the bulk properties of the sample with this system. By making small changes in the above geometry, one can study conversion electron Mössbauer spectroscopy (CEMS), X-ray Mössbauer spectroscopy (XMS) and temperature dependent MS. CEMS and XMS are very useful for surface characterisation.

Data analysis

Raw data from the Mössbauer spectrometer are collected by a MCA and then transferred to a computer for analysis. After folding the stored data, theoretical sub-spectra are then generated by specifying parameters such as isomer shift (IS), quadrupole splitting (δ) and internal magnetic field (H_{int}). The parameters are then varied to obtain the minimum χ^2 value and give the best fit.

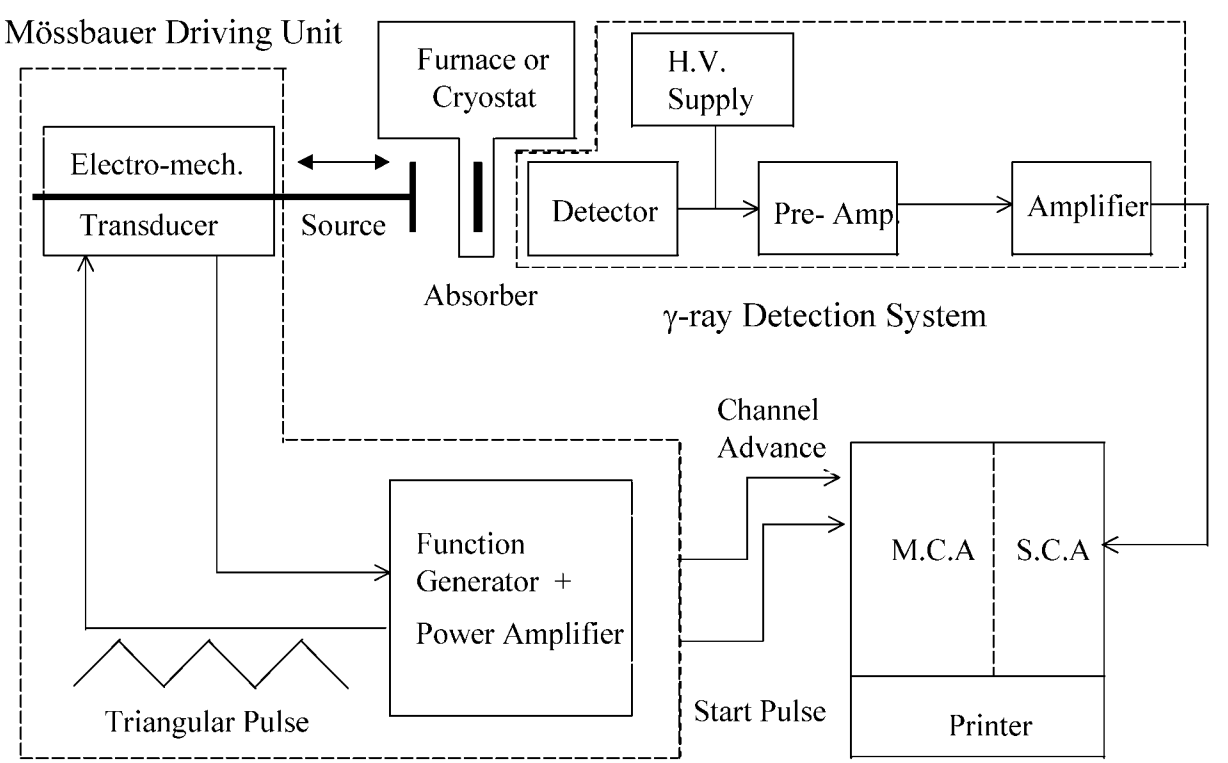

6 Experimental set-up of transmission Mössbauer spectroscopy

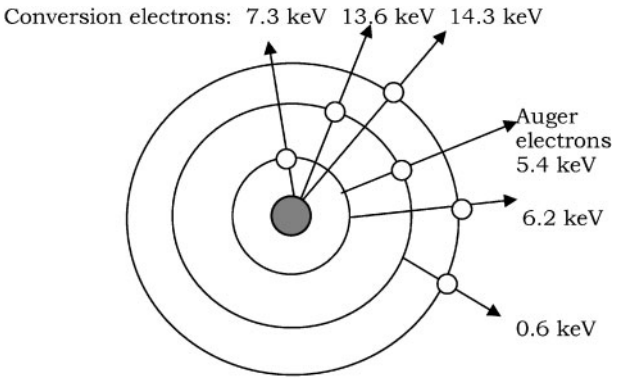

7 Decay scheme of ^{57}Fe nucleus in absorber

Latest advances in the technique

The above discussion is essential for any type of Mössbauer experiment and to understand the Mössbauer spectrum. After the discovery of the Mössbauer effect, several experimental as well as theoretical advances have been made depending upon the experimental demands. In the experimental technique, the most important improvement is in surface studies by MS. For that, the special techniques such as Conversion Electron MS (CEMS), X-ray MS (XMS),[17] and Synchrotron Mössbauer Reflectometry (SMR)[18] have been adopted. Next to transmission MS (TMS), CEMS is most popular to study different surface properties and to study the depth profile in different multilayers. If the absorber is too thick or is an opaque substrate so that γ-radiation cannot pass through or the signal is too small, then this reflective technique (CEMS) is very useful. The basic idea of this technique is as follows.

After absorbing the incident γ-radiation from the source, the Mössbauer nuclei can be de-excited by (i) emission of γ radiation with a probability $N(\gamma)$ and (ii) by internal conversion, i.e. by the ejection of an atomic electron with probability of $N(e)$. The ratio of these two probabilities, $N(e)/N(\gamma)=8{\cdot}21$. So the conversion electron is 8·21 times more probable than direct de-excitation by the emission of γ-radiation. The conversion electron is ejected from the atom with energy $E_c=E_\gamma-E_b$, where E_γ is the energy of the γ-radiation from the Mössbauer nuclei and E_b is the binding energy of the electron in the atom. In the absorber, this ejection of an electron from any of the K, L or M shells creates a hole that can be filled by higher orbital electrons. So the energy release after the transition of the electrons from higher to lower orbits is in the form of X-rays or an Auger electron. The decay scheme of this process is shown in Fig. 7. These decays can be studied by detecting the conversion electrons or Auger electrons by using a gas-flow proportional counter as shown in Fig. 8.

Other techniques such as Mössbauer effect powder diffraction,[19] high pressure Mössbauer studies[20] and phonon assisted Mössbauer effects[21] are also important to mention in this context. In the theory and data analysis of MS, considerable advances have been made. Several recent developments in data analysis by using a new algorithm,[22] in particular, genetic algorithms, fuzzy logic, and artificial neural network[23–25] and first principles calculation[26] of Mössbauer hyperfine parameters are important. In this context, it is important to mention that the application of a genetic algorithm in the study of materials has been discussed in the review article by Chakraborti.[27] Use of new sensors in MS to detect the γ radiation instead of a proportional counter made the system very compact and small in size.[28] The portable Mössbauer spectrometer, named Rover,[29] developed for extra-terrestrial applications, opens up new industrial applications of MS. In recent exploration of Mars, NASA scientists used this new system to study the surface materials on the planet. Use of this portable

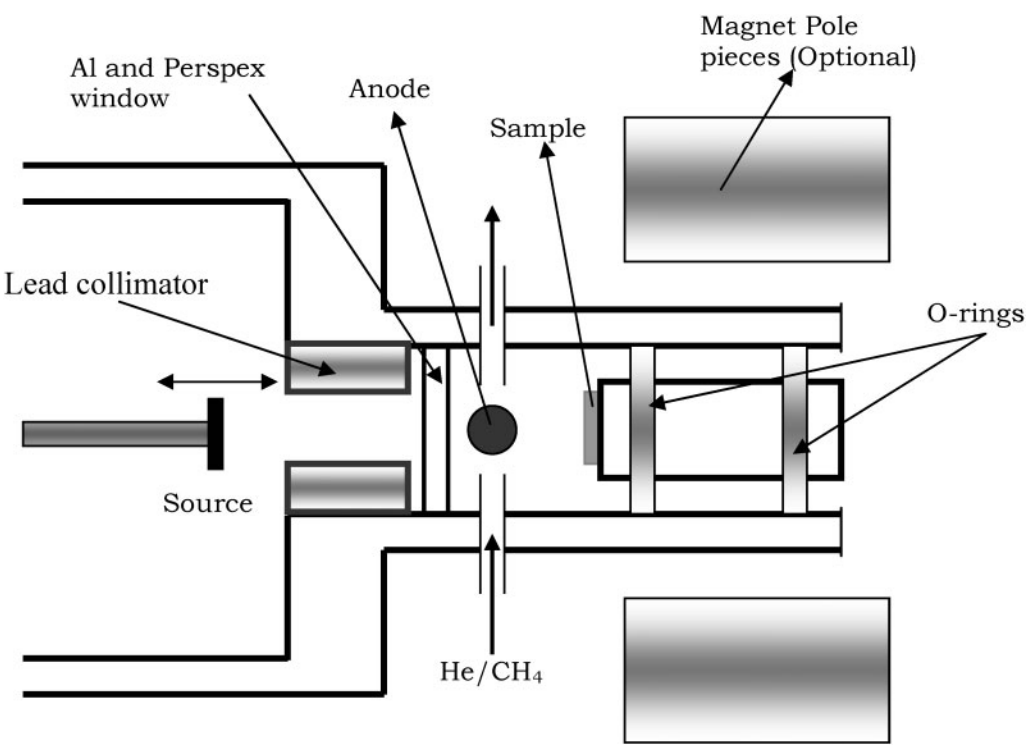

8 Schematic diagram of standard CEMS detector under external magnetic field

Mössbauer spectrometer with automatic data analysis techniques opens up a new era for MS.

The above discussion related to the theory, methodology and the latest developments of the system is brief, but it is a useful introduction to the present review article. In the review, studies of materials by MS will be discussed in different sections. Since this technique is widely applicable in different research fields as discussed earlier, the materials studied by MS are categorised bearing the following points in mind: (i) the nature of the materials and (ii) the aim of the studies. The materials can be categorised into the following groups: (i) alloys, (ii) amorphous, quasicrystalline and nano materials, (iii) corrosion and catalysis, (iv) semiconductors, electronic and optical materials, (v) superconductors, (vi) minerals, and (vi) biological samples. Materials in each section may then be divided into sub-sections depending on the problems of the studies.

Study of materials

Over the four decades since R. L. Mössbauer's discovery, this technique has provided knowledge in basic science, as well as industrial applications. Study of alloys by ^{57}Fe MS gives us valuable information such as phase identification, to calculate the relative percentage of different phases and especially the nearest neighbour effect in the alloys. The contribution that MS has made in the field of alloy studies is beyond the scope of the present overview. In this section, MS studies of different materials will be discussed.

Study of steels

Ferrite, carbon and nitride steels

It has been demonstrated by Huffman and Huggins[30] that MS is very much applicable to the steel industry as a regular monitoring tool and as an important experimental technique for investigating important metallurgical problems related to steel making and steel processing. Starting from ore selection for steel making, characterisation of coal for the blast furnace, the ash and slag, the relative abundance of different phases present in a steel product, study of surfaces and corrosion, MS is essential to study the products and raw materials. MS contributed to understanding the behaviour of different ferrite steels, and related iron nitrides and carbides.

In early work by Chow and Bognor,[31] the amounts of austenite measured in ferrite steel by MS and X-ray techniques are almost same. Formation of austenite in steel increases its toughness. The fracture toughness of nickel bearing austenite steel increased drastically after tempering which forms austenite in the steel. MS can detect the austenite and ferrite as two separate phases in steel. Kim and Schwartz[32] found that fracture toughness increased by 4 and 10 times when tempering was done at room temperature and at 77°C, respectively. MS studies found that part of the austenite was converted into martensite that gives the resultant toughness. Estimation of retained austenite is important to understand the fracture toughness and the other properties of steel. The fractured surface is conventionally studied by back-scattered MS. It is important to mention that an X-ray technique is ineffective owing to the roughness of the surface. A detailed discussion on this topic is given by Rao.[33]

The first studies of iron nitrides and iron carbides were done in 1962–1964.[34–36] Carbon steel systems remain most important in the steel industries. In carbon steel, several researchers studied the formation of austenite and martensite and their relative percentages. Important work was done by Swartzendruber and Bennett.[37] They studied the phase formation on the surface of high carbon steel during surface grinding by using CEMS. Nitriding the iron in the carbon steel improved the hardness and corrosion resistance of the steel. The eight complex structures of different Fe–N phases have varying properties. For example, the α''-$Fe_{16}N_2$ phase has an enhanced Fe-magnetic moment.[38] The Fe–N phase diagram was studied by Kopcewicz and colleagues[39,40] using CEMS after implantation. CEMS experiments by Kopcewicz *et al.*[39] indicate different phases present on the surface of the sample after the treatment. The interaction between the nitrogen atoms and their distribution among the octahedral sites of the γ-fcc lattice in Fe–N austenite was studied by Oda *et al.*[41] They found different phases such as γ_0, γ_1 and γ_2 owing to the effect of different nearest neighbour nitrogen atoms in the iron sites. The effect of annealing on the decomposition and transformation of different phases in iron nitrides was studied by Schaaf.[42] The activation energy for ε-phase to γ'-phase in Fe–N is 0·8 eV and from γ'-phase to α-phase is 1·3 eV. Eight different phases were found in the sample after the treatments as stated before. On the basis of this different range of activation energies, Schaaf[42] studied the homogeneity of Fe subjected to different nitriding processes by CEMS and CXMS. ^{15}N (E=40 keV, $\Phi=2\times10^{17}$ ions cm^{-2}) implanted into unalloyed iron and two steels at room temperature was studied by Marest *et al.*[43] using CEMS. Surface damage by ion implantation on the steel surface and characterisation by CEMS are now important topics in steel research. Moncoffre *et al.*[44] studied nitride phase behaviour as a function of the implantation temperature in nitrogen in a very low alloyed steel XC06 (0·05%C) and an AISI 52100 steel (1·1%C; 1·42%Cr). The nitrogen distribution profiles were obtained using the ^{15}N(p,$\alpha\gamma$)^{12}C nuclear reaction, whereas the chemical state of iron was followed using CEMS.

Ion implanted steels

A number of studies were made on the effect of ion implantation and laser surface treatment of different carbon–nitride steel by CEMS. Koinkar *et al.*[45] studied thin films on different substrates using pulsed laser evaporation of 304 steel specimens and then studied the surface of the film by CEMS. Their study shows that the laser-deposited steel film can serve as a protective coating against thermal oxidation. The AISI M2 high speed steel was implanted with titanium ions at 20°C with different concentrations of Ti^+ per cm^2 and then characterised by CEMS.[46] The α bombardment on the carbonitrides produces nitrogen implantation in low carbon steels, which were studied by the CEMS technique by Ramos *et al.*[47] The results showed that the thermal behaviour of the carbon-nitrides is strongly affected by the presence of helium particles in the nitrogen-implanted region. In addition, low dose helium implantation (10^{14} α-cm^{-2}) produces dissolution and

re-precipitation of ε-$Fe_3(C,N)$ into $Fe_{2+x}(C,N)$ ($x<1$). Jervis *et al.*[48] used excimer laser processing in air to grow thick oxide layers on AISI 304 stainless steel and then characterised the resulting oxide layer using MS. The results show that the resulting oxide, which is grown under rapid quenching conditions, has a spinel structure and a complex composition. Carbon (13 at.-%) and nitrogen (5 at.-%) were found as surface contamination. Titanium ion implantation on steel was reported by Khakani *et al.*[49] In their study, steel samples were implanted with 110 keV titanium ions at fluences ranging from 5×10^{16} to 4×10^{17} Ti cm^{-2}. Analysis of the phases formed was performed using CEMS. Different phases of Fe(Ti) solid solution, α-Fe_xTi_{100-x} and superficial α-Fe-Ti–C amorphous phases were identified. Uglov *et al.*[50] studied the elemental and phase composition, microstructure, microhardness and tribological properties of steels subjected to nitrogen and carbon plasma-immersion ion implantation in different regimes by different techniques, including CEMS, for phase identification. Depending on the resulting target temperature during implantation, different phases such as α'-Fe(C,M)+M_6C+MC (where M stands for: Fe,Cr,W,Mo) to ε-$(Fe,M)_{2+x}(N,C)+M_6(C)$ are formed. With increasing temperature, they observed retained martensite in addition to ε-$(Fe,M)_{2+x}(N,C)$. It has been observed that joint nitrogen and carbon plasma-immersion ion implantation leads to the formation of ε-$(Fe,M)_{2+x}C$ and $(Fe,M)_7C_3$ (M: Cr,W,Mo) carbides. Different phases were studied using MS on the surface layers of plain carbon steel, grey cast iron, and TiB_2/steel after irradiation with a high energy electron beam.[51] In the plain carbon steel with ferrite–pearlite, after irradiation, the pearlite region was transformed to martensite but the ferrite region transformed to kainite. The surface of grey cast iron melted and transformed into a mixed structure composed of eutectic ledeburite and retained austenite. The surface layer of the TiB_2/steel surface-alloyed material consisted of melted and transformed regions. Kholmetskii *et al.*[52] studied the modified surface layer of high speed steel after various kinds of ion implantation. Different ratios of martensite and austenite were found in their experiment depending on the ratio of concentration of nitrides and borides. In their study, they found a change in the distribution of hyperfine fields as a result of different implantation and formation of different phases in the samples.

Deformation studies

Mechanical treatment of steels is important to change their mechanical and structural properties. There are different types of deformation in steels owing to mechanical treatment, and dependent on temperature. MS is very important in this field. It tells us about surface as well as interface properties of the deformed steels. Gavriljuk[53] found that accumulation of carbon atoms from decomposed cementite near the interface of pearlitic steels is due to plastic deformation during cold working in pearlitic steels. This is because the binding enthalpy between carbon atoms and dislocations in ferrite exceeds the solution heat of cementite. Cold deformation induced phase transformations in high carbon steel were reported by Shabashov *et al.*[54] During this process, different phases such as supersaturated solid solution of carbon in bcc iron, an austenite with a high carbon concentration, and metastable ε- and χ-carbides were formed owing to dissolution of the pearlite. Deryagin *et al.*[55] found stable austenite in Cr–Ni steel that exhibits ferromagnetic properties. They suggested this is due to the local increase in Ni concentration in the austenite phase in Cr–Fe steel. In Fe–Mn–C dual phase steel, the variation of retained austenite concentration was studied by Ladriere and He[56] using MS after mechanical deformation and heat treatment. They found that austenite transformed to martensite during deformation and it had been reduced by a considerable amount after the sample was cooled in liquid. Results show that two kinds of austenite exist for austenitic manganese steel before wear. One contains almost no carbon, and the other contains more carbon. The carbon atoms mainly exist in the octahedral interstitial sites of austenite one as nearest neighbours around an iron atom. By using backscattered Mössbauer spectrometry, the microstructural changes in worn surfaces of Mn6 and Mn13 (which are different samples depending upon their compositions) from the friction-induced martensitic transformation for austenitic manganese steels were investigated by Fucheng and Tingquan.[57]

There are other Mössbauer spectroscopic studies of different bulk steels and steel surfaces. The above studies are only a few of them giving the essence of the application of this technique in steel research.

Magnetism and magnetic materials

Properties of magnetic materials are a subject of great scientific and practical interest. Many experimental and theoretical investigations have been carried out to obtain a deeper understanding of the nature of magnetism in solids. Since the discovery of the Mössbauer effect, it has been used as a powerful nondestructive probe of iron magnetic materials. From the measurement of different Mössbauer parameters, one can calculate the magnetic moment of an iron atom and its orientation in the material. In the presence of an external magnetic field, Mössbauer spectroscopic studies can give information about the local susceptibility of the paramagnetic substances and their magnetic anisotropy. Temperature dependence Mössbauer measurements can measure a number of properties in the magnetic materials. In order to determine the magnetic structure (or magnetic order, e.g. ferromagnetic, paramagnetic, diamagnetic, antiferromagnetic, ferromagnetic, etc.) of materials, different techniques such as neutron diffraction, muon spin resonance and relaxation, and MS are important methods. These techniques are complementary to the old magnetisation and susceptibility measurements. Different new magnetic orders such as speromagnetic, asperomagnetic, etc, and some disordered crystalline materials such as spin glass, cluster glass and mictomagnets have also been studied by MS. This section will discuss different magnetic materials studied by MS.

In the first category (ferromagnetic, paramagnetic, diamagnetic, antiferromagnetic and ferromagnetic materials), an important magnetic material well studied by MS is Fe–Al alloy having different relative compositions and preparation routes. It has been said that MS can give us information about different magnetic orders in such materials. This is mainly in two ways, from the nature of the Mössbauer spectrum and through

measurement of hyperfine parameters. Measurement of the hyperfine magnetic field in the ferromagnetic alloys provides a measure of the magnetic moment of the iron atoms in the alloy. In polycrystalline or in amorphous materials, where there are different iron magnetic moments or in other words, different local hyperfine magnetic fields experienced by the iron nuclei, the probability distribution of the hyperfine fields can give us information about the distribution of the iron magnetic moments. Measurement of hyperfine fields and calculation of iron magnetic moments as well as the effect of nearest neighbour environment owing to addition of impurities has been widely studied by several scientists since 1963, using different alloys. Impurities in the alloys change the nature of the spectrum and its line-width. The additional line-width and the change in the nature of the spectrum are taken as indicating the presence of different phases where the nearest neighbour effect has been counted as an independent phase. As an example, one can mention the important study made by Stearns[58] that showed the effect of nearest neighbours on iron hyperfine fields in Fe–Al alloys. In her study, it was shown how the hyperfine magnetic field H at the Fe nuclei in Fe–Al alloys depends upon the number of Al atoms in the surrounding coordination spheres. This approach is used by other workers[59–65] to explain the results of H observed by MS in the Fe–Al system. Stearns[58] interpreted the results in terms of the effect of the solute atoms in the first five nearest neighbour shells. Perez Alcazar and Galvao da Silva[64] considered the effect of first nearest neighbour (nn) and second nearest neighbour (nnn) shells. These workers assumed that the 8Fe nn + 6Fe nnn configuration gives $H_o = 330$ kOe, but this field is reduced to $H = H_0 - n_1\Delta H_1 - n_2\Delta H_2$ where n_1 and n_2 are the number of Al atoms in the eight nearest and the six next nearest neighbour sites of Fe. Following Stearns,[58] they first used $\Delta H_1 = 24$ kOe (the reduction in H for each Fe atom substituted by an Al atom in the nn site) and $\Delta H_2 = 11$ kOe (the reduction in H for each Fe atom substituted by an Al atom in the nnn site). In order to interpret their experimental data better, Perez Alcazar and Galvao da Silva[64] used another empirical relation $H = H_0(1 - \alpha n_1 - \beta n_2)$, where $H = 330$ kOe, α being the value corresponding to $\Delta H_1 = 24$ kOe and β being the value corresponding to $\Delta H_2 = 5$ kOe. Yelusov *et al.*[65] only considered the effects of nn atoms and found that the local hyperfine field H depended non-linearly on the number of nn Al atoms, the fourth and the next (up to eight) nn atom causing H to change more than the first three atoms. Bandyopadhyay *et al.*[66] studied Fe–Al alloys for two different atomic percentages of Al. The samples have been prepared by different heat treatments and processed to see the effect of these routes on the nearest neighbour environment. They found different first and second nearest neighbour configurations in the samples with the different percentages. Moreover, the hyperfine field of different nearest neighbour configurations in different samples follows a regular trend depending on sample preparation. Table 1 shows hyperfine field values for different Fe atom configurations in Fe–Al alloys proposed by different workers including Bandyopadhyay *et al.*[66] In all the above cases, with the increase in impurity concentration in the sample, the lines in the Mössbauer spectra broaden further and give rise to satellite lines owing to the increasing value of the nearest neighbour effect. When metallurgical phase change takes place owing to the addition of impurity atoms, the nature of the spectrum changes and gives a central single line in addition to the broadened sextets. This is common both in Fe–Al[66] as well as in invar alloys of Fe and Ni[67] when the percentage is around 28–30%. So the Mössbauer spectra can easily analyse the metallurgical phases as well as the chemical phases present in the alloys. The same effect due to Cr impurity in bcc Fe lattice was observed by Cranshaw[68] for different atomic percentages of Cr.

One of the most well known and still not fully understood phenomena related to magnetism is the so-called Invar effect. In 1897, Guillaume[69] discovered the original Invar property of the face-centred cubic (fcc) iron–nickel alloys containing about 35 at.-%Ni, which exhibit an anomalously low (almost zero) and constant thermal expansion over a wide region around room temperature. Subsequently, he found the temperature independent elastic behaviour of Fe–Ni–Cr alloys that is now known as the 'Elinvar' effect. The Fe–Ni alloys have different properties depending upon their relative composition and with addition of the third alloying element, i.e. Cr, Va, Mn, etc. Again, all these systems are well studied by MS. In the present review article, some of the recent studies on Fe–Ni, Fe–Pt and some tin based invar alloys will be presented. ^{119}Sn Mössbauer effect and magnetisation measurements have been performed at temperatures between 4·2 and 700 K on an invar alloy (35·8 at.-%NiFe) and ordered FeCo containing tin.[70] Mössbauer results from that study support the model that explains the invar property. In the present study, inter-ionic separation plays an important role that explains the behaviour of the hyperfine interaction. The influence of plastic deformation on the ^{57}Fe and ^{119}Sn Mössbauer parameters of Sn-containing invar alloys was studied by Eliezer *et al.*[71] The cast alloys consist of a matrix having an fcc crystal structure and second-phase stable particles identified as Ni_3Sn_2. Plastic deformation of the specimen containing 4·73 at.-%Sn, the matrix of which contains less than 30%Ni, results in a martensitic transformation, detected by the characteristic lines in the ^{57}Fe Mössbauer

Table 1 Mössbauer parameter *H* (kOe) for different nn and nnn in Fe–Al alloys reported by different authors (reprinted from Ref. 67)

	Reference*			
Configuration	A	B	C	D
8 Fe nn + 6 Fe nn	330	330	330	
(7 Fe + 1 Al) nn + 6 Fe nnn	306	306	312	310–304
(6 Fe + 2 Al) nn + 6 Fe nnn	282	282	288	286–282
(5 Fe + 3 Al) nn + 6 Fe nnn	258	258	264	264–260
(4 Fe + 4 Al) nn + 6 Fe nnn	234	234	229	241–237
(3 Fe + 5 Al) nn + 6 Fe nnn	210	210	167	217–214
(2 Fe + 6 Al) nn + 6 Fe nnn	186	186	122	194
(1 Fe + 7 Al) nn + 6 Fe nnn	162	162	65	
8 Fe nn + (5 Fe + 1 Al) nnn	319	325		
8 Fe nn + (4 Fe + 2 Al) nnn	308	320		310–304
8 Fe nn + (3 Fe + 3 Al) nnn	297	315		295
8 Fe nn + (2 Fe + 4 Al) nnn	286	310		286–282
8 Fe nn + (1 Fe + 5 Al) nnn	275	305		273
8 Fe nn + 6 Al nnn	264	300		264–257

*A, Ref. 58 with $\Delta H_1 = 24$ kOe and $\Delta H_2 = 11$ kOe; B, Ref. 65 with $\Delta H_1 = 24$ kOe and $\Delta H_2 = 5$ kOe; C, Ref. 66, Fig. 4.8; D, Ref. 67.

spectrum as well as by X-ray diffraction. The alloys having a Ni concentration of the matrix greater than 30% do not transform into a bcc structure after plastic deformation. They proposed that because of the high cooling rate during casting and the slow diffusion of Fe and Ni atoms, Fe rich zones form around precipitates, and these zones are responsible for martensitic transformation. Asymmetric Mössbauer spectra of a Fe–41·3 at.-%Ni invar alloy have been quantitatively interpreted by Hesse and Müller.[72] In the temperature range from about 77 K up to the Curie temperature for each spectrum, four parameter values have been obtained. These are the mean hyperfine field H_0, the magnetic field difference h_1 caused by the isotropic contribution of one first Fe-neighbour atom, the corresponding anisotropic difference h_2 and the strength of the anisotropic quadrupole interaction (w). A physical interpretation of these parameters and their temperature dependence has been worked out. The last parameter shows the dependence on the thermal expansion of the lattice. They conclude that there must exist some mechanism by which small changes in the lattice constant cause an enhanced variation of w. The effect of hydrogenation on the internal field in Fe–Ni invar alloy was studied by Sohmura and Fujita.[73] The weak internal field contribution of a Mössbauer spectrum of the Fe–Ni invar alloys was diminished by intense hydrogenation, and instead, the strong ferromagnetic part increased. This effect of hydrogen was interpreted in terms of 3d hole filling with electrons from solute hydrogen in Stoner's band model. Mössbauer measurements on Fe–Ni and on Fe–Pt in the ordered and disordered states at various temperatures and in a longitudinal external field (H_{ext}=50 kOe) have been studied by Gonser *et al.*[74] Hyperfine field distributions of Fe–Ni invar alloys indicate that in addition to the ferromagnetic phase, a second phase or state exists whose magnetic properties seem to be closely related to those of γ-Fe. No other phase or state was detected in the ordered Fe–Pt alloys. Extensive studies on the microstructure and low temperature magnetism of Fe–Ni invar alloys were done by Rancourt *et al.*[75] The Fe–Ni (68–35 at.-%Fe) samples were characterised by MS and vibrating sample magnetometer. The as quenched samples showed the zero field quenched behaviour. They attributed this behaviour to the presence of strong ferromagnetic domains. These domains could be due to the quenched-in crystallographic defects in the sample. Annealing effectively removes these effects, however, in most samples it concomitantly introduced α/γ'-phase precipitation precursors. The 68 at.-%Fe sample in which precursors were not formed (due to the high temperature of its single phase boundary) showed re-entrant spin glass (RSG) behaviour. The RSG behaviour is believed to arise from pinning owing to intrinsic domain wall width scale compositional variations combined with demagnetisation effects and/or normal thermal randomisation. No evidence is seen for a true RSG transition or phase occurring in Fe–Ni alloys. Appearance of concentration oscillations during martensitic $\alpha \rightarrow \gamma$ transformation were studied by Goshchitskii *et al.*[76] They studied the structural and concentration changes, which go together with the reverse martensitic α–γ transformation in metastable austenitic Fe→Ni invar type alloys under slow heating (0·2–0·4 K min^{-1}). The Mössbauer and electron microscopy studies showed that the $\alpha \rightarrow \gamma$ transformation included several stages. (1) At the preliminary stage (523–673 K), nickel was redistributed between martensite and the retained austenite. (2) At the second stage (673–723 K), dispersed plates (10–50 nm thick) of the γ-phase were formed by shear in martensitic crystals. (3) During the third stage (673–723 K), the thin-plate γ-phase was enriched in nickel and depleted in the retained martensite (in accordance with the Fe–Ni equilibrium diagram). (4) At temperatures higher than 723 K (the fourth stage), globular austenite was formed. The globular austenite inherited the concentration inhomogeneity of the $\alpha \rightarrow \gamma$ mixture as nickel concentration oscillations. Varying the degree of nickel redistribution in austenite by special thermal treatment, they found that it was possible to control the thermal expansion coefficient in a broad range. MS under longitudinal external fields (up to 7 T) and SQUID magnetometry (up to 5 T) measurements were carried out on mechanically alloyed γ-fcc $Fe_{100-x}Ni_x$ (x=21, 24, and 27 at.-%) alloys at room temperature by Abdu *et al.*[77] The high field Mössbauer results indicate that a large amount of the material is in the paramagnetic state, giving rise to two spectral components with their effective fields almost linearly dependent on the external field. The in-field Mössbauer spectra of the x=27 at.-% alloy show an additional component with a hyperfine field of ≈21 T, which is attributed to Ni rich (>30 at.-%Ni) ferromagnetic clusters that behave superparamagnetically at room temperature and show a non-linear character in the magnetisation (M–H) curves at low fields. This ferromagnetic cluster phase is also present in the x=21 and 24 at.-% samples but in smaller amounts. Their results indicated that induced hyperfine fields and hence induced moments in the paramagnetic components increase with increasing Ni content.

Ferrimagnetic materials have a net magnetic moment which is aligned on application of an external magnetic field. To understand the magnetic structure, $NiFe_2O_4$ (ferromagnetic material) was studied by Chappert and Frankel.[78] Under no external magnetic field, it shows a spectrum that is overlapping two sextets as a result of two different sites (a and b) in its crystal structure. Under the application of the external longitudinal magnetic field (7 T), the lines in the Mössbauer spectrum owing to Δm=0 transition are absent, and the resultant spectrum shows the overlap of two four-finger patterns owing to the a and b sites in the crystal structure. This is an indication of the collinear magnetic structure in the sample. But the chromium substituted nickel ferrite shows non-zero intensity of the Δm=0 line in the Mössbauer spectrum. This is due to the non-collinear magnetic structure in this sample. A non-zero intensity of the Δm=0 lines had previously been reported by Pollard.[79] That study showed that this was probably partly due to the presence of antiferromagnetic α-Fe_2O_3 as a surface impurity. Antiferromagnets are those where the net magnetic moment is zero in the bulk, but sublattices have equal and opposite magnetic moments. Mössbauer spectroscopy can split these two sublattices and can see an individual sublattice as a particular magnetic phase. Since the structures of the sublattice are the same, so in the spectrum both sub-lattices contribute identical signals in the Mössbauer spectrum. Thus the

spectrum is the addition of the intensities of these two sub-lattices. Therefore there is no difference between the spectrum of a ferromagnetic and an antiferromagnetic material. Both show a six-finger pattern in the spectrum in the absence of an external magnetic field. In the Mössbauer spectra of different antiferromagnetic compounds, under the application of longitudinal magnetic field, the relative intensities of the lines change, and the intensity of the line $\Delta m=0$ is not zero in the spectrum. This is an important clue to differentiate the ferromagnets from antiferromagnetic materials.[80]

The 'spemmagnetism' in the insulators describes a state of matter in which the antiferromagnetic exchange interaction between neighbouring magnetic ions is frustrated, leading to a random, isotropic spin structure. In such material, the spin structure is not affected on application of an external magnetic field, even up to 5 T.[81] Ferey *et al.*[82] studied the magnetic properties of FeF_3 amorphous compounds and found the existence of strong antiferromagnetic exchange interactions. The spectra fitted by Pollard and Pankhurst[83] modelled different ferric insulators from antiferromagnetic exchange interactions in the compounds to explain their speromagnetic properties under a strong magnetic field. They fitted the spectra by assuming the existence of speromagnetism in the samples.

In asperomagnetic materials, there is some preferred orientation of the magnetic spins, hence it possesses a net spontaneous magnetisation. Greneche *et al.*[84] studied the $NiFeF_5(H_2O)_2$ asperomagnetic compound. Here the magnetisation properties are dominated by the iron magnetic moment. Under the application of the external magnetic field, the favoured direction of the magnetic moment appears antiparallel to the magnetic field.

The next series of magnetic materials are spin glasses, cluster glasses and mictomagnetic materials and will be discussed in this section.

For more than 25 years, there has been interest in random magnetic materials and their low temperature behaviour. Such studies led to the discovery of fundamental new types of magnetic ground state, namely, the spin glass phase. In this state, the random freezing of the localised magnetic spins occurs cooperatively, thus generating many unusual properties. In many experiments, the glassy materials show the same types of behaviour. As an example, below freezing temperature, a variety of irreversibility, meta-stability and time dependence effects appear in the magnetic response. Yet the key question remains how the spin system enters the glassy state, since spin freezing occurs at low temperatures when the dynamical fluctuation of the individual spins or spin clusters slowly decreases. Therefore the time/frequency dependent measurements spanning a wide regime (time range 10^{-6} to 10^{-9} s) give very useful information to understand the spin glass. MS can see a fluctuating spin system with a time period of fluctuation of the order of 10^{-7} s. So to study spin glasses, MS is one of the very useful techniques in addition to muon spin resonance. Extensive research on MS of AuFe spin glass was reported by Meyer *et al.*[85] Temperature measurement shows a sudden change of character at around 19·5 K, which is higher than the cusp temperature. They suggested that at low temperature, the spin-glass has a static behaviour but that the true paramagnetic state only sets in at a temperature that is appreciably higher than the cusp temperature. A possibility could be that below the cusp temperature, the system stays in a single 'well', whereas between the cusp and Mössbauer transition temperature (19·5 K here), it is not stable and jumps between different 'wells' where the frequency is lower compared to the Mössbauer frequency scale. Again, it has been found that well above the spin freezing temperature of the spin glass system, there exists a regime where the behaviour of the phase is different from that of a paramagnetic phase. The magnetisation curve is non-linear, and Curie-Weiss behaviour is found only at higher temperature.[86] To understand the dynamics of the magnetic correlation of the spin glass samples in this region, Pösinger *et al.*[87] studied Au(Fe), $Y(Fe,Al)_2$ systems by temperature dependent MS under the application of an external magnetic field and found a correlation of spin over times from 2 to 200 ns when the external field is 13·5 T. They also reported that the lifetime of the magnetic correlation increases with a decrease in temperature and increase in the external magnetic field, but the applied magnetic field and temperature have very little influence on the nature of the correlations. Several recent studies on the binary and ternary spin glass systems are also important. Bauermann *et al.*[88] studied the concentration dependence of the saturation hyperfine field by ^{151}Eu MS in the EuS_xSe_{1-x} spin glass system They found a continuous change of the local magnetic structure along the series. The spin glass phases consist of nearly two-dimensional ferromagnetic clusters, whereas the ferromagnetic states close to the ferromagnetic-spin-glass boundary are phases such as frustrated ferromagnets. They also observed relaxation phenomena in both the spin glass and 'frustrated ferromagnetic' phases. Other spin glass properties in addition to the mixed phases have been observed in the ternary alloys such as FeNiMn and FeNiCr. These magnetic materials exhibit random mixtures of ferromagnetic and antiferromagnetic interactions and have been attracting considerable interest. Depending upon the relative concentration of Fe and Ni, Fe–Ni binary alloys show different magnetic properties. The Fe–Ni alloy having 35 at.-%Ni is known as Invar, and that having a Ni concentration of around 75 at.-% is known as permalloy. However, owing to the γ–α phase transformation, it is not possible to study the antiferromagnetic phase of Fe below 1180 K.[89] Addition of Cr or Mn or V stabilises the γ-phase, and the complete region extending from the antiferromagnetic (Fe rich) to the ferromagnetic (Ni rich) forms within the same crystallographic structure. From the physicist's point of view, the Fe–Ni–Cr (or Mn) ternary alloy system provides several challenging problems. First, no one theory explains the magnetism of 3d-transition metal alloys. Second, the antiferromagnetism of Fe in the fcc-phase arises owing to a negative exchange interaction between the nearest-neighbour (nn) Fe atoms.[89] In such systems, there exist six different exchange interactions. Interactions between Fe–Fe and Cr–Cr (or Mn–Mn) are antiferromagnetic, and all other interactions are ferromagnetic. Huck and Hesse[90] reported the Mössbauer spectroscopic study of the $(Fe_{0\cdot65}Ni_{0\cdot35})_{1-x}Mn_x$ system for $0 \leqslant x \leqslant 0\cdot245$. Temperature dependent Mössbauer spectroscopic measurements show the magnetic phase transition for different compositions in the alloys. The calculated average hyperfine field from hyperfine field

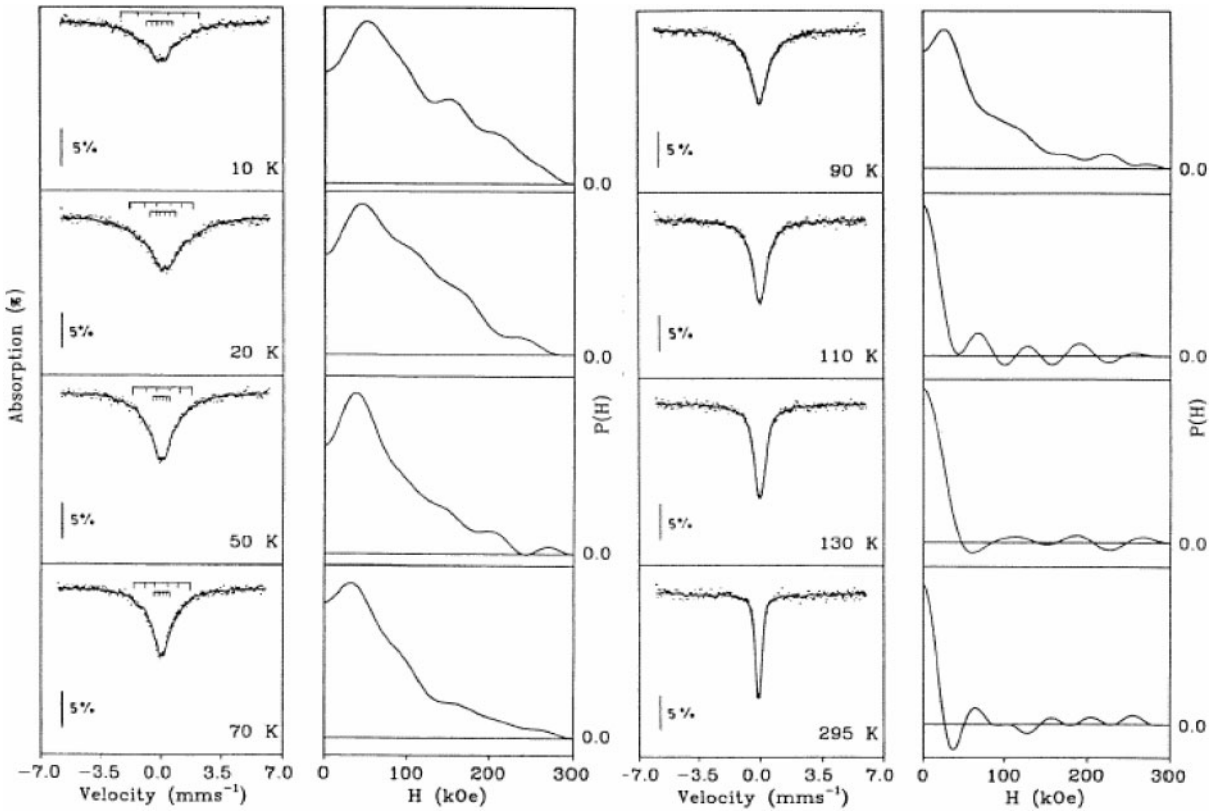

9 Mössbauer spectra of $Fe_{50}Ni_{30}Cr_{20}$ alloy at different temperatures, and corresponding hyperfine-field distributions (reprinted from Ref. 91)

distributions of different compositions for different alloys shows that the variation of the average hyperfine field with temperature is clearly divided into two sections. The first section (from RT to the 2nd transition temperature) of the curve represents the normal course corresponding to the spontaneous magnetisation from initial paramagnetic phase to ferromagnetic phase with transition temperature T_c, the Curie temperature of the sample. The second region starts from a kink representing a mixed ferromagnetic and spin glass phase, known as re-entrant spin glass phase. The other samples with Mn concentrations greater than 14% show direct spin glass transition from the paramagnetic phase. From the calculated values of different transition temperatures, they finally established the magnetic phase diagram of FeNiMn alloys. MS of the $Fi_{80-x}Ni_xCr_{20}$ ($14 \leqslant x \leqslant 30$) system for different Ni compositions has been reported by Bandyopadhyay[91–93] and Bandyopadhyay *et al.*[94,95] The magnetic phases studied in such alloys indicated that these alloys are paramagnetic at room temperature and show different types of magnetic phase transition with decreasing temperature.[89] At room temperature, all spectra are singlets and show line broadening with slight asymmetry with decrease in temperature. Typical Mössbauer spectra of the sample for $x=20$ and corresponding hyperfine field distributions are shown in Fig. 9. Different Mössbauer parameters are then calculated from the hyperfine field distribution curve. The Curie temperature (T_c) of this alloy calculated from the temperature dependence of the average hyperfine field was 130 K. To understand the local magnetic order of this alloy below the Curie temperature, the hyperfine field distribution curves are then fitted by two independent Gaussians. Each Gaussian represents a particular type of magnetic order. Mössbauer spectra are then generated theoretically for these two different iron sites, and the resultant spectra then overlap with the experimental spectra obtained at different temperatures to check the quality of the Gaussian fitting. Figure 10 shows the two Gaussian fits of the hyperfine field distribution curves at low temperature. Variation of normalised area under the curves explains the different interactions present in the sample at low temperature. At low temperature, though the alloy shows ferromagnetism, the interactions between Fe and Fe are antiferromagnetic. Since the ferromagnetic interactions dominate the antiferromagnetic interactions, the sample looks like antiferromagnetic clusters in a ferromagnetic matrix, where the local environment of the former is Fe rich, and the latter sites are Fe poor. Alternately, if the antiferromagnetic clusters are negligible, then the sample can be viewed as ferromagnetic spin clusters and an infinite (or long range) ferromagnetic matrix, like the re-entrant spin glass state. Keeping all these aspects in mind, the hyperfine field distributions have been fitted with two independent Gaussians of different peaks and width following Weiss.[96] On the basis of the above discussions, the two Gaussians on the low and high field sides of the hyperfine field distributions, $P(H)$, have been assigned as the Gaussians originating from Fe atoms in the low field clusters and in the high field ferromagnetic matrix, respectively. It is to be noted that evenafter decomposing the hyperfine field distributions into two Gaussians, the value of $P(H)$ at $H=0$ is still very high. This is because Fe atoms in low field clusters are very small and hence not resolved totally. So they contribute a non-zero value of $P(H)$ at $H=0$ in the hyperfine field distributions, as does the presence of a paramagnetic

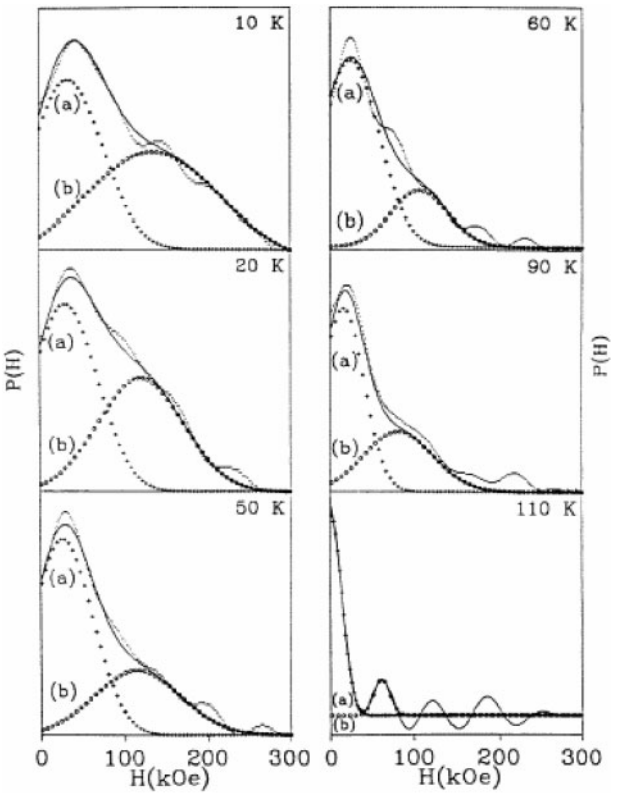

10 Two-Gaussian fits to *P(H)* distribution versus *H* curves at different temperatures; curves (a) represent low field-side Gaussians (+) and curves (b) high field-side Gaussians (•••) (reprinted from Ref. 91)

phase. Existence of mictomagnetic clusters have been found in the alloy with a Ni concentration of 26 at.-%.[92] To study the lattice dynamics of the $Fe_{80-x}Ni_xCr_{20}$ (x=30, 26 and 19) samples, the values of the centre shift of the Mössbauer spectra taken at different temperatures have been measured.[94] A non-zero contribution from the second term of the above expression arises as a result of the relativistic effect whenever the source and absorber are at different temperatures, and is known as the thermal shift. This temperature dependent part of the centre shift is caused by the time dilation resulting from thermal motion of the γ-ray-emitting and -absorbing nuclei. In this way, the Doppler shift is related to the lattice dynamics of Debye solids. By using the minimum-standard-deviation method, the experimental second-order Doppler shift data relating to the values of the centre shift, have been fitted,[94] which gives the value of Θ_D as 461, 458 and 454 K for x=30, 26 and 19, respectively. There is hardly any change in δ_{SOD} below the transition temperature. This indicates that below the transition temperature, there is no effect from the electronic structural anomaly or phonon softening of the $Fe_{80-x}Ni_xCr_{20}$ alloys. The softening corresponds to the case of lattice vibration when the average velocity $<v^2>$ decreases. Again, the expression for $<v^2>$, which has been used for fitting the experimental data holds for a harmonic crystal.[94] So, one can conclude that below the transition temperature, the vibrational motion of Fe atoms remains harmonic. The average velocity decreases below the transition temperature, as discussed earlier. The decrease in $<v^2>$ reflects the absence of vibrational instabilities in the lattice below the magnetic phase transition from paramagnetic to a new state.

Metallic glasses

An amorphous solid is the state of solid materials where there is no long-range order in the positions of the atoms. Depending upon the preparation method, the solid material can be formed as an amorphous material. For instance, common window glasses, most polymers and even some amorphous metallic alloys can be prepared under special processing conditions, such as rapid solidification and ion implantation. The most common method to produce amorphous solids of a particular metallic composition is by rapid solidification of the mixture from its molten state. Metallic glasses (MGs), which are obtained by rapid quenching (10^6 to 10^8 K s^{-1}) of metallic melts, are also non-crystalline or amorphous like oxide glasses, but at the same time are different from the latter in several ways. They are primarily made of metallic elements, and their bonds are purely metallic bonds. The amorphous metallic alloys can be prepared by other routes, such as ion implantation, but these alloys are not like rapidly solidified metallic alloys. The structure of a rapidly solidified alloy is like glass and is known as metallic glass. Here the term glass refers to amorphous alloys where silicon is a common element.

The first metallic glass produced by direct quenching from the melt in the laboratory was made by Professor Paul Duwez and co-workers at the California Institute of Technology.[97] Research activity has developed during the last four decades in many fields of amorphous materials because of their basic science and their technological interests, mainly on structural aspects, and on thermodynamic, mechanical, and magnetic properties which have stimulated applied studies. MGs exhibit high hardness and high stiffness, high electrical resistivity, non-magnetocrystalline anisotropy, soft ferromagnetism and high resistance to corrosion. At present, fundamental interest in MGs exists since the discovery of the nanocrystalline materials because of their better magnetic performance.[98] MS is an excellent tool to investigate MGs because it can select resonating nuclei of a particular species and can read the nature of their immediate surroundings. Using CEMS, one can study the surface properties of the MGs.

^{57}Fe MS has contributed to the investigation of the structural properties, magnetic properties and the magnetic anisotropy of iron-based MGs and more recently of iron-based nanocrystalline alloys. In addition, one can correlate the magnetic texture with the history of the quenching process. MS can tell us about the effective or internal magnetic field at the nucleus, through the so-called hyperfine field (H_{int}). Analysis of the internal hyperfine field at different sites gives the probability distribution of the hyperfine field, $P(H)$.

In addition, the intensities of intermediate lines describe the orientation of H according to the γ-ray beam direction, i.e. the mean magnetisation direction. In the case of crystalline ferromagnetic alloys, the orientation of the magnetic spin along the easy direction of magnetisation originates from magnetocrystalline anisotropy in magnetic domains. In case of amorphous systems like metallic glass, there is no magnetic anisotropy, but the magnetoelastic anisotropies play an important role for MGs. The domain structure strongly depends on the magnetostrictive behaviour of the alloy (sign and magnitude) and on the internal stresses

induced during the quenching process.[99] In MGs containing about 75% of transition metals, one generally observes a preferred orientation of ferromagnetic domains, also called magnetic texture, which is clearly evidenced by MS through the relative intensity of lines 2 and 5. By using the angular dependence of the magnetic hyperfine interaction, it is possible to obtain information about the average spin orientation from the intensity ratio of the second and first lines (I_2:I_1) or (I_5:I_6) corresponding to $\Delta m=0$ and $\Delta m=\pm 1$ nuclear transitions. The relative intensities are given by: $I_2:I_1=4\sin^2\theta/(1+\cos^2\theta)$, where θ is the angle between orientation of spins and the direction of propagation of γ-rays. For a magnetic spectrum with a six-line pattern, $I_2:I_1=4$ or 0 when all spins are aligned perpendicular ($\theta=90^\circ$) or parallel ($\theta=0^\circ$), respectively, to the γ-rays. The ratio of $I_2:I_1$ becomes 2 for a random orientation, $\theta\approx 55^\circ$. Therefore, magnetic texture can be completely described from two independent MS of the same composition or with the presence of small impurities recorded under different conditions. The different conditions may be the presence of thermal stresses induced during the solidification procedure or may be after producing some damage in the MGs.[100] The stress in the MGs is biaxial in the bulk favouring in-plane magnetic domains, whereas the compressive stresses at the surface originate from the out-of-plane domains.[101] When the metallic glass ribbons exhibit thickness fluctuations owing to surface defects of the substrate, one can correlate the local magnetic textures obtained by scanning the width of the ribbon, with the microtopology of the surface.[102] On the other hand, MS can give us information about the structure and stress relaxation effects in the case of low temperature annealed MGs from the hyperfine field distribution and magnetic texture, respectively. Mössbauer spectra of amorphous wires suggest the presence of magnetic domains with radial and axial orientations in the outer surface and the bulk, respectively.[101] Extensive work on the study of the crystallisation of Fe–B–Si MGs was reported by Bandyopadhay[103–106] and Bandyopadhyay and colleagues.[107,108] The amorphous state of metallic glass is metastable in nature. Upon annealing, these amorphous alloys change from amorphous to crystalline through an intermediate nanostructured state, depending on their composition, annealing temperature and time period of annealing. The magnetic properties in the new crystalline state are different from that of the amorphous state. This kinetic process of crystallisation is determined by the temperature and time period of heat treatment. Upon annealing, the MGs tend to relax and become denser by atomic rearrangement. The atomic structure of the amorphous alloys may be 'locally distorted non-stoichiometric quasicrystalline'.[103] This gives rise to a large number of structurally inequivalent sites in metallic glass and causes their characteristic magnetic parameters such as exchange interactions, magnetic moments, hyperfine fields, etc. to have a distribution of values instead of unique values. Further, this distribution changes if the sample is annealed. The nature of these changes is determined by the composition of the metallic glass, the annealing temperature and time periods. As the temperature of annealing approaches the precipitation of other compounds, this evolution process also affects the changes in the probability distributions of the hyperfine fields, $P(H)$. Crystallisation kinetics in the Fe–B–Si MGs has been investigated by Banerjee *et al.*[109] A study of the crystallisation mechanism of some iron-based metallic glasses by MS and X-ray diffraction was reported by Nagarajan *et al.*[110] The crystallisation was found to depend essentially on the mutual solid solubility of the ternary element with the transition metals as well as on the metalloid concentration. They found that in a Fe–Ni–Mo–B metallic glass, introduction of Ni stabilised the $(Fe–Ni)_3B$ phase whereas Co and Si destabilised the $(Fe–Co)_3B$ and $(Fe–Si)_3B$ phases which are absent in the final equilibrium products. The nearest neighbour configuration of iron atoms in the solid solution is also discussed.

The effect of annealing on $Fe_{79}B_{16}Si_5$ metallic glass has been reported by Bhatnagar and Ravi.[111] It is well known that amorphous alloys contain a large number of structurally and magnetically non-equivalent sites that can be effectively characterised by determining the distribution of $P(H)$. Bandyopadhyay[103–106] reported the effect of the annealing temperature (T_C) and time period (t) on the evolution of $P(H)$ of the metallic glass $Fe_{79}B_{16}Si_5$ (Si5) and $Fe_{78}B_{13}Si_9$ (Si9) near and below the crystallisation temperature. Mössbauer spectra and corresponding variation of hyperfine field of $Fe_{79}B_{16}Si_5$ with time period of annealing and at fixed temperature are shown in Fig. 11. Mössbauer spectra taken at different temperatures and for different time periods have been analysed by two methods. Using a least-squares fit method for the experimentally measured Mössbauer spectra, different crystalline phases have been identified and the results are shown in Table 2 for $Fe_{79}B_{16}Si_5$ annealed at 748 K for different times. In the second part of the analysis, Window's method[338] has been applied to determine the probability of hyperfine field distributions, $P(H)$, of the Mössbauer spectra. Careful observation of the hyperfine field distributions of the MS below the crystalline temperature shows two minor changes: (i) the peak position shifted slightly about the peak position of the as-received sample and (ii) a slight bulge developed on the left wing making the peaks more asymmetric.[104] This behaviour is due to the contributions from small random perturbations and the texture effect of the sample during different annealing temperatures and time periods. The similar nature of $P(H)$ (not shown) indicates that the sample retained its amorphous nature below 673 K. The experimental spectrum of $Fe_{79}B_{16}Si_5$ at 748 K, $t=1$ h decomposed into eight subspectra related to the different phases precipitated, which could be identified as α-Fe, α-(Fe–Si) with five different nearest neighbours (nn), Fe_3B and Fe_2B.[103] The analysis of other spectra for $t\sim 2$ h shows that Fe_3B appears to have been formed at three iron sites having $H=224$, 267 and 289 kOe. On the other hand, the Fe_2B phase shows an average value of $H=238$ kOe. Before the crystallisation process starts at 748 K, the sample contains different nanostructured clusters, where they are strongly influenced by the boundary atoms of the clusters. All these effects cause wide distributions in the $P(H)$ of MS below the crystallisation as shown in Fig. 11. The hyperfine distributions were then fitted by using a number of Gaussian curves where each Gaussian curve represents a particular site in the sample. The results show four peaks that correspond to the following phases:

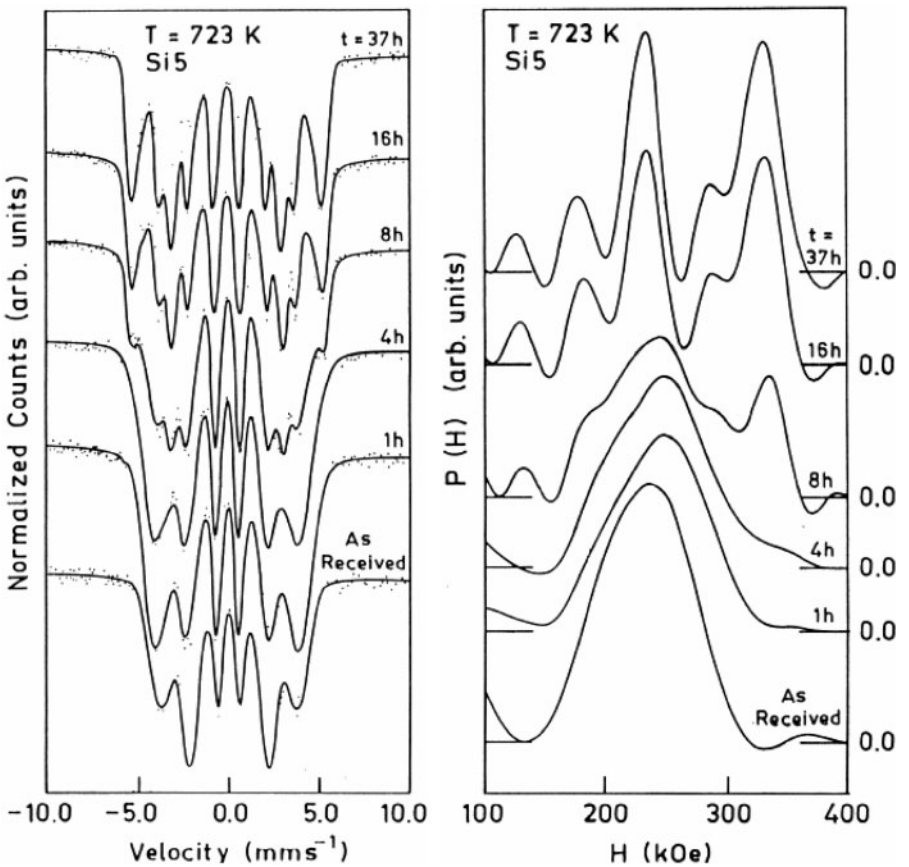

11 Mössbauer spectra and corresponding hyperfine field distributions of $Fe_{79}B_{16}Si_5$ metallic glass annealed at 723 K for different times (reprinted from Ref. 104)

Table 2 Different Mössbauer parameters assigned for different phases present in $Fe_{79}B_{13}Si_5$ sample annealed at 748 K for different time intervals

	H_{eff}, kOe (error: $\pm$4 kOe)	Assignments	Annealing time, h	H_{eff}, kOe (error: $\pm$4 kOe)	Assignments
0	241	Amorphous	4	333	α-Fe
				327	α-(Fe, Si 8nn)
				311	α-(Fe, Si 7nn)
				287	α-(Fe, Si 6nn)
					t-Fe_3B
				270	t-Fe_3B
				240	α-(Fe,Si 5nn)
					Fe_2B (average)
				227	t-Fe_3B
				197	α-(Fe,Si 4nn)(?)
1	333	α-Fe	6	334	α-Fe
	327	α-(Fe,Si 8nn)		328	α-(Fe,Si 8nn)
	310	α-(Fe,Si 7nn)		311	α-(Fe,Si 7nn)
	288	α-(Fe,Si 6nn)		288	α-(Fe,Si 6nn)
		t-Fe_3B			t-Fe_3B
	265	t-Fe_3B		265	t-Fe_3B
	241	α-(Fe,Si 5nn)		236	α-(Fe,Si 5nn)
		Fe_2B (Average)			Fe_2B (average)
	226	t-Fe_3B		225	t-Fe_3B
	196	α-(Fe,Si 4nn) (?)		196	α-(Fe,Si 4nn) (?)
2	332	α-Fe	8	334	α-Fe
	327	α-(Fe,Si 8nn)		329	α-(Fe,Si 8nn)
	311	α-(Fe,Si 7nn)		312	α-(Fe,Si 7nn)
	286	α-(Fe,Si 6nn)		287	α-(Fe,Si 6nn)
		t-Fe_3B			t-Fe_3B
	269	t-Fe_3B		265	t-Fe_3B
	240	α-(Fe,Si 5nn)		238	α-(Fe,Si 5nn)
		Fe_2B (average)			Fe_2B(average)
	227	t-Fe_3B		226	t-Fe_3B
	200	α-(Fe,Si 4nn)(?)		201	α-(Fe,Si 4nn)(?)

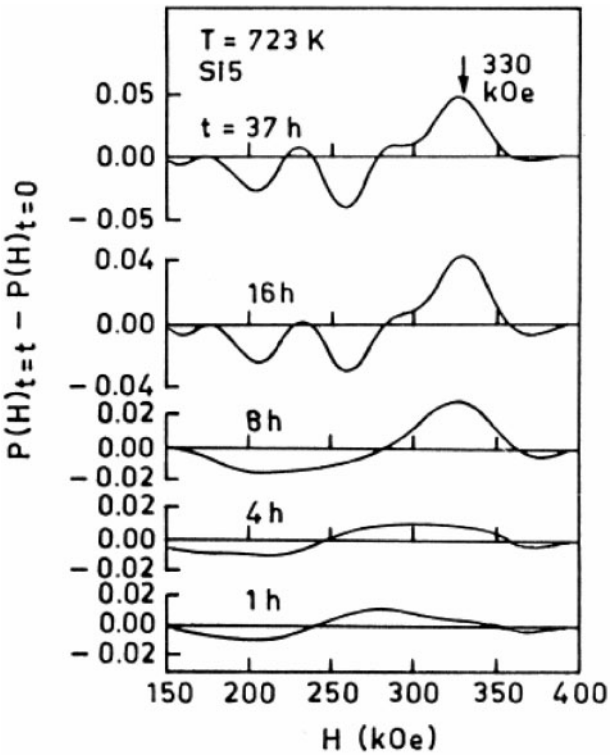

12 Difference hyperfine field distributions of $Fe_{79}B_{13}Si_5$ sample annealed at 748 K for different time intervals (reprinted from Ref. 104)

(i) $H_{peak}\approx317$ kOe: α-Fe, α-(Fe,Si 8nn), α-(Fe,Si 7nn);
(ii) $H_{peak}\approx276$ kOe: α-(Fe,Si 6nn), t-Fe_3B;
(iii) $H_{peak}\approx222$ kOe: α-(Fe,Si 5nn), Fe_2B (average), t-Fe_3B, α-(Fe,Si 4nn);
(iv) $H_{peak}\approx170$ kOe: α-(Fe,Si other nn?).

The observed evolution of average hyperfine field distributions in the studies reported by Bandyopadhyay[103–106] is similar to the time evolution of $<H>$ in the binary amorphous $Fe_{83}B_{17}$ alloy observed by Kosimura and Takahashi.[112] This behaviour could be explained by the clusters model and structural relaxation in amorphous alloys.[113,114] In order to understand the evolution of $P(H)$, Bandyopadhyay[103–106] calculated the difference $[P(H)_{t=t}-P(H)_{t=0}]$ plotted versus H as shown in Fig. 12 for different values of t at 748 K. It shows that the field components around $H=200$ kOe and 262 kOe decrease whereas the components around $H=230$ and 327 kOe increase with t. The vertical arrow indicates the H-value characteristic of α-Fe. The behaviour observed in Fig. 11 explained in terms of phase precipitation results show that first stage α-(Fe,Si) and metastable Fe_3B are formed while further heating leads to the second stage involving the decomposition of the metastable Fe_3B into Fe_2B and α-Fe.[103] There are several other studies on surface and structural properties of different metallic glasses using MS. The present discussion gives a brief outline on the contribution of MS in the research of MG systems.

Rare earth materials

Rare earth materials represent a growing market. These materials have expanding applications in markets as diverse as rechargeable batteries, advanced ceramics, permanent magnets, metals, catalysts, magnets, metallurgy, glass and ceramics, optical data storage, lasers, fibre optics, phosphors and superconductors. MS has been used to study rare earth compounds, and it has added valuable scientific knowledge in the understanding of these materials. Rare earth hard magnets to rare earth intermetallic compounds, rare earth superconductors, rare earth multilayer compounds, rare earth ceramics and other different rare earth compounds have been studied by this technique. In this section, some selective studies of rare earth compounds of different compositions will be discussed.

Rare earth (RE) magnets have revolutionised the properties and applications of permanent magnets. They offer many advantages, and have drastically increased flux compared to traditional magnets with comparable volumes. The discovery of the rare earth intermetallic compound $Nd_2Fe_{14}B$ in 1984[115–117] opened a new era of research on the Fe rich permanent magnet. At present in the world market, the value of the total production is shared by low cost ferrites (55%), Nd–Fe–B based materials (25%), the SmCo magnet (10%) and AlNiCo magnets (10%). The Nd–Fe–B based magnet is attractive from an industrial as well as a basic scientific point of view. The three major intermetallic permanent magnetic materials are tetragonal $R_2Fe_{14}B$, tetragonal $R(Fe,M)_{12}$, rhombohedral or hexagonal $R_2(Fe,M)_{17}$ and their related hydrides, carbides and nitrides. Recently, it has been found that the interstitial modification of these rare earth compounds by nitrogen and carbon, forming nitrides and carbides, can improve their magnetic behaviour.[118,119] The crystal structure of these compounds is important to understand their magnetic behaviour by different experimental techniques, including MS.

Table 3 shows crystal structures and site occupancies of these compounds. Numerous Mössbauer studies of the alloys in the $R_2Fe_{14}B$ (R=Y, La, Ce, Pr, Nd, Sm, Gd, Tb, Dy, Ho, Er, Tm, Lu) series were reported in the period 1985–1986.[120–126] Alloys with $Nd_2Fe_{14}B$ crystal structure have been investigated by several groups.[127,128] The space group of this system is $P4_2/mnm$.[128,129] The existence of some α-Fe and some impurities such as $R_{1+\varepsilon}Fe_4B_4$ in $R_2Fe_{14}B$ has also been reported.[130] In $Nd_2Fe_{14}B$, the six Fe sites have relative populations 4:4:8:8:16:16. Therefore it is difficult to identify the equally populated Fe sites in the Mössbauer spectrum. The best and most common approach is to assign

Table 3 Crystal structures and sites of three main rare earth compounds of general expression $R_2Fe_{14}B$, $R(Fe,M)_{12}$ and $R_2(Fe,M)_{17}$

Phase	Space group	R sites	Fe, M sites	N, C, H sites
2:14:1	$P4_2/mnm$ (number 136)	4f and 4g	$16k_1$, $16k_2$, $8j_1$, $8j_2$, 4c, 4e	H only in $8j_3$, $16k_3$, $16k_4$ and $4e_2$
1:12	$I4/mmm$ (number 139)	2a	8f, 8i, 8j	2b
2:17 (rhombohedral)	R3*m* (number 166)	6c	6c, 9d, 18f, 18h	9e
2:17 (hexagonal)	$P6_3/mmc$ (number 194)	2b and 2d	4f, 6g, 12j, 12k	6h

equipopulous sites on the basis of their measured hyperfine field and nearest neighbour coordination; sites with higher Fe and lower R elements must have a higher value of hyperfine field and vice versa. A detailed study of the temperature dependent hyperfine field at different sites in $R_2Fe_{14}B$ compounds shows that the variation of the hyperfine fields at different sites is different. This could explain the crystal structure and existence of a short Fe–Fe bond antiferromagnetic interaction in $Nd_2Fe_{14}B$ alloy.[131,132] Variation of the hyperfine field at an Fe-site is closely related to neutron diffraction experiments, but it is not true for all other iron sites in the crystal structure. Boge *et al.*[133] used ^{155}Gd MS to study $Gd_2Fe_{14}B$ to estimate the dominant crystal field term from the measured effective field gradient (EFG) at the ^{155}Gd nucleus. Coehoorn and Buschow[134] have cautioned that the assumption of a strict proportionality between the EFG term, V_{zz}, and the second-order crystal field lattice coefficient is, at best, tenuous. Other permanent magnetic materials are made from the interstitial modification of R-Fe based intermetallic compounds by nitrogen or carbon.[118,119] All these compounds have at least 80 at.-% Fe, but still Mössbauer spectra are complicated owing to a complex crystal structure. Coey and Qi[135] and Qi *et al.*[136] studied the effect of nitrogen on the R_2Fe_{17} compounds. When the nitrogen binds with R_2Fe_{17}, it forms $R_2Fe_{14}N_3$. The value of the hyperfine field for both R_2Fe_{17} and $R_2Fe_{14}N_3$ shows that the addition of nitrogen to R_2Fe_{17} increases the iron magnetic moment by 15%. On the other hand, the addition of carbon at the same atomic per cent reduces the effect by a few per cent. The addition of nitrogen and carbon to the R_2Fe_{17} as interstitial elements gives the inertial induced volume expansion, and as a result the ratio of ΔIS (isomer shift) to $\Delta \ln V$ increases to 1·8 mm s^{-1}, but this effect is only 0·7 mm s^{-1} for carbon.[135] The resultant increase in this ratio is due to the volume expansion and opposing electron transfer from iron to nitrogen or carbon. Qi *et al.*[136] explained this opposing electron transfer in terms of Miedema's model of electron density at the Wigner-Seitz cell boundary. Intermetallic nitride phases in $R_2Fe_{17}N_x$ have been studied by Persiano and coworkers,[137,138] where R is Pr. They found a saturated $Pr_2Fe_{17}N_{3-\delta}$ phase, where δ=0·2 in the non-homogenised sample and some unaffected Pr_2Fe_{17} under some strain. The calculated Mössbauer parameters were explained on the basis of three different phases and particle size as (i) central saturated nitrides, (ii) intermediate stressed Pr_2Fe_{17} and (iii) an unaffected external Pr_2Fe_{17}. The major drawback of the nitrides and carbides is their chemical instability at higher temperature. They decompose completely into α-Fe and different rare earth nitrides or rare earth carbides. It has been found that addition of Si stabilised the compounds. By starting with $R_2Fe_{17-x}Si_x$ powder, the carbides can be made by heating in a CH_4 atmosphere at 700°C for approximately 2 h, and these compounds are stable up to 900°C. For $Sm_2Fe_{17-x}Si_xC_y$ (x=1, 2 and 3 for y=2·7, 2·3 and 2·0, respectively),[139] it was found that in these compounds, cell volume increases by at least 4–6% over the Si range from 1 to 3. Addition of Si decreases the cell volume as well as the lattice parameters, and the result can be attributed to the increase in Curie temperature. Rare earth boro-carbides

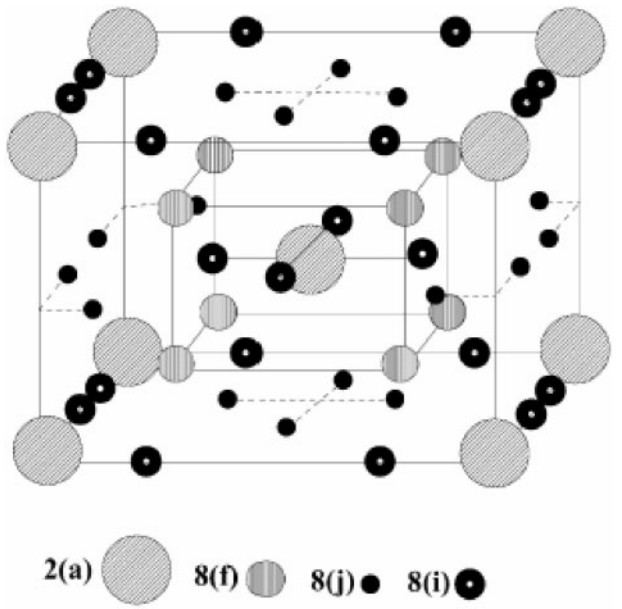

13 Schematic representation of RFe_4Al_8 crystal structure

such as $R(Ni_{0.99}Fe_{0.01})_2B_2C$ (R=Y, Gd, Tb, Dy, Ho and Er) are studied by Mössbauer measurement.[140] The measured isomer shift and quadrupole splitting are found to be the same for all R except Y. Quadrupole splitting decreases with increasing ratio of the *c*/*a* of the crystal parameters. This trend can be explained by the change in the geometrical factor in the crystal structure which is mainly due to the changes in the lattice constants.

The effect of the hydrogenation, decomposition, desorption, recombination (HDDR) process, particularly with regard to magnetic properties and microstructures on Nd–Fe–B anisotropic magnetic powders is also important because of formation of texture.[141–143] This addition also reduces the cost of the material. It generates a textured submicrometre microstructure during heating of $Nd_2Fe_{14}B$ powders under hydrogen atmosphere and later followed by desorption.[143] Anisotropy of the resultant materials treated via the above route is affected both by disproportion processing parameters as well as the presence of the additives.[143] Saccone *et al.*[144] studied the $Nd_{14\cdot01}Hf_{0\cdot08}Fe_{78\cdot91}B_7$ alloy first after hydrogenation–disproportionation treatment between 700 and 950°C, and then the same alloy was treated at constant temperature under constant pressure. MS showed the presence of different boride phases such as Fe_2B, and t-Fe_3B and their quantity in the treated Nd–Fe–B sample. It is important to mention that the substitution of iron by cobalt and the addition of elements such as gallium, zirconium, niobium, hafnium, tantalum, etc. were found to be very effective in inducing magnetic anisotropy in Nd–Fe–B magnetic powders.[141,145]

RFe_4Al_8 compounds are another member of the group of rare earth compounds with the general formula RM_4Al_8 where R is any 3d transition metal element. All RM_4Al_8 compounds crystallise in the tetragonal form with a $ThMn_{12}$ type crystal structure (Fig. 13) which belongs to the I4/*mmm* space group.[146] The magnetic properties of all these compounds can be explained by a molecular field model considering different magnetic

sub-lattices in the crystal structures.[147] In all such compounds, the interaction between R–Fe is less than one-half of the inter sublattice Fe–Fe interaction. Ordering of rare earth elements in such compounds only takes place at very low temperatures. According to Buschow and van der Kraan,[147] this is due to a small interaction in R–Fe and due to that particular type of crystal structure which leads to a vanishingly small molecular field at the site of R under the antiferromagnetic ordering of Fe moments. Mössbauer spectroscopy[148] and neutron diffraction[149] have confirmed the complex antiferromagnetic (AF) ordering in RFe_4Al_8 compounds. Recent work on RFe_4Al_8 (R=Ce and Sc) has been reported by Gaczynski and colleagues.[150,151] The temperature dependent Mössbauer study of RFe_4Al_8 (R=Ce and Sc) shows a sextet Mössbauer spectrum at low temperature. It then vanishes with increasing temperature. This change is usual in MS and is an indication of onset of Fe spin ordering at low temperature. The ordering temperatures reported from these studies for the above compounds are 165 K and 225 K, respectively. But these temperatures are different in magnetic susceptibility measurements, where the ordering temperatures are found to be 130 K and 125 K for Ce and Sc. These differences may be due to the local probe detection ability of MS. Another study shows that the addition of Ce and Sc to RFe_4Al_8 as $Ce_{1-x}Sc_xFe_4Al_8$ ($0<x<1$)[151] always gives antiferromagnetic ordering in the Fe sublattice below 130 K. The effective magnetic moment decreases with the Sc content, whereas the Neel temperature T_N is not affected by substitution of Sc for Ce. The substitution of Al atoms into the M-sublattice in the $Dy[(Fe_{0\cdot7}Co_{0\cdot3})_{1-x}Al_x]_x$ and $Dy[(Fe_{0\cdot4}Co_{0\cdot6})_{1-x}Al_x]_x$ series was studied to determine the influence of the 3d electrons on the magnetism of R–M compounds by ^{161}Dy MS.[152] The structural properties of glassy hard magnetic amorphous ribbon $Nd_{50}Fe_{40}Al_{10}$ were studied by Mössbauer measurements and by Chiriac *et al.*[153] Low temperature Mössbauer measurement in this compound shows a number of asymmetrical lines that can be ascribed to the non-equivalent local environment of Fe atoms. The Mössbauer spectra of the $Sm_2Fe_{17-x}Al_x$ solid solutions (x=0, 0·5, 0·75, 1, 3, and 4), which crystallise in the rhombohedral Th_2Zn_{17} structure, have been measured between 85 and 295 K.[154] The spectra have been analysed with a model based on the binomial distribution of aluminium near neighbours calculated from the aluminium site occupancies derived from neutron diffraction measurements on $Nd_2Fe_{17-x}Al_x$ solid solutions. This analysis which is based on the binomial distribution of aluminium near neighbours, indicates that the Mössbauer spectra are sensitive to the spin reorientation occurring between x values of one and three. This also confirms that the aluminium site occupancies are independent of the rare earth element in the $R_2Fe_{17-x}Al_x$ solid solutions. They calculated the value of the iron magnetic moment at its sites, and revealed important covalent bonding between iron and its aluminium near neighbours.

Several other rare earth compounds were studied by Mössbauer techniques.

In the above section, the discussion addressed important rare earth magnets. We will now discuss perovskite rare earth materials. Perovskites are a large family of crystalline ceramics that derive their name from a specific mineral known as perovskite. The parent material, perovskite, was first described in the 1830s by the geologist Gustav Rose, who named it after the famous Russian mineralogist Count Lev Aleksevich von Perovski.

Perovskite is the most abundant mineral on Earth and has been of continuing interest to geologists for the clues it provides to the planet's history. It is believed that the Earth's lower mantle is similar to the upper mantle, which provides the geological interest. The upper mantle is 80% (Mg, Fe)SiO_3 and the lower mantle is believed to be the same or perhaps up to 90–100% perovskite. The principal perovskite structure found in ferroelectric materials is a simple cubic structure containing three different ions of the form ABO_3. The A and B atoms represent 2+ and 4+ ions, respectively, while O is the O^{2-} ion. This ABO_3 structure can be thought of as face centred cubic (fcc) with A atoms at the corners and the O atoms on the faces. The B atom completes the picture and is located at the centre of the lattice. This A atom is the largest of the atoms and consequently increases the overall size of the AO_3 (fcc) structure. As a result, there are minimum energy positions off centred from the original octahedron that can be occupied by the B atom. Shifting of this atom as a result of applied electric fields causes the structure to be altered, creating electric dipoles. There are several types of such materials. In this section, some of the important Mössbauer spectroscopic studies of these materials will be discussed. Several structures of ABO_3 materials were reported by Wang *et al.*[155] Another important study was made by Haung *et al.*[156] on the perovskite oxide superconductor $Ba(Pb,Bi)O_3$ using ^{121}Sb MS. From the variation of quadrupole moment and isomer shift with temperature, they found an antiferromagnetic phase transformation in the sample at a temperature around 240 K. The change in the isomer shift in the sample with temperature is small which they explained through the Sb–O bonds with some hybridised orbital character. MS was used to study the $CaFeO_3$, $SrFeO_3$ and $Sr_2LaFe_3O_3$ materials at low temperature and at high pressure (up to 70 GPa) with an external magnetic field of 7 T to see the pressure–temperature magnetic phase transition.[157] It was found that the high pressure and magnetic field at low temperature switched the electronic ground state of these materials to a uniform-charge and ferromagnetic state. Mössbauer spectroscopic studies of $Sr_{2-x}Ca_xFeRO_6$ double perovskite series at low temperature showed the iron in three different metal nearest neighbour locations due to the displacement of Fe and Re ions.[158] These materials are important for novel spin electronic and magnetic sensor device applications. From the variation of isomer shift and hyperfine field values, it has been concluded that in such materials, the iron ions show an intermediate valence state (between Fe^{3+} and Fe^{2+}) with an effective electronic configuration $3d_{(5+y)}$, where y decreases from 0·3 to 0·2 as x increases. The change in quadrupole value for $x \geqslant 1{\cdot}0$ confirms the cubic to monoclinic structural transformation in these compounds. Other studies are also reported by several researchers. In fact, MS studies of pervoskite materials give us much valuable information about its structure and the change of its structure with different external parameters which permit us to understand these

rare earth compounds for present as well as future applications.

Multilayer samples

The discovery of a giant magnetoresistance (GMR) effect in 1988[159] was a breakthrough in the study of magnetic multilayers. Since then, the properties of layered magnets, at the atomic level, have attracted much attention,[160–162] particularly those of a two-phase distribution of hard and soft magnetic materials. From a theoretical point of view, detailing the magnetic behaviour of a hard magnetic substrate coated with a soft Fe layer, was first reported by Goto *et al.*[163] They showed, both theoretically and experimentally, that a critical bending field, which is proportional to w, where w is the thickness of the soft magnetic layer, characterised the onset of the exchange spring. Bowden *et al.*[164] extend this discussion to a discrete bilayer and multilayer exchange spring system. From a theoretical point of view, all these reports are important to understand the magnetic behaviour of different multilayer samples. CEMS is an important tool to study different multilayer samples. Some of those studies will be presented here.

In Fe/Cr multilayers, because of the antiferromagnetic interlayer coupling through the Cr layer, magnetisation of adjacent Fe layers is oriented antiparallel.[165] In such multilayer samples, as a result of application of an external field, the magnetisation of Fe layers is aligned parallel which causes the resistivity to decrease greatly. From the spin dependent scattering, the GMR can be understood qualitatively, but is still not very clear. So from a fundamental physics viewpoint, this system is very interesting as a research problem. Again from a technical viewpoint, the exploration of the conditions to further increase the magnetoresistance (MR) ratio is an attractive challenge. It is theoretically supposed that the MR depends on the spin-dependent scattering that occurs at the interface sites.[166] So the nature of interface layers is very important for MR. The roughness of the interface is especially important. By applying MS, the interface roughness on an atomic scale can be estimated. Another interesting point to study in multilayer samples is the magnetism in non-magnetic multilayer materials because of the coupling of the magnetic layer with the non-magnetic isotopes in the non-magnetic layer. For the study of magnetism in a non-magnetic material, hyperfine field measurement by the non-magnetic Mössbauer isotope (^{197}Au and ^{119}Sn) provides much information. Some studies on magnetic and non-magnetic multilayer materials will be discussed in the following section.

As with other Mössbauer studies in multilayer systems, the ^{57}Fe isotope plays a major role. To study the interface of the multilayer, purposefully the samples were doped with ^{57}Fe at some selective positions to study interface magnetic interactions through the hyperfine field distributions. A typical example is the Mössbauer transmission studies on polycrystalline Fe/V multilayers.[167] Because the ^{57}Fe in a ferromagnetic Fe matrix depends upon its nearest neighbour, the change in the hyperfine field at the interface sites of the ^{57}Fe atoms owing to the presence of a non-magnetic nearest neighbour environment is seen in the line broadening of the Mössbauer spectra. From that information, the compositional profile of the Fe/V interface was estimated, and the range of intermixing was derived to be within a few atomic layers. Extensive work on this system was reported by Nordström *et al.*[168] They studied the CEMS spectra of several Fe/V multilayer samples and then calculated the hyperfine field distributions. The wide distributions in the hyperfine field calculated by them were assigned as an interface of roughness of about three monolayers. They also found evidence of interlayer coupling in the hyperfine field distributions which influences the hyperfine field of the iron layer.

The influence of the interfaces on the magnetic properties of Fe/Ag and Fe/Cu multilayers was reported by Kuprin *et al.*[169] In these samples, dependence of magnetic behaviour of ultrathin Fe layers on the width of the interfaces was investigated for (Fe(110)/Ag(111)) multilayers with thin interfaces and (Fe(111)/Cu(111)) multilayers with wide interfaces. ^{57}Fe CEMS down to 50 K was employed to show that Fe layers are not uniform, to characterise interfaces, and to distinguish between static and relaxation behaviour. This allowed unambiguous interpretation of temperature dependences of susceptibility and spontaneous magnetisation upon crossover to an island structure of the Fe layers. Magnetic structures of interfaces in Fe/Cr (001) multilayers were studied by Uzdina *et al.*[170] by CEMS. Temperature dependence of magnetic properties of Fe/Ag multilayers was studied by Balogh *et al.*[171] They found the magnetic properties to be strongly influenced by Ag impurities when the thickness of Fe is less than 1·4 nm, but when it is higher than that, the Curie temperature decreases. They also studied the superparamagnetic behaviour of the system by MS. By using theoretical modelling that includes ballistic deposition with subsequent coating of some atoms on the surface, the data were explained. Mössbauer spectroscopic studies of ternary multilayers were reported by several researchers[172,173] after irradiation of the samples by heavy ions. The results indicate the phase formed at the interface after irradiation of Cr/Ni/Fe multilayers is due to electronic energy loss similar to that in the case of thermal diffusion and keV ion beam irradiation.

Much work has been reported on Re/Fe multilayers as a result of their potential magneto-optical applications. Perpendicular magnetic anisotropy and perpendicular orientation of the magnetic moments at room temperature can be modulated in Re multilayers of thickness less than 20 Å.[174] Bland[175] studied the magnetic anisotropy between in-plane and out-of-plane magnetic alignments in a variety of multilayer systems using MS to observe the (Fe) magnetic orientation. The surface anisotropy in [Fe(x Å)/Au (20 Å) (111)]$_{80}$ multilayers for $x=5$, 10 and 20 Å is $0{\cdot}9\times10^{-3}$ J m^{-2}. In the same report, the out-of-plane magnetic components were observed for $DyFe_2$, YFe_2 thin film and $DyFe_2(x\text{Å})/YFe_2(y\text{Å})$ multilayers. In transitional metal layers, the crystalline volume anisotropy is outweighed by the dipole shape anisotropy, and rare earth atoms have significantly larger single ion or crystal field anisotropy. Therefore incorporating these atoms into multilayer systems, using MS and CEMS, Thomas *et al.*[176] studied the role of crystalline volume anisotropy in the overall anisotropy of the multilayer samples.

Study of Au/M (some other element) and Sn/M multilayer samples using ^{197}Au and ^{119}Sn sources,

respectively is slightly different from the usual Mössbauer studies. In the case of the ^{197}Au Mössbauer study, as a result of the high energy of the gamma rays of the source and its very short lifetime, measurements have to be made in a laboratory with reactor facilities. Mössbauer spectroscopic studies with these isotopes were reported by Kobayashi *et al.*[177] The sample temperature was always maintained at 16 K to avoid the heating effect. As a result of the comparatively high energy of the gamma radiation from the source, the thickness of the Au layers in the multilayer samples is large in general. Different Au/Fe, Au/Co and Au/Ni samples were studied by varying the Au thickness in the samples. The observed interface hyperfine field varies in accordance with the magnitude of the bulk 3d metal magnetisation.

Another candidate in the non-magnetic Mössbauer spectroscopic study is ^{119}Sn, and this isotope is widely used in several studies in multilayer research. Emoto *et al.*[178] studied the Au/Sn/Au multilayers by inserting a Sn layer in Au. The large distribution of the hyperfine field in these multilayers suggests that the spin polarisation is spatially varying and is not uniform even in one monolayer.

In another study, Gupta *et al.*[179] reported the effect of swift heavy ion irradiation of Fe–Tb multilayers using X-ray reflectivity and CEMS measurements. They found that 80 MeV Si ion irradiation increased the interfacial roughness linearly with irradiation dose. MS measurements provide evidence of segregation of Fe and Tb atoms in the intermixed region, which may be the cause of the observed increase in the interfacial roughness. The as-deposited multilayer exhibits a large perpendicular magnetic anisotropy, which shows a monotonic decrease with irradiation dose. They concluded the observed decrease in perpendicular magnetic anisotropy to be the combined effect of the stress relaxation in the bulk of the layers and an increase in the interfacial roughness.

In summary, both transmission MS and CEMS study of a multilayered sample tell us about the physics at the junction region of multilayers through the measurement of hyperfine fields and their distributions.

Nanomaterials

Study of small dimensional materials, named nanostructured materials, has recently become an active research field in the area of solid state physics, chemistry and engineering. Evidence of this interest is provided by a large number of conferences,[180–182] reports,[183–186] books,[187–191] and a new journal (*Nanostructured Materials*) has been devoted to the subject. There are several reasons for this. One is the need to fabricate new materials, on a finer scale to continue decreasing the cost and increasing the speed of information transmission and storage. Another is that nanostructured materials display novel and often, enhanced, properties compared to traditional materials, and show possibilities for new technological applications. In the present review, possibilities of new research on nanostructured materials and findings will be discussed.

Nanostructured materials produced by primary crystallisation of amorphous alloys consist of fine crystalline grains embedded in the residual amorphous matrix.[192] Since the grain sizes are smaller than the magnetic interaction length, the local magnetocrystalline anisotropy is averaged out by the exchange interactions. This together with suitable magnetostrictive properties leads to soft magnetic behaviour superior to that of amorphous alloys, which means a higher magnetisation and greater stability of properties on further annealing.[193,194] These microcrystalline materials are in a non-equilibrium state; therefore, the properties depend not only on the composition but also on the preparation conditions. Thus, identification of various phases during a nanocrystalline process, as well as a good insight into the corresponding nucleation and growth mechanism are clues for a better understanding of the physics properties of these materials. Several studies have been carried out to examine a nanomaterial by Mössbauer spectroscopic techniques. In this section, a brief discussion of those studies will be presented.

An excellent review article was presented by Greneche[195] on the study of the structural and magnetic properties of nanostructured oxides by MS. ^{57}Fe Mössbauer spectroscopic measurements with and without application of an external magnetic field can easily distinguish the different Fe particles in the nanomaterials from their behaviour through different hyperfine structures. The Larmor precession time of the nuclear Fe magnetic moment ($t_M \sim 5 \times 10^{-8}$ s) allows superparamagnetic fluctuation of the nanoparticles within the Mössbauer window, $t_m \sim 2 \times 10^{-7} - 5 \times 10^{-10}$ s. When $t_M > t_m$, the spectrum looks like a broad line doublet, whereas magnetic splitting is observed for $t_M < t_m$.

Nanocomposite material (α-Fe–Al_2O_3) prepared by a sol–gel method was studied by Haung *et al.*[196] Small magnetic particles usually exhibit high saturation magnetisation and high coercivity. Both of these properties are required for most technological applications. For instance, it has a high signal-to-noise ratio for magnetic recording. In comparison to other magnetic metal particles, the iron particle has high magnetisation but also two weaknesses: oxidation of the particle surface and low coercivity. The studies by Haung *et al.*[196] on the reduction process showed that $FeAl_2O_4$ is present as the intermediate phase between α-Fe_2O_3 and α-Fe below 700°C. The relative weight of metallic iron increases with the reduction temperature up to 900°C. But nanocomposite α-Fe–Al_2O_3 is resistant to oxidation up to 300°C. Annealing of α-Fe_2O_3 nanoparticles and its effect on magnetic properties was reported by Vasquez-Mansilla *et al.*[197] Annealing of α-Fe_2O_3 samples prepared by the chemical route leads to recrystallisation without a change in its mean size and modifying the crystalline anisotropy energy of the nanoparticles leading to a change in the reversible–irreversible regime and in the Morin transition behaviour.

In reports of Mössbauer spectroscopic studies of nanomaterials, an important group is Finemet/Nanoperm alloys. Nanocrystalline soft magnetic materials were made by crystallising amorphous ribbons of specific families of the (Fe,B)-based alloy. This new class of materials is characterised by 10–25 nm sized grains of a (bcc) (Fe,X) phase consuming 70–80% of the total volume, homogeneously dispersed in an amorphous matrix. The Japanese have pioneered and developed these materials, especially insofar as the impact on major industrial applications is concerned. As a result of research to date, two families of alloys show the best

performance characteristics and have emerged as the leading candidates for application: Fe–Cu–Nb–B–Si (the '*Finemet*' family) and Fe–Zr–(Cu)–B–(Si) (the '*Nanoperm*' family). The Finemet family is characterised by an optimum grain size of about 15 nm, provides a saturation induction of about 1·2 T, and exhibits very good properties at high frequencies, comparable to some of the best Co-based amorphous materials. On the other hand, the grain sizes consistent with optimum performance are larger, around about 25 nm, in the Nanoperm family. The distinguishing feature of the Nanoperm family of alloys is the very low energy loss exhibited at low frequencies (60 Hz), offering the potential for application in electrical power distribution transformers. The nanocrystalline materials are obtained by crystallising precursors cast as amorphous alloy ribbons. The amorphous alloys typically crystallise in two stages: a magnetically desirable bcc-(Fe,X) phase appears first, followed by a boride phase, the presence of which is deleterious to good, soft magnetic behaviour. In the optimised chemistries, the separation between the two crystallisation events is large (~150 K), so that crystallising heat treatments may be conducted above the temperature of the first event, while safely avoiding the onset of the other.

In 1988, Yoshizawa *et al.*[198] reported that Fe–Si–B–Nb–Cu based amorphous alloys exhibit excellent soft magnetic properties on nanocrystallisation. The values of magnetic parameters such as permeability, saturation flux density, coercive force, etc. make these materials suitable for a wide range of technological applications. The role of combined addition of Cu and Nb to the alloys was found to be decisive in the nanocrystalline microstructure and thus, became a topic of extensive research. The magnetic behaviour of these materials is extremely sensitive to the nanocrystalline microstructure and thus, controlling the nanocrystalline microstructure from the amorphous precursor is the key issue in the industrial application of these materials.[199] Thus, knowledge of correlation between the structure and magnetic behaviour along with compositional dependence is required to determine the most appropriate composition for tailoring the magnetic properties. A complete and rigorous structural characterisation, during the nanocrystalline process of a particular alloy, is of fundamental importance in order to understand magnetic behaviour. It also becomes essential to understand the critical roles that surfaces and interfaces play in nanostructured materials, owing to the very high specific surface areas of nanoparticles and the large areas of interfaces in the nano-assembled forms. In the following section, a brief description is presented of the research status of this system using MS.

A systematic Mössbauer spectroscopic study of Fe–Cu–B–Nb–Si Finemet alloys was reported after heat treatment and under application of a radio frequency (rf) magnetic field.[200–204] In all of those studies, the basic aim was to see the formation of nanostructured phases in the as received Finemet materials after different heat treatments and under the application of an external magnetic field. Nanostructured magnetic materials consisting of nanophase particles in an amorphous matrix exhibit soft magnetic properties. Both the nanocrystalline and the amorphous grain boundary phases are ferromagnetic at room temperature, and the excellent soft magnetic properties of this composite system occur as a result of averaging over two phases. Thus, to understand the soft magnetic properties of nanocrystalline alloys, it is important to study the magnetic behaviour of both the amorphous matrix and nanocrystalline grains, and the interactions between them. Because of the small crystalline size, the nanocrystalline particles are single domain particles and may exhibit interesting magnetic properties associated with single domain particles. Hesse and colleagues[200–204] studied the phase analysis of the Mössbauer spectrum of the annealed Finemet alloys to observe the crystalline kinetics in the sample with annealing. The hyperfine field distributions of different annealed samples provided information about the amorphous as well as the crystalline phases in the alloy. They observed the interaction between the amorphous and nanocrystalline particles and the growth of the magnetic order from small particles to large clusters. It is known that a distribution of magnetic moment in the amorphous matrix in addition to the exchange interaction gives the temperature dependent fluctuation parameter. They studied the nearest neighbour effect of Cu and Nb atoms on the Fe magnetic moment from the nature of the hyperfine field distribution. With the growth of the crystalline phase, the grain boundaries of amorphous phases decrease, and for a sufficiently thin grain boundary layer, the dimensionality can be taken as two, instead of three. In their study, they observed the low dimensional magnetic behaviour in the samples. They also measured the blocking temperature of the nano phases in each stage of annealing.

They obtained information about the magnetic anisotropy and magnetostriction by applying the radio frequency magnetic field on the sample during MS. The radio frequency magnetic field causes two types of effects on the Mössbauer spectra of the nanostructured materials: (i) the appearance of side bands and (ii) its collapse. The side bands are due to force vibrations on the absorber matrix that modulates the Mössbauer resonant absorption cross-section energy with the radio frequency field. These vibrations induce magnetostriction that causes the side bands in the spectra. When magnetostriction vanishes, the side bands disappear. The radio frequency collapse is caused by the radio frequency magnetic field itself. In soft magnetic materials, the magnetisation direction changes depending upon the frequencies of the applied magnetic field. Because the hyperfine magnetic field vector is strongly coupled with the magnetic moment of the atom, it also starts to change direction in response to the applied radio frequency magnetic field. When the frequency of the radio frequency magnetic field is higher than the Larmor frequency and the radio frequency field amplitude is high enough to overcome local anisotropies in the sample, then the magnetic hyperfine field at the site of the Fe nucleus will be averaged to zero. This causes complete collapse of the lines in the Mössbauer spectrum. As a result of this collapse, a quadrupole doublet or a single line will appear in the spectrum. From the collapse, they estimated the magnetic anisotropy in the sample. The radio frequency collapsed central doublet accompanied by the radio frequency side band, indicates that the sample under study is magnetostrictive. With annealing, new crystalline phases

appear in the samples and hence, a part of the magnetic moment would follow the external radio frequency magnetic field and hence, the collapse owing to radio frequency would be different. From this behaviour, the softness of the materials can be estimated. Some reports by Chattopadhyay and colleagues[205–207] give important results on Finemet alloy research. They prepared $Fe_{73·5}Cu_1Nb_3Si_{13·5}B_9$ Finemet alloy by a melt-spin technique. To see the change in microstructure, the as received Finemet alloys were then annealed at different temperatures for 1 h and studied by several techniques. These studies were made to detect different nanocrystalline phases in an amorphous matrix. Next, the magnetisation measurements of the annealed samples were carried out and the data analysed using a spin wave model to get an idea about the mean squared value of the range of exchange interactions in the nanocrystalline materials. It was found that these values are much smaller than those observed in crystalline ferromagnets.[205] In another report,[206] the samples ($Fe_{73·5}Cu_1Mo_3Si_{13·5-x}Al_xB_9$, $x=0$, 1, 3 and 5) were prepared by mechanical ball milling, and several magnetic measurements were performed to see the variation of magnetisation (M_s) and coercivity (M_c) as a function of Al content (x). They found that M_s and M_c both decrease with the content of Al in the sample. In the study by Raja *et al.*,[207] the Finemet alloys were prepared using a vibrating ball mill method under an argon atmosphere. The measurements of the Finemet alloys with the same composition prepared by melt-spin were then compared. They found that though composition-wise both alloys are the same, their behaviour after annealing differs. According to their study, the soft magnetic properties of the samples made by mechanical ball milling are much inferior to that produced by melt-spin. The critical grain size of the nanocrystalline phase in the melt-spun samples was found to be 10 nm. Room temperature Mössbauer spectrometry, magnetostriction and magnetic measurements of two-phase nanocrystalline $Fe_{76·5}Cu_1Si_{13·5}B_9$ alloy have been studied by Szumiata *et al.*[208] to observe the structural and magnetic properties. The composition of both the crystalline grains and the amorphous remainder has been derived for samples subjected to various heat treatments. The observed type of evolution of the effective magnetostriction constant basically points to the strong relaxation process of internal stresses in the course of crystallisation. Zorkovska *et al.*[209] studied the effect when Fe was substituted by Al up to 7 at.-% in Fe–Cu–Nb–Si–B Finemet alloys. All samples annealed at 550°C are nanocrystalline, with more or less ordered α-Fe(Si,Al) grains; the DO_3 like ordering was the most dominant in samples with 5 and 7 at.-%Al. In the as-quenched state, Al linearly decreased the magnetisation, but up to 3 at.-%, the Al enhanced the Curie temperature of the alloy. The Curie temperature of the crystalline phase and the magnetisation in annealed samples abruptly decreased, when there was more than 5 at.-% Al in the alloy. The magnetic anisotropy induced in the ribbons of the $Fe_{73·5}Cu_1Nb_3Si_{13·5}B_9$ alloy in the course of stress annealing combined with the nanocrystallising anisotropy was investigated by Dmitrieva *et al.*[210] Different nanocrystalline phases formed during the above treatments were studied by MS. Analysis of the Mössbauer results showed that the content of the Fe–Si phases depends neither on the exposure time nor on the value of the induced magnetic anisotropy constant. The $Fe_{66}Cr_8CuNb_3Si_{13}B_9$ nanocrystalline alloy with a low fraction of crystalline phase (~15%) has been studied by Mössbauer spectrometry over a wide temperature range, ~4·2–800 K.[211] The temperature dependences of the hyperfine parameters were measured in ordered Fe–Si alloys. It was found that the thermal evolution of the hyperfine field of the crystalline phase exhibits a kink at a temperature close to the Curie point of the amorphous matrix. This effect was explained in terms of suppression of the interphase exchange interactions at the ferromagnetic–paramagnetic phase transition of the amorphous matrix and superparamagnetic fluctuations of the magnetisation in single-domain grains.

Miglierini *et al.*[212] reported the CEMS study of Nanoperm nanocrystalline alloys with composition FeMXB (M=Mo, Nb, Ti; X=Cu, Au). Their results show the significant alteration of the short-range order before crystallisation. This is due to the rearrangement of the atoms and possibly to diffusion. Magnetic hyperfine fields obtained by transmission and CEMS show differences between the short-range order of bulk and surface regions. They also studied the variation of the spectrum and corresponding hyperfine field distribution of $Fe_{80}Mo_7CuB_{12}$ and $Fe_{80}Mo_7AuB_{12}$ Nanoperm alloys annealed at different temperatures for 1 h.

Superparamagnetic behaviour in the nanoparticles is commonly studied by MS. $CoFe_2O_4$ magnetic nanoparticles were prepared and characterised by Kim *et al.*[213] The field-dependent and temperature-dependent magnetisation measurements and Mössbauer spectra measured at various temperatures showed that the cobalt ferrite nanoparticles prepared at a temperature lower than 40°C are entirely superparamagnetic at room temperature with a blocking temperature (T_B) of around 80 K and those, prepared at temperatures higher than 60°C, consisted of superparamagnetic and ferromagnetic components with T_B higher than 400 K. For the latter, the fraction of superparamagnetic components decreased as the precipitation temperature increased with increased particle size. Nanostructured materials prepared by Fe ion implantation into an MgO crystal were reported by Hayashi *et al.*[214] CEMS was used to identify physical states of the implanted iron. CEMS shows that the transition from superparamagnetism to ferromagnetism in the precipitated iron nano-clusters critically depends on the implantation dose and post-annealing. With increasing dose over $2·0\times10^{17}$ ions cm^{-2}, a ferromagnetic component appears in the Fe implanted MgO samples. Nanocrystalline Fe–O alloys, prepared by milling and then annealing of Fe_2O_3 and α-Fe were studied by MS.[215] After milling, these two components produce FeO and α-Fe nanoparticles with the presence of a solid solution of oxygen in iron. More milling time and annealing produces amorphous $Fe_3O_4+\alpha$-Fe with average crystal size of 20 nm. Mössbauer spectroscopic studies of other nanostructured materials have been reported by several groups.[216–218] In nanocrystalline Fe–M–B (M=Zr, Pr, Cr, etc.) alloys, the α-Fe grains were embedded in the residual amorphous matrix showing excellent soft magnetic behaviour.[216,217] Fe–B–Si–Al nanoparticles prepared by mechanical ball milling show the presence of superparamagnetic α-Fe particles in the matrix.[218] The relative amount of the

superparamagnetic phase increases with increasing milling time, and it appears as a single central line in the spectrum. Another study of superparamagnetic nanophase formation was reported by Wang and Li.[219] The $Ni_{1-x}Zn_xFe_2O_3$ nanoparticles (Fe–Zn ferrite) show superparamagnetic behaviour at room temperature for x values from 0 to 1. The same compounds show magnetic phases at 77 K. This has been explained as the magnetic ordering in the nanophase particles at low temperatures. It is well known that the magnetic properties of composite materials depend upon the chemical composition of crystalline and amorphous phases and can be controlled by adding small amounts of other elements. In transition metal metalloid metallic glasses, it has been found that addition of a small amount of Nb helps in forming small grain boundaries and results in the formation of nanocrystalline phases in the residual matrix. The effects of the addition of Nb to $Co_{21}Fe_{64-x}Nb_xB_{15}$ (x=3, 5 and 7) alloys were reported by Kane *et al.*[220] All the as prepared samples are amorphous and, after annealing for 1 h at different temperatures, all the samples show the formation of a nanocrystalline phase. The increased Nb causes higher disorder in the atomic structure as well as in the spin texture of as-quenched alloys. According to their study, the first stage of crystallisation leads to the formation of the Fe_3Co phase embedded in a residual amorphous matrix. In the second stage of crystallisation, the $(FeCo)_2B$ phase is formed. The magnetic properties of the nanocrystalline $Fe_{74}Cu_1Nb_3Si_{12}B_{10}$ alloy annealed at 573, 623, 673 or 700 K for 1 h and then at 823 K (crystallisation temperature) for 0·5 h are investigated by MS to examine the softness of the materials.[221] ^{57}Fe Mössbauer and magnetisation studies were performed on $Fe_{25}Se_{75}$ alloys, produced by mechanical alloying. The MS results show a doublet of a paramagnetic $FeSe_2$ alloy in the spectra of samples milled from 3 to 52 h. For milling times longer than 52 h, the spectra showed formation of a high temperature Fe_7Se_8 iron selenide, which is a ferrimagnetic phase, together with the FeSe paramagnetic compound.[222]

Several other reports have discussed the science and technology of nanomaterials using different techniques including MS. Here, a brief contribution of MS in this field has been discussed.

Semiconductors

Progress in semiconductor technology is accompanied by progress in the knowledge and control of intrinsic and extrinsic defects in these materials, i.e. of vacancies or self-interstitials and dopant or impurity atoms, respectively, because defects improve or deteriorate the quality of a semiconductor depending on their electrical properties and respective environment. In this area of research of semiconductor materials, radiation physics has an important role, and MS also has an important role. The combination of magnetic materials with underlying III–V electronic device structures leads to new potential applications involving integrated information processing and non-volatile storage.[223,224] The ferromagnetic metal semiconductor system, as an example, iron–gallium arsenide (Fe/GaAs), which is now very popular, can be prepared by epitaxial growth of iron films on GaAs substrates. In addition, ion beam sputtering and magnetron sputtering techniques also showed the ability to grow high quality ferromagnetic thin films on a GaAs semiconductor substrate. In this context, it is important to mention the work by Monteverde *et al.*[225] They studied the solid state reaction between monocrystalline AlGaAs(100) and polycrystalline Fe films, having thickness in the range of 50–100 nm using X-ray diffraction, CEMS and TEM (transmission electron microscopy). The Fe films were deposited on ion-etched semiconductor substrates using an ion-beam-sputtering technique. It has been found that, in the as-deposited state, the thickness of the interfacial zone never exceeds 1·5 nm, a value comparable to that obtained for Fe films deposited by molecular beam epitaxy. The interface reaction of the Fe films was also studied after annealing in vacuum at 400°C for 1 h. The orientation of the magnetisation and the grain size of the deposited metallic layers were studied by CEMS and transmission MS for as-deposited, as well as annealed films. The results show the existence of Fe_2As grains that formed owing to interdiffusion after annealing. These grains were observed in the AlGaAs substrate, exactly under the Fe/AlGaAs interface, having a triangular shape. They also analysed the orientation relationship between the Fe_2As grains and the substrate.

A novel approach to create substitutional and interstitial ^{57}Fe Mössbauer sites in silicon at elevated temperatures is reported by Gunnlaugsson *et al.*[226] In this method, radioactive $^{57}Mn^+$ ($T_{1/2}$=1·5 min) ions have been implanted with 60 keV energy into silicon crystals at 400–800 K. As a result of annealing of the radiation damage during the ^{57}Mn lifetime, the Mn atoms are found on substitutional lattice sites. In the subsequent decay of ^{57}Mn to the Mössbauer state of ^{57}Fe, an average recoil energy of 40 eV is imparted on the daughter ^{57}Fe atom. This leads to a relocation of the majority of ^{57}Fe atoms into interstitial sites, and the remainder stay on substitutional sites. The Mössbauer spectra in their studies show that at 451 K (p++-Si) or 475 K (n+-Si), there is no line broadening, and the spectra are dominated by two lines assigned to substitutional Fe (Fe_S) and interstitial Fe (Fe_i) at the tetrahedral site. As the temperature is increased to 567 K or 669 K, they observed a clear broadening of the interstitial lines in both crystals. At still higher temperatures, the corresponding lines disappeared from the spectra which were dominated by two lines assigned to the formation of Fe-vacancy pairs. They have given the relationship between the line width of the interstitial line in the Mössbauer spectra and the macroscopic diffusion coefficient as $\Gamma=\Gamma_o+(12\hbar cD/E_o l^2)$, where Γ_o is the experimental line width measured in units of the Doppler velocity, $\hbar$ is Planck's constant, c the velocity of light, E_0 the energy of the Mössbauer γ-radiation (14·4 keV) and l=0·235 nm, the elementary jump length, assuming a direct interstitial diffusion mechanism. They found that the difference $\Delta\Gamma=(\Gamma-\Gamma_o)$ is directly proportional to the diffusion coefficient. Their experimental data show that the broadening in p^{++}-Si is consistently larger than in the n^+-Si, i.e. the Fe_i^+ diffusivity is considerably larger than the Fe_i° in the investigated temperature range. These MS data have substantially contributed to a clarification of controversial experimental results reported for the charge state dependence of the diffusivity of interstitial Fe in Si.

Mikhlin *et al.*[227] studied the monoclinic and hexagonal pyrrhotites leached in 1 mol L^{-1} HCl and exposed to air at 100% and ~10% relative humidity for up to 5 months and then studied using MS and other techniques. The amorphous, nonequilibrium, iron-depleted layer (NL) produced by leaching amounted to half of the residual mass and was composed of predominantly low spin ferrous iron and polysulphide anions. Neither alteration of the underlying pyrrhotite nor new iron sulphide phases (pyrite, pyrrhotite, etc.) crystallised from the amorphous NL were found. The NL decomposition was faster in a wet rather than dry environment, and the oxidation of the NL was much more rapid than that of starting pyrrhotites. The intensity and quadruple split of the Mössbauer signal from the product (an isomer shift of 0·36 mm s^{-1}) were found to increase with the aging, indicating that the NL structure becomes more rigid, and the singlet Fe(II) gradually converts to Fe(III). Roy *et al.*[228] studied Mössbauer spectra of $Fe_{2-y}Zn_yMoO_4$ spinel ferrites in their paramagnetic state. Paramagnetic Mössbauer spectra of all samples showed broad absorption peaks owing to the presence of Fe^{2+} and Fe^{3+} ions on both sites (A and B) of the spinel lattice. From the Mössbauer parameters, similar isomer shift and quadrupole splitting values on different iron sites have been found. These sites are $Fe_A{}^{2+}$, $Fe_A{}^{3+}$, $Fe_B{}^{3+}$ and $Fe_B{}^{2\cdot5+}$, $Fe_B{}^{2\cdot5+}$ representing the presence of the Fe^{2+} and Fe^{3+} ions on the B-sites, which take part in charge hopping. The results of electrical resistivity and magnetic measurements support charge hopping between Fe^{2+} and Fe^{3+} ions on B-sites. Ehm *et al.*[229] studied the crystal structure of $Fe_{0\cdot47}NbS_2$ using X-ray powder diffraction. $Fe_{0\cdot47}NbS_2$ crystallises in the space group $P6_{322}$. The niobium atoms are coordinated trigonal prismatically by sulphur atoms. Sandwiches of NbS_2 are stacked onto each other along the *c* direction, separated by van der Waals gaps. The iron atoms are located inside the van der Waals gaps on three symmetrically nonequivalent positions. The distribution over these three positions is not uniform. The valence state of the iron atoms was investigated by MS. This shows that the iron is predominantly ferric and high spin, but a minor part is low spin. Becze-Deák *et al.*[230] studied $Fe_{0\cdot01}Zn_{0\cdot99}Se$ by MS. A doublet in the Mössbauer spectrum of $^{57}Fe_{0\cdot01}Zn_{0\cdot99}Se$ below room temperature is assigned by them to Fe^{2+} impurity pairs. Low temperature Mössbauer emission experiments, ZnSe:^{57}Co polycrystal and powder sources exhibit the nucleogenic Fe^{1+} valence state below 45 K as an after-effect of the electron-capture decay of ^{57}Co. Above 8 K, the proportion of the nucleogenic Fe^{1+} decreases owing to thermally activated $Fe^{1+}\rightarrow Fe^{2+}$ relaxation. The activation energy is estimated to be 0·004 eV. Whereas nucleogenic Fe^{1+} is absent in ZnSe:^{57}Co single crystal spectra, increasing proportions are detected in samples with an enhanced specific surface. The formation model of the nucleogenic Fe^{1+} is extended to other zinc chalcogenides, and a tentative model is developed which shows the role of the surface electric field in limiting formation of nucleogenic Fe^{1+} in well crystallised source samples. Kim *et al.*[231] studied perovskite $La_{0\cdot67}Ca_{0\cdot33}Mn_{0\cdot97}{}^{57}Fe_{0\cdot03}O_3$ prepared by a sol–gel method. X-ray diffraction, Rutherford back-scattering spectroscopy, Mössbauer spectroscopy and vibrating sample magnetometer techniques were used to investigate the magnetoresistance and magnetic properties of the sample. Using X-ray diffraction, they found crystalline $La_{0\cdot67}Ca_{0\cdot33}Mn_{0\cdot97}{}^{57}Fe_{0\cdot03}O_3$ as a cubic perovskite structure with a lattice parameter 3·859 Å. Mössbauer spectra of $La_{0\cdot67}Ca_{0\cdot33}Mn_{0\cdot97}{}^{57}Fe_{0\cdot03}O_3$ have been taken at various temperatures ranging from 4·2 K to room temperature. Analysis of ^{57}Fe Mössbauer spectrum data has considered nearest-neighbour interactions and anisotropic hyperfine field fluctuation. Analysis of ^{57}Fe Mössbauer data in terms of the local configurations of Mn atoms has permitted the influence of the magnetic hyperfine interaction to be monitored. The saturation magnetisation of $La_{0\cdot67}Ca_{0\cdot33}Mn_{0\cdot97}57Fe_{0\cdot03}O_3$ is found to be 68 emu g^{-1} at 77 K. The Curie temperature, T_C, is determined to be 210 K. The temperature dependence of the resistance under zero and 10 kOe applied fields shows that a semiconductor–metal transition, T_{SC-M}, occurs at 200 K. The relative magnetoresistance, MR was found to be about 45%. Takeda *et al.*[232] synthesised the solid solution $Ca_{1-x}Sr_xFeO_3$ under high oxygen pressure. They investigated its structural and electronic properties by MS and other techniques. The system was found to be divided into an orthorhombic region for $0\cdot05 \leqslant x \leqslant 50\cdot5$, a cubic region for $0\cdot85 \leqslant x \leqslant 51\cdot0$, and a mixed region at $x \approx 0\cdot6$. In the orthorhombic region, they found a well defined metal–semiconductor transition region wherein the transition temperature decreased with increasing x from 0 to 0·4. Mössbauer measurements on the low temperature (LT) phase of $Ca_{0\cdot8}Sr_{0\cdot2}FeO_3$ confirmed the occurrence of charge disproportionation. MS with the help of other techniques finally determined that the two crystallographically different Fe–O octahedral bonds created in the low temperature phase were both almost regular in shape but decrease with increasing temperature.

This discussion gives a brief idea about the application and important role of MS in semiconductor research.

Superconductors

From the beginning of the science of superconductivity, MS has been important to understand its physics. It is mostly applied to study the magnetic phase transition in magnetic superconductors. In non-magnetic superconductors, it is very useful to study the structural and charge distributions of the compounds. In the case of magnetic superconductors, iron is part of the composition. But in the non-magnetic superconductors, to study the structure and charge distribution, it has to be doped externally by replacing one of the constituents to a certain degree without disrupting the lattice structure. Therefore, in the latter case, the iron atoms are present in the superconductor compounds as defects. Rare earth MS also plays an important role in superconductor science. In the case of magnetic superconductors, an important focus of study is the relation of the temperature in superconductivity and antiferromagnetic ordering in the superconductors. Several review articles have been published on the magnetic properties of high temperature superconductors (HTCS) and MS.[233–235] High T_C superconductors have a layered structure with CuO_2 planes responsible for superconductivity. Felner and Nowik[235] reported that whenever a sufficient amount of cations are present outside these CuO_2 planes

to make superconductivity disappear, a static long-range antiferromagnetism is induced in these planes. Moreover, substitution of Cu in the sites responsible for superconductivity even by non-magnetic ions, suppresses both superconductivity and magnetic order. On the basis of these two facts, they concluded that, in the studied HTSC systems, superconductivity and antiferromagnetism are closely related, and they compete with each other. Also they rarely can coexist. They found that in all cases, the Neel temperature for the antiferromagnetic state of the superconducting systems is directly proportional to T_C, the superconducting transition temperature in the same sample. Among the other MS studies of superconductors, the rare earth MS is very common. There has been considerable interest in $RuSr_2GdCu_2O_8$ superconductor since the discovery of coexistence of a superconducting phase with magnetic ordering in this compound.[236] Magnetisation and neutron scattering experiments indicate that there are two distinct types of magnetic ordering, one associated with the rare earth sublattice and the other with the Ru sublattice.[237] Kruk *et al.*[238] studied the magnetic behaviour of the above sample by ^{155}Gd and ^{99}Ru MS. From the measurements of H_{eff} and the relation of H_{eff} to the Gd magnetic moment with respect to the crystallographic axis, they studied the magnetic structure of the compound. The magnetic ordering is found to have a two-dimensional character owing to the layered structure of the unit cell. On the other hand, the ^{99}Ru MS confirms that all the Ru magnetic moments are ordered in the superconducting state. The magnetic hyperfine field and the isomer shift of Ru also give information about its valence state. For these compounds with an oxygen ligand, the isomer shift increases as the oxidation state of Ru increases. $REBa_2Cu_3O_7$ (where RE is Eu, Y), the so-called 1-2-3 compounds, are important high T_C oxide superconductors. In this series of superconductors, direct information on the Cu ion site at the atomic level is important to understand the superconductivity mechanism, and MS is an excellent source for that information.[239] Gao *et al.*[240] studied the chemical bond properties and MS in $REBa_2Cu_3O_7$ compounds. In their study, Mössbauer isomer shifts of ^{57}Fe doped in $REBa_2Cu_3O_7$ and ^{119}Sn doped in $REBa_2Cu_3O_7$ were calculated by using the chemical environmental factor. They found that the chemical bond parameters play the main role in explaining the Mössbauer isomer shifts in high T_C superconductors. Escamilla *et al.*[241] studied the effects of iron substitution on the superconducting and structural properties of $(Y_{0\cdot8}Pr_{0\cdot2})Ba_2Cu_{4-x}Fe_xO_8$. They found that, with increasing iron concentration, the rate at which T_C diminishes with x is the same as for the $YBa_2Cu_{4-x}Fe_xO_8$ system, but faster than in the $YBa_2Cu_{3-x}FexO_{7-\delta}$ system. The Mössbauer spectra of the different samples (in addition to X-ray diffraction) indicate that the iron atoms occupy the Cu(1) sites of the double $(CuO)_2$ chains in fivefold coordination. The bond length decreases as x is increased in the case of the Cu(1)–O(4) bond, but the Cu(2)–O(4) bond increases. They conclude these changes may be due to the presence of O(5) atoms, which in turn affect the charge-transfer mechanism between the $(CuO)_2$ double chains and the CuO_2 planes where superconductivity takes place. They also concluded it could be responsible for the rate of decrease in T_C. Li *et al.*[242] studied the effect of Fe-doping on superconductivity, transport and microstructure by measurement of Hall coefficients, MS and the calculation of the point-charge-effective-valence model (PCEV model) in Fe-doped $Tl_{0\cdot5}Pb_{0\cdot2}(Sr_{0\cdot8}Ba_{0\cdot2})_2Ca_2(Cu_{1-x}Fe_x)_3O_y$ (Tl-1223) superconductors. In the concentration range of Fe (x= 0–0·05), both zero-resistance temperature (T_{CO}) and carrier concentration (n_H) decrease linearly with increasing Fe dopant. Mössbauer measurements are performed to investigate the microstructure of Fe–O defects. In addition, they investigated the atomic position of the Fe dopant and the electric field gradient (EFG) on Fe sites by using a PCEV model. Measurements of quadrupole splitting and results of model calculation confirmed a small shift of the Fe ion relative to the original centre of the CuO chain, and in Fe–O defect clusters, Fe dopants can lead to excess oxygen atoms entering the lattice. To explain the decrease in T_C and carrier concentration, they suggested that microstructural distortion and excess oxygen defects induced by Fe doping encourage localisation of the cruising carrier on CuO planes as a cause. Similar types of studies were made by Kuzmann *et al.*[243] on T1-based superconductors on introduction of the Mössbauer nuclei ^{57}Fe, ^{119}Sn and ^{151}Eu into the sample. The doped Tl-based superconductors were then characterised by measuring the critical temperatures, critical currents, microstructure and composition of the sample in superconducting and secondary phases. The samples were then analysed by ^{57}Fe and ^{151}Eu MS. They found that the incorporation of Eu into the superconducting phase favoured formation of the Tl-1212 phase. The isomer shift and the electric field gradient derived from the ^{151}Eu spectra were consistent with Eu^{3+} at the Ca site. The ^{57}Fe Mössbauer spectra indicated two different micro-environments of Fe^{3+}, and they were assigned to Fe^{3+} substituting Cu between the two Ca layers and between the Ca and Ba–Sr–O layers. Li *et al.*[244] studied the effects of Sn-doping on the local microstructure in $La_{2-2x}Sr_{2x}Cu_{1-x}Sn_xO_4$ (x= 0·075,0·090, 0·110) superconductors by MS. Their results show that the Sn ions in the 4+ valence state dominantly occupy Cu sites rather than the La(Sr) site and increase effective oxygen content. From the point of view of the effective oxygen content (or excess oxygen), the role of Sn dopant on the carrier concentration was discussed in their report. They also attempted to explain the higher value of transition temperature T_C in (Sr,Sn)-doped $La_{2-2x}Sr_{2x}Cu_{1-x}Sn_xO_4$ samples based on the amphoteric effect of Sn-doping on the concentration. Using ^{57}Fe and ^{119}Sn MS and other techniques, Kuzmann *et al.*[245] studied the Fe and Sn doping of a Hg-containing 1223 high temperature superconductor. Fe was incorporated into the superconducting lattice and decreases the T_C values from 112 K for the undoped to 105 K for the Fe-doped phase, whereas Sn preferred secondary phases. They found two high spin Fe^{3+} microenvironments in the sample attributed to Fe^{3+} ions occupying the square pyramidal and the square planar Cu sites in the superconducting phase. Korostin *et al.*[246] reported a ^{57}Fe Mössbauer study of Bi-2212 superconductors from 30 to 295 K in order to investigate vibrations of the Cu-sites in the CuO sub-lattice planes. They measured the recoilless fractions for ^{57}Fe occupying Cu sites within the bulk of grains and at the

grain surfaces of the Bi-2212 sample. Their results showed that the dependence of recoilless fraction on temperature has no anomalies in vibrations of the Cu-sites in the CuO_2 planes. Anomalous changes of their mean-square displacement have not been observed near the transition temperature to the superconducting state.

The above discussion gives a brief idea of the main use of MS to study superconductors, mainly to study the local environment of the Mössbauer nucleus in the sample, their vibration modes in the chain or in a particular plane in the crystal structure.

Minerals

It is well known that ^{57}Fe MS is a very sensitive and useful technique available for identifying and determining the relative amounts of different iron compounds present in complex materials. The first applications of the Mössbauer effect involved the investigation of minerals in 1960 by Solomon.[247] Since then, more than 2500 publications have addressed the investigation of minerals. A review of publication statistics for MS has been reported by Stevens *et al.*[248] In particular, ^{57}Fe MS has been applied to the analysis of iron bearing minerals both in their as found state and after thermal and chemical beneficiation. One useful application of such studies involves the monitoring of the kinetics of ore dressing of minerals so that the degree and nature of conversion from one iron ore compound to another can be ascertained at each stage of ore dressing. Several studies have been reported on soils, samples of deep-sea sediments, astrological samples from the moon and Mars, coal, and different minerals containing iron by transmission and back-scattered MS. In the present section, a brief description of the application of MS in all of these applications will be described.

MS is useful for regular monitoring of the iron compounds during ore processing in several ferrous and non-ferrous industries and can be found in the proceedings of international symposiums on 'Industrial applications of the Mössbauer effect'. In an earlier study,[249] the kinetics of the roasting process of pyrite minerals was observed by ^{57}Fe MS and X-ray diffraction. These studies provided a valuable understanding of the kinetics of roasting and indicated the optimum time period for efficient transformation of pyrite into the magnetic oxides α-Fe_2O_3 and γ-Fe_2O_3. Bandyopadhyay *et al.*[250] studied the roasting process of chalcopyrite minerals by MS. Among the copper-bearing minerals, chalcopyrite is one of the most abundant forms containing copper, iron and sulphur in almost equal parts. Extraction of copper from chalcopyrite involves two stages: (i) smelting and (ii) refining. After the first operation (i.e. smelting), crude copper is separated, whereas the second operation involves refining the copper to a pure metal (>99·9%Cu). The smelting operation is then followed by flotation and partial oxidation. Partial oxidation carries the roasting mineral ore within a strictly controlled temperature range and limited flow of air to eliminate some of the sulphur. In the stages subsequent to partial oxidation, the roasted material is heated in a reverberatory furnace at much higher (1200°C) temperatures.[251] At this stage, ^{57}Fe MS is a very useful technique for monitoring the ore dressing of a chalcopyrite mineral, so that the degree and nature of conversion from one iron compound to another can be ascertained at each stage. It also helps to monitor the air and water contamination during partial oxidation of the ore. A recent review on the treatment of chalcopyrite was reported by Prasad and Pandey.[252]

Mössbauer spectra of chalcopyrite samples measured at room temperature, roasted in a controlled air steam, at 500 and 650°C for different time intervals are shown in Fig. 14. The Mössbauer spectrum of an as received sample (t=0·0 min) decomposed into one sextet and two doublets. The sextet is assigned to chalcopyrite and one doublet to pyrite. Another doublet is assigned to the paramagnetic nature of chalcopyrite following the work of Lipka *et al.*[253] On the basis of the observed phases in the spectra, Bandyopadhyay *et al.*[250] suggested a possible mechanism to explain the formation of different iron compounds at 500°C and 650°C by proposing a reaction scheme as follows

$$CuFeS_2 \rightarrow FeSO_4 \rightarrow \alpha\text{-}Fe_2O_3 \text{ and } FeSO_4 + O_2 \rightarrow Fe_2SO_4$$

It may be pointed out that Razouk[254] has proposed the following mechanism for the oxidation of chalcopyrite

$$2CuFeS_2 + 6O_2 \rightarrow Cu_2S + Fe_2(SO_4)_3; Cu_2S + \frac{5}{2}O_2 \rightarrow CuO + CuSO_4$$

and then

$$3CuO + Fe_2(SO_4)_3 \rightarrow 3CuSO_4 + Fe_2O_3$$

Both reactions proposed by Bandyopadhyay *et al.*[250] and Razouk[254] are of the same type. At 650°C, the reaction scheme proposed by Bandyopadhyay *et al.*[250] is different from that at 500°C as follows

Stage I $CuFeS_2 \rightarrow FeS_2$ (at 620°C and t=1–2·5 min)
Stage II $FeS_2 \rightarrow$(intermediate steps)$\rightarrow FeSO_4 + \alpha$-$Fe_2O_3$
Stage III $FeSO_4 \rightarrow \alpha$-$Fe_2O_3$

It is known[249] that the precise nature of sulphide formed is determined by the time period for which the roasting is carried out, and that FeS and Fe_2O_3 can be thermally oxidised into α-Fe_2O_3.[255] On the basis of the other reaction schemes,[255] the scheme (stages I–III above) suggested by Bandyopadhyay *et al.*[250] is tenable, and explains the Mössbauer spectroscopic measurements of the transformation of roasting kinetics of chalcopyrite at different temperatures. In this context, it is important to mention the roasting kinetics study of pyrite by MS by Shyu *et al.*[256] *In situ*, ^{57}Fe MS has been used to study the decomposition of pyrite of various sizes and pyrite in coal in an oxygen atmosphere at different temperatures between 25 and 400°C. Their study showed that the oxidation of pyrite in coal occurs mainly in three steps as follows

(i) Pyrite to iron sulphate between 25°C and 310°C
(ii) Iron sulphate to γ-Fe_2O_3 between 310°C and 325°C and
(iii) γ-Fe_2O_3 to α-Fe_2O_3 between 325°C and 400°C.

From the conversion of pyrite in the coal and in mineral pyrite, it has been concluded that the oxidation of the two types of pyrite is entirely different, and the oxidation of pyrite in coal is highly influenced by the coal constituents.

As a regular monitoring tool, Klingelhöfer *et al.*[257] obtained quantitative details of the reaction products at different stages of the processing or reduction of iron ore

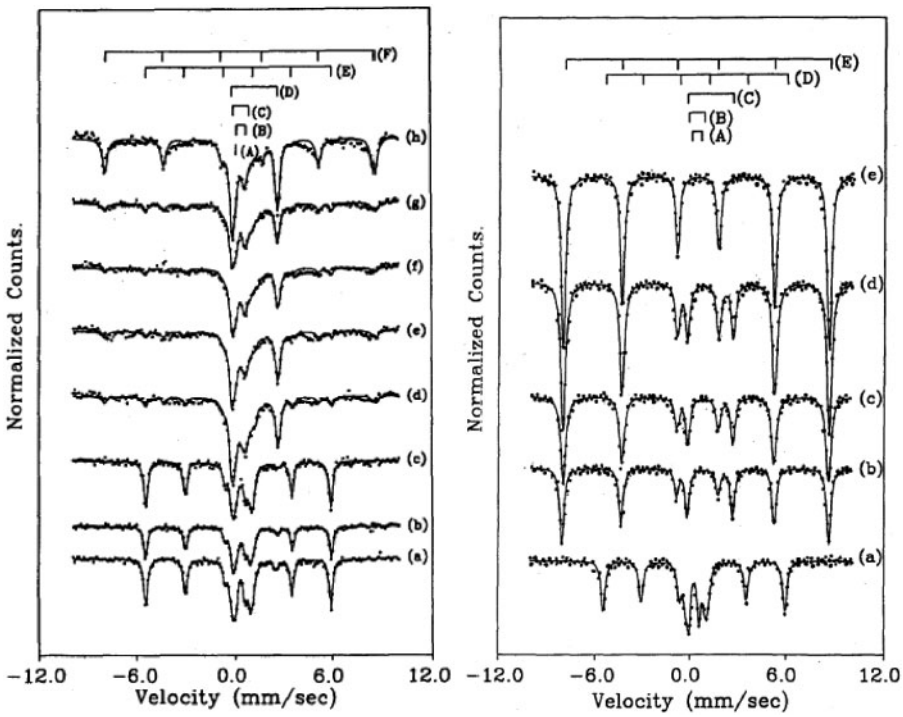

14 Left: Room temperature Mössbauer spectra of chalcopyrite roasted at 500°C for different time intervals, *t*=(a) 1·0, (b) 2·0, (c) 3·0, (d) 5·0, (e) 10·0, (f) 15·0, (g) 20·0 and (h) 40·0 min; lines at top indicate characteristic peak positions in Mössbauer spectra of (A) $Fe_2(SO_4)_3$, (B) pyrite, (C) see text, (D) $FeSO_4$, (E) chalcopyrite and (F) α-Fe_2O_3; Right: Room temperature Mössbauer spectra of chalcopyrite roasted at 650°C for different time intervals, *t*=(a) 1·0, (b) 2·5, (c) 3·0, (d) 5·0, (e) 10·0 min; lines at top indicate characteristic peak positions in Mössbauer spectra of (A) pyrite, (B) see text, (C) $FeSO_4$, (D) chalcopyrite and (E) α-Fe_2O_3 (reprinted from Ref. 215)

collected from different industries. They showed an accuracy of ± 2 wt-% which was in good agreement with results obtained from chemical analysis. As an extension of this method of examining reaction products, they have also demonstrated the applicability of *in situ* MS during operation of a pilot plant, as an important means of obtaining optimal control over the operating cycle of the reactor. The use of this portable Mössbauer spectrometer (discussed in the section 'Latest advances in the technique' above) offers both the prospect of 'real-time' measurements as well as on site evaluation of mineral findings. MS of the transformation of magnetite to haematite and vice versa using different treatments has been widely studied. In the present section, some will be discussed. It is basically the study of the transformation of iron oxides from one form to another. It could be done thermally,[258] chemically[259,260] and mechanically.[261] Mazo-Zuluaga *et al.*[258] studied synthetically prepared pure and copper doped magnetite by several techniques including MS. The samples were heated in air between RT and 800°C at several heating rates. They found that the heat treated pure samples consisted only of well crystallised haematite, whereas the copper doped samples when heat treated at 350°C consisted of mixtures of magnetite, maghaematite and haematite. The relative amount of different phases depends on the amount of doped copper as well as on the heating time. This transformation is not direct, but goes through the formation of maghaematite as an intermediate phase. MS, X-ray and DTA techniques in their study have supported this. Another study of the effect of Cu(II), Ni(II) or Co(II) ions on conversion of goethite to magnetite under different conditions using MS was reported by Mohapatra *et al.*[259–261] In their studies, crystalline goethite samples were prepared by coprecipitation using ferric nitrate, sodium hydroxide and metal (Cu, Ni or Co) ion solutions, and the samples were studied by XRD, TEM, TG-DTA in addition to MS. The converted products obtained by the addition of Cu and Ni ions showed only magnetite that was found to be ferrous ion deficient, whereas the converted product obtained using Co(II) contained 67% total iron, and magnetite was the major phase. Another independent phase in the second type of conversion due to the presence of Co(II) was nanocrystalline Fe_2O_3 with a small amount of absorbed water and sulphate. Betancur *et al.*[262] studied the dynamics of transformation of haematite (α-Fe_2O_3) to magnetite (Fe_3O_4) by two solid-state reaction methods. The first method consists of a thermal treatment under a 20% H_2 and 80%N_2 atmosphere at 375°C, and then the study of phase evolution as a function of the thermal treatment time ranging from 0 to 25 min with a 2·5-min interval. In the second method, a planetary ball mill treatment involves inducing the phase transformation from 0 to 6 h with hourly measurements using room-temperature MS and X-ray diffraction analysis. Results show a well behaved structural transformation for which Fe_3O_4 as a single phase was found for treatment times above 12·5 min in the case of the thermally treated samples. A less stoichiometric magnetite was obtained characterised by a distribution of hyperfine fields for milling times above 3 h in the case of the ball milled samples. Their work evaluated the transformation taking place through the intermediate states by computing the degree of oxidation and evolution of the relative areas, which closely follows

an exponential-type behaviour. Stewart *et al.*[263] studied the effect of ball milling with milling time of haematite (α-Fe_2O_3) by Mössbauer and susceptibility measurements. Ball milling treatment for 30 min reduced anhydrous bulk haematite grains to nanometric sizes. For milling times of 15 min to 2 h, the haematite crystal suffers an anisotropic lattice dilation, and by Mössbauer experiments it was found that the process alters the effective Morin temperatures. The transition occurs less sharply than for the non-milled material and spreads over a maximum extent of 50 K for a milling time 30 min. In addition, the disorder brought about by milling reduces the magnetic response in the weak ferromagnetic state of α-Fe_2O_3. The modification of Morin temperature could be due to the anisotropic dilation of the unit cell that affects the whole grain and is related to the nanometric grain sizes achieved.

Another effect of mechanical ball milling is mechanochemical transformation. Mechanochemical reactions are initiated by the application of a mechanical force. It has been shown that solid state mechanochemical reactions can be initiated by milling the reactants in a high energy ball mill. Oxidation/reduction reactions occur at room temperature during mechanical milling and have been applied by Warris and McCormic[264] to refine pyrite (FeS_2) at room temperature. It is known that pyrite is the most common sulphide host for gold, and in refractory pyrite samples, gold is encapsulated in the pyrite matrix, so it is important to break down the matrix by cyanidation. It has been found by MS and other techniques that pyrite can be oxidised mechanochemically as a sulphate without the production of sulphur dioxide gas.

Mulaba-Bafubianandi *et al.*[265] studied the fast online determination (5 min) of the Fe^{3+} to Fe^{2+} ratio in selected industrial minerals such as stilpnomelane, chromite and ilmenite. A miniature Mössbauer spectrometer was used for these industrial online analytical studies. Fe^{3+}/Fe^{2+} ratio increased from 0·14 to 2·26 when going from ilmenite to stilpnomelane. The measurement time was 5 min per point of the spectrum. The results from the Mössbauer analysis are in good correlation with those from the conventional chemical method. Its usefulness in raw materials selection, and on natural chromite minerals classification based on (a fast) Fe^{3+}/Fe^{2+} ratio determination has been shown in their studies.

Several studies have been reported on minerals processing by different biochemical routes, and MS has been used as an important monitoring technique in this process. An important and interesting study was carried out to investigate the mechanisms and biogeochemical processes occurring during magnetite reduction by iron reducing bacteria using MS and other techniques.[266] Reduction experiments were performed with biogenic and synthetic magnetite in well defined solutions. Synthetic magnetite in a bacteriological growth medium was inoculated with either aerobically or anaerobically grown cells. Fe(II) production was determined by HCl extraction of bioreduced samples in different buffer media, and the resulting solids were characterised by MS and other techniques. It was found by MS that the extent and rate of biogenic magnetite reduction in the bicarbonate-buffered medium were higher than that in the PIPES-buffered medium. In the HCO_3-buffered solutions, Fe(III) in the biogenic magnetite was reduced to Fe(II), and siderite precipitated. In the PIPES-buffered medium, Fe(III) in biogenic magnetite was also reduced to Fe(II) with no trace of secondary mineral phases. Electron microscopy and MS results indicate that the reduction process involves dissolution–precipitation mechanisms as opposed to solid state conversion of magnetite to vivianite or siderite. It is known that a microbial biofilm consortium enriched from shield surface water is able to mediate geochemical cycling of iron within the biofilm. Using this idea, Brown *et al.*[267] leached iron from Fe(II) containing minerals such as magnetite, biotite and ilmenite to Fe(III) in a colloidal suspension. In the next stage of the processing, the Fe(III) was then reduced to Fe(II) by iron-reducing bacteria that behave as electron acceptors. They found different iron compounds as precipitates depending on the ratio of iron to carbon in the media and upon the local environment by using Mössbauer and X-ray diffraction spectroscopy. MS has shown different precipitation as ferrous hydroxide, vivianite, ferrihydrite and haematite, which then become incorporated into stratified iron deposits such as banded iron formations. Many more Mössbauer spectroscopic studies of minerals have been reported in journals such as *Mineral Engineering*, *Hydrometallurgy* and in journals related to chemistry, physics and metallurgy.

In addition, MS has been widely used to study the minerals from the moon and Mars. A number of studies on meteorites have been reported. Because such studies concern minerals in meteorites from the moon or Mars, this discussion has been included in the section of minerals. Since the astronomical studies are a specialised branch in physics, they need some introduction. In recent years, the most important success in astronomical research was the Mars exploration in 2003 by the American space agency (NASA) and by the European space agency (ESA). The inclusion of a specially designed portable 'Miniaturized Mössbauer Spectrometer' (MINMOS II) in the NASA Mars exploration Rover (MER) and ESA's Lander Beagle 2 is one of the greatest successes in the history of MS. This was possible owing to tremendous advances in the design of the MINMOS II.[268] A detailed description of the Mars Mössbauer spectrometer has been given in an article by Klingelhöfer *et al.*[269] It weighs less than 500 g and is $50 \times 50 \times 50$ mm^3. The working principle of MIMMOS II is based on the back-scattered technique. To analyse the spectra of rocks and minerals on Mars, a huge data bank (Mars mineral spectroscopy database) has been created (http://www.mtholyoke.edu/go/mars). The goal of this web site is to provide an easily accessible data set of Mössbauer spectra of minerals collected over a range of temperatures, in order to provide suitable analogue spectra for data acquired on remote surfaces such as Mars. Complementing these data will be both reflectance FTIR data, collected at Brown University's RELAB facility, and Raman spectra collected by Jill Pasteris at Washington University St. Louis. After collection at Mount Holyoke, Mössbauer spectra are then posted on that site. FTIR and Raman spectra will also be collected through 2004–05. This database is accessible to all, and it contains information about the minerals and the original data of Mössbauer spectra. Many minerals and rocks from Mars have been observed or predicted from

other terrestrial research. Previous Mars missions, namely Viking and Mars Pathfinder revealed Si, Al, Fe, Mg, Ca, K, Ti, S and Cl to be the major constituents in soil and rock from the red planet. The selected minerals are organised according to their Mössbauer parameters, main site substitutions, behaviour as a function of temperature, and a ranking as found on Mars. In addition, an identification system based on Artificial Neural Networks was implemented which can make a fast and precise mineral identification from the experimental Mössbauer parameters at a given temperature. A Mössbauer spectrometer is fitted on each of the Mars Exploration Rovers (MER), named Spirit and Opportunity, and are still on Mars, researching rocks and soil samples. Following are some of the interesting facts discovered on the Martian surface and described data analysis.[270]

A Mössbauer spectrum captured by the Mössbauer spectrometer onboard the Mars Exploration Rover Spirit shows the presence of three different iron-bearing minerals in the soil at the Rover's landing site. One of these minerals has been identified as olivine, a shiny green mineral commonly found in lava on Earth. The other two have yet to be defined. The discovery of olivine implies the soil consists at least partially of ground up rocks that have not been weathered or chemically altered. The Mössbauer spectrometer uses two pieces of radioactive cobalt-57, each about the size of pencil erasers, to determine with a high degree of accuracy the composition and abundance of iron-bearing minerals in Martian rocks and soil.

The next Martian Mössbauer data obtained was a kind of rock, named Adirondack rock, which contains different iron-containing minerals. The analysis of the Adirondack rock shows that it is a type of volcanic rock, known as basalt. Specifically, the rock is what is called olivine basalt that contains magnetite and pyroxene. These data were acquired by Spirit's Mössbauer spectrometer before the Rover developed communication problems with Earth. The shiny green minerals, called olivine minerals, were also found in the spectrum sent from MER Opportunity's landing site, named Meridiani Planum. The same spectrum was also seen at the MER Spirit's landing site, Gusev Crater. Based on these data, scientists believe the soil at Meridiani is made up in part of fine-grained volcanic basalt. The next data were sent by the MER Opportunity's Mössbauer spectrometer, and show the presence of an iron-bearing mineral called jarosite in the collection of rocks, named 'El Capitan.' 'El Capitan' is located near where the Rover landed. The central doublet part in the Mössbauer spectrum specifically indicates a jarosite phase, which contains water in the form of hydroxyl as part of its structure. These data indicate water-driven processes exist on Mars. Three other phases are also identified in this spectrum: a magnetic phase, attributed to an iron oxide mineral; a silicate phase, indicative of minerals containing double-ionised iron (Fe^{2+}); and a third phase of minerals with triple-ionised iron (Fe^{3+}). The Mössbauer data and microscopic view of the surroundings of the landing site of MER Opportunity show two types of grains, named, blueberries and empty berries. The upper line shows data for a region dubbed 'Berry Bowl,' which contains a handful of the spherelike grains dubbed 'blueberries.' The lower line represents an area called 'Empty' next to Berry Bowl that is devoid of berries. Berry Bowl's spectrum still shows typical outcrop characteristics, but also exhibits an intense haematite signature, seen as a 'magnetic sextet.' The data collected by MER Opportunity's Mössbauer spectrometer at various spots in the 'Eagle Crater' show a basaltic mineral composition with minor amounts of haematite. Basalts are volcanic minerals and haematite is an iron-bearing mineral often formed in water. Evidence of haematite was also found in the rock named 'Pot of Gold,' located at the Gusev Crater. This was discovered by the MER Spirit's Mössbauer spectrometer by examination of the surface of the rock. The analysis shows a typical basaltic, or volcanic, rock mixture of non-haematite iron-containing minerals with haematite minerals in the Gusev Crater. Haematite, found on Earth, can be formed in three different ways: in standing water, in small amounts of hot fluids (hydrothermal processes), and in volcanic rock. Scientists are planning further observations of this and other rocks in the area, which they hope will yield more information on the haematite's origins.

In a review article, Dyar and Schaefer[271] discussed detailed MS on the surface of the Moon. The present study includes a list of potential Fe-bearing minerals on the Martian surface and discusses the properties of some of those minerals by MS. Morris *et al.*[272] reported the Mössbauer spectroscopic studies of lunar minerals, their relations to other minerals data and their utilisation in lunar mineralogical exploration. Other Mössbauer spectroscopic data of lunar minerals are available from different lunar conferences[273–277] and a book by Mitra.[278] Out of the investigated minerals, some of the Fe-bearing minerals are very common and they are pyroxene, ilmenite, olivine, amorphous Fe^{2+} glass, metallic iron and Fe–Ni alloys. Morris *et al.*[272] also discussed the effect of the solar wind on the lunar surface. Bland *et al.*[279] reported studies of meteorites in the understanding of planetary science. Room temperature Mössbauer spectroscopic studies of bulk meteorite samples were done to understand the weathering history of meteorites, and to develop a model to understand the rate at which meteorites arrive at the Earth's surface. These data are helpful to clarify the preterrestrial and early solar system processes that have formed these meteorites. In this article, Bland *et al.*[279] discussed the weathering of ordinary chondrite as measured by MS, defining weathering rates in different climatic regions and the flux of meteorites to the Earth. They used an absolute measure of alteration to understand isotropic effects, with relevance for the preterrestrial alteration of some meteorites along with MS and X-ray diffraction to study the mineral abundance in carbonaceous chondrite meteorites.[278] Here, chondrite is one type of stony meteorite. Details of different meteorites have been discussed in that article.[278] These are some examples of the use of MS in astronomical studies.

In the last section of the present discussion, a brief description of the application of MS to study coal and related materials will be presented.

MS has been widely applied to characterise the iron minerals in coal. Most of the iron minerals in coal are available in the form of sulphur compounds, mainly as pyrite (FeS_2). Coal is an important source of energy, and the associated possible hazardous environmental pollution from coal has led to considerable research to

understand fully the different compounds present in coal and how the compounds transform during processing and utilisation in power plants and industry, for example in the steel industry. The suitability of coal for industrial and other applications depends on the constituents of the coal. Characterisation of different coals is an important step. MS is an ideal technique for the identification of iron-bearing minerals in coal. Detection and quantitative estimation of iron-bearing minerals, such as pyrite, are extremely relevant for power plants and the steel industry. The main use of coal can be divided into three groups as: steam production, steel industry and synthetic fuel production. The presence of sulphur as iron compounds in coal and coke produces sulphur dioxide and other corrosive products. These sulphur products produce damage in the blast furnaces, and other chambers where the coal and coke are useful. Therefore it is important to characterise the phases present in coal and coke and determine the amounts of pyrite and other iron sulphide compounds. A journal '*Fuel*' is dedicated to publishing research on Mössbauer spectroscopic studies of coal and coke. An important study that has been cited several times to date, was reported by Huffman and Huggins.[280] They reported MS studies of iron minerals and mineral derived phases in coal, coke and other coal related minerals. A number of iron–sulphur compounds were assigned in the samples from their Mössbauer parameters as pyrite, siderite, marcasite, different $FeSO_4$ compounds, jarosite, troilites and several $Fe_{1-x}S$ compounds. These are the minerals commonly available in coal. In addition to the above sulphur compounds, they were reported a number of silicate phases, clay minerals and siderite. Different tables presented in that study are very useful for assigning the sulphur, silicates and clay compounds in coal using MS. They also studied the transformation of different phases in coal compounds during high temperature carbonisation. Their studies were divided into three categories, coke prepared in a small oven for research, coke prepared in a large oven for commercial purposes and residues from high temperature studies of coal. They found different volatile materials in high siderite content coal samples. From the data obtained by MS during coal carbonisation, they suggested the following transformation of iron–sulphur compounds

$$\text{Pyrite } (FeS_2) \Rightarrow \text{troilite } (FeS) + \text{pyrrhotite } (Fe_{1-x}S)$$

$$\text{Illlite} + \text{other clays} \Rightarrow \text{ferrous glass}$$

$$\text{Siderite} \Rightarrow \text{metallic Fe} \xrightarrow{\text{cooling}} \text{metallic Fe} +$$

Fe oxides (magnetite and haematite).

A new method to determine pyritic sulphur in coal and troilitic plus pyrrhotitic sulphur in coke has also been suggested by them. Taneja and Jones[281] studied iron-bearing minerals in coal and in coal ash by temperature dependent MS to study the variation of Mössbauer parameters. During ashing of coal, the changes in iron compounds studied by them suggested the following transformations

$$\text{Pyrite} : FeS_2 \Rightarrow \alpha - Fe_2O_3; \text{Siderite} : FeCO_3 \Rightarrow \alpha - Fe_2O_3;$$

$$\text{ankerite} : [(Ca,Fe,Mg)CO_3] \Rightarrow Mg_xFe_{3-x}O_4$$

and other phases.

Several Fe^{2+} phases in clays in coal samples transformed to Fe^{3+} phases as glasses, silicates and oxides. Asami *et al.*[282] studied the chemical kinetics using MS during gasification of brown coal and char with carbon dioxide. After reacting with CO_2, they found the transformation of Fe_3C to γ-Fe, α-Fe and CO at the initial stage of gasification. Finally, Fe_3O_4 and FeO are the dominant species when reaction time was prolonged. Medina *et al.*[283] proposed an iron-catalysed CO_2 hydrogenation mechanism for natural gas formation in coal beds. They used $Fe(NO_3)_3 \cdot 9H_2O$ as starting material in the generation of the active catalyst, iron metal, to produce Fe_2O_3. Then Fe_2O_3, the precursor to the active catalyst, was reduced at 200°C under a hydrogen atmosphere. After the reaction, methane in the produced gas was typically greater than 90%. MS shows that under those conditions, 6% of the iron oxide is reduced to metal, which is believed to be the catalytically active species. The same group studied the low temperature iron- and nickel-catalysed reactions leading to coalbed gas formation.[284] Hydrocarbon hydrogenolysis and CO_2 hydrogenation in the presence of Fe/SiO_2 and Ni/SiO_2 catalysts are potential mechanisms contributing to natural gas formation in coalbeds. Reaction temperatures were selected to resemble natural coalbed conditions. The oxides (Fe_2O_3 and NiO) were used as precursors of the active catalysts (Fe and Ni metals) in their study and were reduced at 200°C under a hydrogen atmosphere. MS showed that 6% of the iron oxide was converted to the metal whereas in the case of nickel, oxygen titration showed that the extent of reduction to the metal was 29%. The resultant fractions of the active metals in coals are adequate to catalyse generation of appreciable amounts of methane over geological time. In another report, the carbonisation of iron-treated loy-yang coal was reported by Ozaki *et al.*[285] Ahmed *et al.*[286] characterised Spanish coal by MS and FTIR at room temperature and at 80 K. In all samples, the main sulphur content is pyrite, and in some samples they found the existence of jarosite in lignite, brown and sub-bituminous coal, whereas iron carbonates are present mainly as siderite in bituminous and semi-anthracite coal. Using the data from FITR and other studies including MS, they calculated the aromaticities of different coal samples and graded the coal. The process of oxidative desulphurisation of sulphur rich Ukrainian coal was studied by Pysh'yev *et al.*[287] in the temperature range of 623–723 K by the flow of an air/steam mixture in the fluidised bed reactor. MS was applied to study the reaction products after every step of thermal treatment. The pyritic sulphur that constitutes most of the sulphur oxidises selectively under these conditions. At lower temperature (623 K), the ferrous sulphates and pyrite oxidised to ferric sulphate. At 673 K and higher temperatures, FeS_2 oxidised to α-Fe_2O_3 and SO_2. In the desulphurisation reaction processes, FeS_2 first transformed into pyrrhotite at 698 K. They suggested different transformation reactions on the basis of the experimental results. Anshits *et al.*[288] studied the morphology and composition of different magnetic microspheres and cenospheres recovered from fuel ashes being formed in combustion of Irsha-Borodinskii lignite and Kuznetskii coal by SEM, electron probe micro-analysis and MS. The morphology of globules, crystallite size and defect structure of different phases were studied to established the basicity of the glass phase. It

was shown by them that the catalytic activity of magnetic microspheres and cenospheres in the reaction of deep oxidation of methane is determined by the spinel phase and depends on the extent of its accessibility and type of defect structure. Using MS, Waanders *et al.*[289] investigated different iron minerals present in South African coal from various coal fields and in coal ash, after industrial and laboratory combustion processes, to determine the changes that occur in these phases during weathering. Different iron phases in coal were found in the form of sulphur compounds such as pyrite and jarosite, while other iron bearing minerals such as illite and ankerite also occur, along with a trace element in kaolinite, a major clay mineral present in coal. The amounts of these minerals vary considerably in coal samples from six coal-producing areas in South Africa. Apart from these minerals, the non-iron-bearing minerals were identified and found to be mainly quartz, clay minerals and carbonates. Differences in mineral composition were found between the coals from the different regions. Ash samples, obtained from the Lethabo electricity power plant, South Africa, were investigated. At the high temperatures (≈1400°C) of combustion in the power plant, fly ash and agglomerates are produced, and the Mössbauer spectra showed two poorly developed doublets, typical of glass. In the laboratory simulation, carried out at temperatures ranging from 200°C to 1200°C, it was clearly observed how the pyrite changed to haematite and finally was taken up in the glass in addition to the haematite that formed. The high contents of calcium present, identified by SEM analyses, resulted in the agglomeration of the fly ash. The weathering products were also identified using the same techniques, and it was noticed that the pyrite changed to a sulphate when the wet coal was exposed to air-drying.

The above discussions illustrate the ^{57}Fe MS study of minerals in various fields. There are other reports on MS studies of minerals.

Archaeological samples

Archaeology tries to reconstruct the culture and history of past societies that do not have any information or have very poor information at the present time. It mainly studies the past material culture of everyday life in the society. It uses a whole variety of methods and tools such as survey and excavation, environmental analysis with pollen or glacial records, palaeobotany and palaeozoology, scientific and historical dating methods, historic and iconographic sources, material analysis of found artefacts, etc.[290] Different experimental techniques have been used to study the archaeological samples found from different places, including MS. MS has been applied to study different archaeological samples such as ceramic and non-ceramic materials, coins, pottery, paintings, etc.

The use of different chemical methods that have been borrowed from natural sciences is known as archaeochemistry.[291] MS plays a dominant role in archaeometry too. Material analysis has two categories, the first is the characterisation of the material of objects, which gives information about the provenance of the material, and the second is the characterisation of the manufacturing of the objects, which helps to reconstruct ancient techniques. The provenance of an object or its raw material can tell us about its resources, trade contacts and economic systems.[291] In the following section, different archaeological materials studied by MS are presented.

Ceramic materials

In archaeological study, information about the area of production of the archaeological samples is important. Materials and decorative patterns of medieval or renaissance archaeological ceramics samples are very similar in most cases. Therefore an exact attribution of these samples to a certain area of production is not always possible by stylistic considerations or macroscopic observations. In such cases, ^{57}Fe MS study is a very useful tool to gain knowledge about the historical provenance of the sherds from the iron-bearing species in the materials. The first work on the application of Mössbauer spectroscopy in such cases was in Italy on the study of Venetian and Paduan (Padova, Veneto, this city is one of the cultural and economic centres in the northeast of Italy) potsherds (ascertained by typological and stylistic criteria) by Stievano *et al.*[292] From the chemical analysis of the Paduan sherds, it has been found that these sherds are richer in P_2O_5, CaO and Al_2O_3, but poorer in MgO and Na_2O than the Venetian ones. Mineralogical analysis, on the other hand, shows that the Venetian ceramic bodies are more fine-grained compared with those from Padua, indicating the use of compact, well seasoned clays with small accumulation content. Temperature dependent MS studies of all these samples between 80 and 293 K show a quadrupole doublet attributable to Fe^{3+}, and a magnetic sextet attributable to iron oxides. The change in intensities of these two components with temperature indicates that two different species, octahedral high spin Fe^{3+} and the superparamagnetic iron oxides (mainly haematite) contribute to the quadrupole doublet. In some of the samples in both the Venetian and Paduan groups, an additional Fe^{2+} component is present. It indicates that the baking conditions were reducing for those samples. From the quadrupole splitting values of the Fe^{3+} component, a baking temperature between 1000°C and 1100°C was inferred for all samples.[293,294] The ratios of Fe^{2+} to Fe^{3+} in all investigated samples obtained from MS were then compared with the chemical analysis results and these showed that the MS alone could describe the chemical–physical environment of the iron atoms in artistic ceramics,[292] but could not differentiate the Venetian and Paduan pottery. Combined mineralogical, chemical and Mössbauer data with stylistic and typological criteria can give a detailed and definitive answer to different questions in archaeology related to these samples.[292–294] Another interesting study was reported by Lazzarini *et al.*[295] on about 40 archaeological samples (plates, cups, lamps, jars, etc.) found from a site at Tell Afis (this site lies between Ebla and Aleppo and has been excavated by the Italian team working at Ebla for more than 20 years), in the north west of Syria by physico-chemical and mineropetrographic analysis including ^{57}Fe Mössbauer spectroscopy. Room temperature Mössbauer spectra of 10 samples showed almost identical spectra. Analysis of these spectra gave a magnetic sextet of iron oxide and a quadrupole doublet of trivalent iron. The homogeneity of the Mössbauer data is in agreement with the common origin of the raw clays. The combination of Mössbauer data with the mineralogical results showed the presence

of well conserved calcite and the absence of calcium silicates formed during the baking process with an approximate baking temperature between 600°C and 700°C.[295]

Study of firing techniques

The firing techniques determine the quality of ceramic production or metal work. To maintain a high quality product during the firing process, the temperature and the atmosphere have to be controlled. ^{57}Fe MS is one of the best methods for technological studies of firing techniques as it can be applied to all iron containing materials involved in the firing process.[292] All kinds of ceramics, like pottery, moulds and parts of furnaces, as well as non-ceramic materials like slags and glass can be studied by Mössbauer spectroscopy. All measurements on fired ceramic materials give information on firing temperatures, kiln atmospheres and also the firing cycles.[293]

Archaeological clays

Using MS, Ortalli *et al.*[296] studied two different samples collected from two different provenances. In their work, they first tried to clarify the provenance of black pottery from Umbria (Italy). The MS results show the presence of a small amount of divalent iron together with the paramagnetic doublet of Fe^{3+} iron and the magnetic sextet representing iron oxides. Presence of Fe^{2+} indicates a reducing atmosphere during the firing of the ceramics, which is quite common for black pottery. They also estimated a difference in firing temperature, which is about 200°C for the two samples collected from the two different provenances. This difference could be due to the two different pottery manufacturing processes and techniques that were present in Umbria, in spite of the homogeneity of style and texture of the ceramic bodies in the two provenances. The same group[296] also dealt with the provenance of votive bond clay cakes in burial accessories of a group of 10 tombs of the necropolis of Colfiorito (Foligno, Perugia). These clay cakes are quite similar in colour and cohesiveness to local light clay known as 'Terra Angelica' that has been used for a long time for the therapeutic purposes. In this case, ^{57}Fe Mössbauer spectra at 80 K of a sample of the clay cakes and of a sample of 'Terra Angelica' were compared. Both spectra showed the presence of a dominant doublet of Fe^{3+} with similar parameters and of a minor component of Fe^{2+}. The similarity between the spectra of these two samples indicates that the two clays have the same origin.

Non-ceramic material

It is well known that Mössbauer spectroscopy allows the study of different non-ceramic archaeological materials such as glass, gold, iron, slags, or phenomena such as the corrosion of metals and the weathering of non-metals by MS. The colour of glass is mainly caused by metal compounds added to the glass. It depends on the oxidation state of the metal ions and various factors like the glass composition and the kiln atmosphere. MS study of these materials can give detailed information on some of these features. MS studies of antique glasses give information on the chemical state of the iron.[297] MS is also used to study the chemical state of tin and antimony in glasses or glazes.[298] Study of slag by MS is always important for the reconstruction of the metal melting process and metal production.[299] MS of slag can easily identified the mineral phases in it and can give information about the furnace temperatures and atmospheres used during the melting process.

Archaeological pottery samples

MS studies of different ceramic and non-ceramic archaeological samples found at different places can give us an idea about the existing technology during that time. Further analysis of these results can also give us an idea about the patterns or changes in technology. This also can reflect larger economic, social, or political processes or events. The artistic style of pottery is tied to the culture of the society, practices and ideas about how pots are made as they are related to the local ecology. There may be many ways to make a cooking pot given available materials but the particular clays chosen and the techniques used to form, finish, and fire the vessels are linked to the organisation of the potters, the perception of different raw materials and fuels, their social identity and the integration of pottery-making with other activities. MS has been applied in pottery analysis. Different materials exhibit a variety of Mössbauer spectra[300,301] that give information about the variations in the clay sources, different techniques used by different people or chronological differences. Study of several samples by MS makes it possible to group the spectra into types that represent standard production procedures used during that time.[300,301]

Study of surface glazes

In the field of archaeological studies of pottery and ancient porcelain, there is actually no essential difference between them. Therefore, the archaeological study of ancient porcelain materials deals with the surface glaze. Using CEMS, Hedges[302] related the colours ranging from blue, green and yellow to red to the chemical state of the iron in Chinese glazed porcelains. The Mössbauer spectra of moon-white Ru porcelain glaze of the Yuan dynasty were also reported.[303,304] They showed the existence of three iron components, Fe^{2+}, Fe^{3+}, and a magnetically split component of Fe_3O_4 with a total of 60% of Fe^{2+} [303,304] When the glaze is fired in a reducing atmosphere, it undergoes nitrification at about 950°C and recrystallisation above 1000°C. Based on the value of the quadrupole splitting and the intensity of the Fe^{2+} component, the original firing conditions were deduced to be 1150 ± 50°C in a reducing atmosphere.[302]

Mineral drugs

The use of minerals as medical drugs is about 2000 years old. In this context, it is important to mention that in the famous Chinese herbal medicine book 'Shen Nong's book of Materia Medica' between the age of 100 AD and 180 AD, 365 kinds of drugs were recorded. Out of those, 46 are mineral drugs. In 1578, Chinese pharmacologist, Li Shizhen, gave a detailed description of 375 different mineral drugs in the book 'Compendium of Materia Medica'. Qin and Li[305] studied about 100 samples out of 375 of Chinese mineral drugs by MS and other techniques and presented their pharmaceutical and curative mechanism.

Ancient bronze and coin samples

Mössbauer studies of bronzes (Shang Dynasty in China, 1600–1100 BC) make use of ^{119}Sn MS. This can

distinguish the alloyed tin and tin oxide in the samples. These alloyed tin or tin oxides could have been present right from the time of production of the bronze artefact or may have formed in the course of time. Zheng and Hsia[306] studied bronzes of the Shang Dynasty by ^{119}Sn MS. Wu *et al.*[307] studied a Chinese bronze mirror from the Han Dynasty by ^{119}Sn MS. They found that on the surface of the bronze mirror, tin is present as Sn(IV) oxide and as a Cu–Sn alloy. Zhang *et al.*[308] studied the surface of the 'Heiqigu' bronze mirror of Han Dynasty (206 BC–AD 220) and the Tang Dynasty (AD 618–907) by ^{119}Sn Mössbauer measurements, both in transmission and back-scattering geometries. They concluded that the tin is present as Sn(IV) oxide on the surface, whereas a Cu–Sn–Pb alloy was found to prevail beneath the surface. Depth profile CEMS measurements of the same sample showed that the tin oxide compound gradually changed from Sn^{4+} oxide on the surface to the Cu–Sn–Pb alloy in the interior.[308]

Ancient paints and less common archaeological samples

^{57}Fe MS has been applied to characterisation of ochre (present in the ancient paintings as pigments), usually iron oxides or hydroxides or mixtures of these two. Several samples from painted tombs, located in Caere and dating from the first half of the 7th to the 6th century BC were studied by Calogero *et al.*[309] Some imported red ochre (from the Island of Elba, known as the source of red ochre in central Italy in Roman and Etruscan times) was also investigated. Room temperature Mössbauer spectra of the red ochres, both the local and imported, show a large magnetic splitting. This splitting is due to the presence of haematite and goethite in different percentages. Comparing these data with the painted samples, it has been found that there is virtually no goethite in the painted sample or it could be there in the form of superparamagnetic phase of particle size less than 15 nm. The observed broad sextet in the spectrum is assigned as poorly crystallised haematite. Mössbauer spectra of the painted samples are typically doublets as a result of the compounds of Fe^{2+} and Fe^{3+}. The Fe^{3+} can be due to silicates and in the form of superparamagnetic oxides. The hyperfine parameters of the divalent iron, on the other hand, are in agreement with the presence of chlorite. Jiang[310] reported the MS study of ancient paint of Western Han Dynasty. The paint is on an ancient grave of a queen of Han Dynasty. According to ^{14}C dating, this grave is 2235 ± 77 years old. It was found that the components of the primary paint were mainly FeOOH and FeS_2 (pyrite) and the history of the paint was traced. Gauzzi *et al.*[311] studied an Etruscan axe from the National Etruscan Museum of Villa Giulia in Rome. A powdered sample extracted from the core of this object was studied by ^{57}Fe Mössbauer spectroscopy, XRD, SEM, EDX and DSC. The room temperature Mössbauer spectrum of the powdered sample exhibits two sextets with different fields, the dominant one having a field around 34 T and the minor one with an internal magnetic field of 50 T. The two sextets merge into a single sextet at 80 K. The dominant sextet is assigned to goethite, whereas the less intense one is assigned to haematite. An intense quadrupole doublet was also found in the room temperature spectrum that had virtually disappeared at 5 K. This could be due to the superparamagnetic relaxation of the iron oxyhydroxides. The XRD and EDX studies also show the presence of crystalline goethite and other elements such as Si, alkaline-earth metals and sulphur. From the decomposition pattern of goethite into haematite, DSC analysis of the dehydration of the sample up to 653 K supports the presence of goethite in the sample.

Study of fossils

Trivalent and divalent iron compounds are commonly seen in animal fossils and can be detected by MS. An example is the vertebrate bone sample from a Malay crocodile with a known age of 3000 years, studied by MS. The iron in the fossil is present in the Fe^{3+} state with a small amount of Fe^{2+}. From the ratio of Fe^{3+}/Fe^{2+}, it has been concluded that the fossilisation process has not yet been completed.[312]

In summary, both transmission and CEMS studies of archaeological samples including the ancient paintings and fossil give us information of archaeological interest.

Biological samples

MS is a very useful technique to study the iron containing biological molecules and model compounds. This part of the present review deals with the application of MS in biomedical research. Oshtrakh[313] studied the structural heterogeneity and functional changes in protein using MS. He found that these changes are due to the small variations of the iron electronic state and stereochemistry. The results showed the relationship of the structural variations with Mössbauer parameters of iron containing proteins and demonstrated the possibilities to obtain new information at the molecular level in biomedical research. Iron containing proteins can recognise oxygen and electron transport (haemoglobin and cytochromes), enzyme functions (catalysis), oxygen and iron storage (myoglobin and ferritin or haemosiderin), and iron transport (transferrin, lactoferrin). The main physiological functions of iron containing biomolecules are related to their molecular structure and iron state.[314–319] These reports show that Mössbauer spectroscopic study of iron containing biological molecules is very useful to understand the structure and functional relationship in the molecules.

The iron storage proteins, haemoglobin and ferritin, contain an iron polynuclear core in the form of hydrous ferric oxide. Most biomedical studies using MS were made with these two very important proteins. Haemoglobin contains iron. It is the oxygen carrier in the body which consists of two pairs of non-equivalent subunits associated in a tetramer. Each subunit contains a protein chain bound with the iron–porphyrin complex (heme) and oxygen molecule that reversibly binds with the heme ferrous iron. It is known that a large number of normal haemoglobin variants in both humans and other animals differ in the primary structure and in oxygen affinity. The process of oxygen binding and releasing by haemoglobin is accompanied by the protein conformational transitions initiated by spin change of the heme iron: Fe(II), S=2→Fe(II), S=0 and Fe(II), S=0→Fe(II), S=2, respectively. Therefore, the heme iron electronic structure plays an important role in the protein structures and functional relationships.[313] In the experimental study of haemoglobin by MS, Mössbauer parameters indicate the electron irradiation leading to oxyhaemoglobin

deoxygenation and the formation of two ferric compounds first, and then to formation of ferrous and ferric compounds in haemoglobin with small structural variations in heme.[313] The ferritin molecule core has up to 4500 ferric ions. It releases iron molecules and when more molecules are added, starts growing into a cluster. Oshtrakh[320] studied small variations of the molecular structure and the iron state in the iron containing ferritin protein. Mössbauer studies of human normal fetal haemoglobin in deoxy-(HbF), oxy-($HbFO_2$) and carbonmonoxy-(HbFCO) forms were done at 87 K by Oshtrakh and Semionkin.[321] Both haemoglobins differ in their molecular structure and functions. Haemoglobin A consists of two pairs of α- and β-subunits whereas haemoglobin F consists of two pairs of α- and γ-subunits. It was found that the values of quadrupole splitting for both deoxy- and oxy-forms of haemoglobin A and F were different. These differences may be related to small variations of the heme iron stereochemistry in both the deoxy- and oxy-forms of haemoglobin while the strong bond of Fe(II)–CO, smoothes away any small structural variations of the heme. Bell *et al.*[322] studied temperature dependent MS of human normal ferritin and haemosiderin. The Mössbauer spectra demonstrated superparamagnetic behaviour of the small FeOOH particles with different amounts of iron in the cores of ferritin and haemosiderin. Mössbauer hyperfine parameters for both proteins were the same; however, the iron content in haemosiderin was higher.[322] Variation of protein structure is related to various diseases such as haemoglobinopathies and also malignant diseases. Therefore studies of protein structure are indirectly related to the detection of different diseases. Study of this structural variation of protein by MS is advantageous because MS is a noninvasive, nondestructive technique which does not require any chemical treatment of the protein samples during studies and thus avoids all artefacts caused by such treatments. In many cases, MS can identify the iron-containing compound or at least determine the charge state, spin state and coordination of the iron with the investigated tissue. Haemoglobinopathies are molecular diseases related to the synthesis of anomalous haemoglobin in the body. Abnormal haemoglobin molecules are unstable and have different functions. Bill *et al.*[323] studied Hemoglobin Zürich (HbZ) in deoxy-, oxy- and carbonmonoxy-forms. It has amino acid substitution in the distal heme region of β-subunits as His E7(63)→ Arg. It was found that temperature dependent quadrupole splitting for HbZ and HbA had a very small difference whereas those for $HbZO_2$ and $HbAO_2$ had more significant differences. This result demonstrates the influence of structural change in the distal heme region on the Fe(II)–O_2 bond and the iron electronic structure. The values of quadrupole splitting for HbZCO and HbACO were the same as a result of the strong Fe(II)–O_2 bond. The temperature dependence of quadrupole splitting of normal A and abnormal haemoglobins in deoxy-form has also been reported elsewhere.[324,325]

The iron core structure in ferritin and haemosiderin proteins of patients with haemoglobinopathies was studied by several researchers.[326–329] MS studies of liver haemosiderin from patients with primary idiopathic haemochromatosis (PH) and with secondary haemochromatosis (SH) caused by β-thalassemia treated by multiple transfusions were found in two different states of the iron core: superparamagnetic and magnetic at 4·2 K respectively with different superparamagnetic blocking temperatures. The structure of the iron core in haemosiderin of patients with PH and SH is related to a more highly ordered goethitelike structure (α-FeOOH) of SH haemosiderin. Recently, MS was applied to detect iron concentration in different cells with Parkinsonian, malignant and malaria diseases.[330] The concentration of iron in the substantia nigra (SN), the part of the brain which is involved in Parkinson's disease, has been found to be $\sim$160 $\mu g\ g^{-1}$ wet tissue and $\sim$670 $\mu g\ g^{-1}$ dry weight, both in control and Parkinson's samples using MS. Mössbauer spectra of ferritin, obtained at different temperatures show very characteristic features, owing to the supermagnetism of the iron core. This together with the different Mössbauer parameters found in whole SN and in isolated NM (nucleomelanin), suggests that most of the iron observed in isolated NM became attached to NM during the isolation procedure.[330] The spectra from SN which were separated from brains, which had been stored in formalin for longer periods, were different from those observed in fresh frozen tissues. Nevertheless, the concentration of iron found in formalin-stored samples was the same as in fresh samples.

MS has also contributed to the study of blood disease. With MS, large amounts of non-Hb iron were found in erythrocytes of patients with β-thalassemia major and intermedia, with Hb-H disease, with sickle cell anaemia and with other haemoglobinopathies. Depending on the spectra obtained at different temperatures, this disease can be detected by finding an additional compound, such as ferritinlike iron, at higher temperature. Large amounts of ferritinlike iron were observed in red blood cells (RBC) affected by several blood diseases. Deferral removed iron from serum, but not from red blood cells. MS of normal RBC shows two doublets corresponding to oxy- and deoxy-Hb. In β-thalassemic RBC, besides the doublets corresponding to oxy- and deoxy-Hb, an additional component was identified as due to ferritinlike iron. The f-factor of the ferritinlike iron is much larger at higher temperatures than that of Hb iron and the subspectrum corresponding to ferritinlike iron. At 4·1 K, this subspectrum splits into a well defined magnetic sextet.

MS was applied to the study of malaria by looking at rat RBC infected with *Plasmodium berghei* parasites *in vivo* and at human RBC infected with *P. falciparum in vitro*.[331,332] The iron in the malarial pigment of rats infected by *P. berghei* was found to be trivalent with high spin. It was found that the f-factor of pigment iron at higher temperatures is much larger than that of Hb iron. At 4·1 K, part of the pigment iron yields a magnetic sextet. The iron compound in the malarial pigment of human blood infected by *P. falciparum* was found to be heminlike, whereas the pigment iron in rats infected by *P. berghei* was different from any known iron porphyrin. MS is also used to study ferritin and to distinguish several types of Fe(II) and Fe(III) species in it. PH dependence of Mössbauer spectra, and the subdependence on four subspectra such as Fe(III) relaxation spectrum, Fe(III) cluster doublet, Fe(III) dimer doublet, Fe(II) doublet, and the effect of varying the number of Fe atoms/molecules on Mössbauer spectra, dependence on the time the sample is held at room temperature, bonding strength of different species

are all parameters which MS depends upon to study ferritin.[333] Though the Mössbauer effect has the disadvantage of being a slow technique (at least 1 day), its advantage is that it provides the possibility of determining straightforwardly the oxidation state of iron, and it allows the identification of various iron surroundings within the protein and the quantitative determination of the relative amount of each species present. By mixing ^{57}Fe and ^{56}Fe in the samples, processes can be investigated, which cannot be seen directly by any other technique. By measuring Mössbauer spectra in different variants, which were frozen at different times after iron loading, it was possible to follow the changes in the amount of different iron species. This measurement is based on the above parameters, and this is how MS characterises ferritin. In the present study, four different Fe(III) and two different Fe(II) species were identified; they are isolated Fe(III) atoms, Fe(III) dimers, small iron aggregates, large iron aggregates and divalent iron.[333] The process of storing iron molecules from their uptake by the ferritin protein from a solution of Fe_2SO_4 to the building of the iron core in a ferritin protein has been widely studied by Bauminger and Harrison.[334] Mössbauer studies on horse spleen and human recombinant ferritins showed the path of iron through five different Fe(III) species and two Fe(II) intermediate species. Among them, a peroxo-bridged and an oxo-bridged dimer, a monomer, small iron clusters and large iron aggregates are present. The path that evolves is: free Fe(II) in solution→2Fe(II) protein-bound sites→peroxo Fe(III) dimer→μ-oxo-bridged Fe(III) dimer→Fe(III) monomers→small Fe(III) clusters→large ferrihydrite-like clusters. In agreement with other methods, it has indicated that the threefold channels play a major role in enabling Fe(II) entry into the protein. The oxidation takes place first at the di-nuclear centre and later also on the iron core. In order to establish the different roles of H and L chains and in order to identify the sites on the protein shell where oxidation takes place and the different iron species form, variants of recombinant L (rHuLF) and H (rHuHF) homopolymers,[335] in which some amino acids were altered by site directed mutagenesis, were examined by MS.[336] It has been found that the iron clusters form faster in rHuLF protein. When Fe(II) oxidation takes place on the core surface of ferritin, the oxidation stoichiometry changed from $2Fe(II)/O_2$ to $4Fe(II)/O_2$ and produced water instead of peroxide. This process is actually minimising the production of hydroxyl radicals that are responsible for tissue damage. The formation of a peroxo dimer was the first oxidation step and its conversion to a μ-oxo-bridged dimer within a few seconds of the formation of peroxo dimers. Mainly monomers, but possibly also dimers, can then move into the inner surface of the ferritin molecule where they start to form the iron core clusters which can then attract Fe(II) and oxidise on the mineral surface.[337]

From the above discussion, it is understood that MS gives useful information about different properties of the biological sample and the amount of iron in it. It shows that the MS technique determined various structural changes in the molecules and plays a major role in determining the iron content. In biomedical studies, it has many applications including studies dealing with protein molecules and diseases. Mössbauer studies of some iron containing biomolecules and model compounds demonstrate the possibilities of various structural changes in the molecules by determining the electronic and magnetic states of iron. Variations of Mössbauer hyperfine parameters are related to modification of the iron environment in molecules as well as changes in biological functions. Both possibilities are very important for biomedical research because one can study various pathological states of the body at the molecular level.

Conclusions

MS is a widely applicable tool to investigate both microscopic and macroscopic properties. Mössbauer spectra provide a valuable complement to conventional techniques in characterising magnetic, chemical and structural properties of materials. It gives information on the magnetic moment and on the type of magnetic order of the iron atoms in the materials studied. Measurements of the isomer shift and quadrupole splitting give additional information and, together with hyperfine field data, provide a useful check on the chemical and metallurgical analysis of the samples under study. This technique also demonstrates the possibility to observe changes in the quantity of iron containing molecules. Variations of Mössbauer hyperfine parameters may be related to modification of the iron environment in the molecule as well as changes in biological functions. The present review article has given a brief discussion of the application of MS in materials research from nanoscience to astrophysics and including biology and biotechnology.

Acknowledgements

I would like to thank Professor N. Chakraborti and Dr T. S. Sudarshan for their keen interest in this work.

References

1. R. L. Mössbauer: *Z. Physik.*, 1958, **151**, 124; *Naturwissenschaften*, 1958, **45**, 538; *Z. Naturforsch. A*, 1959, **14**, 211.
2. N. Benczer-Koller and R. H. Herber: in 'Chemical application of Mössbauer spectroscopy', (ed. V. I. Goldenskii and R. H. Herber); 1968, New York, Academic Press.
3. U. Gonser: in 'Mössbauer spectroscopy', (ed. U. Gonser); 1975, Berlin, Heidelberg, Spinger-Verlag.
4. N. N. Greenwood and T. Gibbs: 'Mössbauer spectroscopy'; 1971, London, Chapman and Hall.
5. G. M. Bancroft: 'Mössbauer spectroscopy, an introduction for inorganic chemists and geochemists'; 1973, London, McGraw-Hill.
6. A. Vertes, A. Kores and K. Burger: 'Mössbauer spectroscopy'; 1979, Amsterdam, Elsevier Scientific Publishing Co.
7. V. G. Bhide: 'Mössbauer effect and its applications'; 1973, New Delhi, Tata McGraw-Hill.
8. I. J. Gruverman (ed.): 'Mössbauer effect methodology', Vols. 1–9; 1964–1974, New York, Plenum Press.
9. H. Wegener: 'Der Mössbauer Effekt'; 1966, Mannheim, Bibliographisches Institut AG.
10. S. Margulies and J. R. Ehrman: *Nucl. Instrum. Methods*, 1961, **12**, 131–137.
11. Proc. 4th Int. Symp. on 'Industrial applications of the Mössbauer effect', ISIAME, 2000, Virginia Beach, Virginia, August 2000, *Hyperfine Interact.*, 1998, **112**.
12. Proc. 5th Int. Symp. on 'Industrial applications of the Mössbauer effect', ISIAME'96, Johannesburg, South Africa, November 1996, *Hyperfine Interact.*, 2001, **136**.
13. Proc. Int. Conf. on 'Applications of the Mössbauer effect', ICAME'97, Rio de Janeiro, Brazil, September 1997, *Hyperfine Interact.*, 1998, **113**; *Hyperfine Interact.*, 1998, **C3**.
14. Proc. Int. Conf. on 'Applications of the Mössbauer effect', ICAME'99, Garmisch-Partenkirchen, Germany, September 1997, *Hyperfine Interact.*, 2000, **126**.

15. Proc. 6th Latin American Conf. on 'Applications of the Mössbauer effect', LACAME'98, Cartegena de Indus, Colombia, September 1998, *Hyperfine Interact.*, 1999, **122**; *Hyperfine Interact.*, 1999, **C4**.
16. Proc. 6th Latin American Conf. on 'Applications of the Mössbauer effect', LACAME 2000, Caracas, Venezuela, September 2000, *Hyperfine Interact.*, 2001, **133**.
17. D. C. Cook: *Hyperfine Interact.*, 2002, **141–142**, 21–34.
18. D. L. Nagy, L. Bottyan, L. Deak, B. Degroote, J. Dekoster, O. Leupold, M. Major, J. Meersschaut, R. Rüffer, E. Szilagyi and A. Vantomme: *Hyperfine Interact.*, 2002, **141–142**, 459–464.
19. U. Kripalani, M. W. Regehr and B. Fultz: *Hyperfine Interact.*, 2002, **139–140**, 667–672.
20. F. J. Berry: *Hyperfine Interact.*, 2002, **144–145**, 381–390.
21. A. Achterhold, W. Sturhahn, E. E. Alp and F. G. Parak: *Hyperfine Interact.*, 2002, **141–142**, 3–12.
22. D. G. Rancourt and J. Y. Ping: *Nucl. Instrum. Methods B: Beam Interact. Mater. Atoms*, 1991, **58**, 85–97.
23. H. Ahonen, P. A. De Souza Jr and V. K. Garg: *Nucl. Instrum. Methods B: Beam Interact. Mater. Atoms*, 1997, **124**, 633–638.
24. Z. Klencsar: *Nucl. Instrum. Methods B: Beam Interact. Mater. Atoms*, 1997, **129**, 527–533.
25. P. A. De Souza Jr, R. Garg and V. K. Garg: *Hyperfine Interact.*, 1998, **112**, 275–278.
26. D. Guenzburger, D. E. Ellis and Z. Zeng: *Hyperfine Interact.*, 1998, **113**, 25–36.
27. N. Chakraborti: *Int. Mater. Rev.*, 2004, **49**, 246–260.
28. E. Molins and A. Roig: *Hyperfine Interact.*, 2002, **141–142**, 125–129.
29. P. A. De Souza Jr, V. K. Garg, G. Klingelhöfer, R. Gellert and P. Gütlich: *Hyperfine Interact.*, 2002, **139–140**, 705–714.
30. G. P. Huffman and F. E. Huggins: *AIP Conf. Proc.*, 1982, **84**, 149–201.
31. H. K. Chow and R. L. Bognor: in 'Developments in applied spectroscopy', Vol. 8, (ed. E. L. Grave); 1970, New York, Plenum Press.
32. K. J. Kim and L. H. Schwartz: *J. Phys. Coll.* 1976, **C6**, 405.
33. K. R. P. M. Rao: in 'Industrial applications of the Mössbauer effect', (ed. G. J. Long and J. G. Stevens); 1985, 153–170, New York, Plenum Press.
34. W. J. S. Takei and R. L. Ruby: *Phys. Rev.*, 1962, **126**, 49–52.
35. G. N. Belozerski and Tu. A. Nemilov: *Fiz. Trved. Tela (St. Petersburg)*, 1963, **5**, 3350.
36. T. Shinjo, H. Itoh. H. Takaki, Y. Nakamura and N. Shikazono: *J. Phys. Soc. Jpn*, 1964, **19**, 1252.
37. L. J. Swartzendruber and L. H. Bennett: *Acta Metall.*, 1972, **6**, 737–742.
38. J. M. D. Coey: *Phys. Worlds*, 1993, **6**, 25.
39. M. Kopcewicz, J. Jagielski and A. Turos and D. L. Williamson: *J. Appl. Phys.*, 1992, **71**, 4217–4226.
40. M. Kopcewicz, J. Jagielski and G. Gawlik: *Nucl. Instrum. Methods B: Beam Interact. Mater. Atoms*, 1995, **95**, 208–212.
41. K. Oda, K. Umezu and H. Ino: *J. Phys. Condens. Matter*, 1990, **2**, 10147–10158.
42. P. Schaaf: *Hyperfine Interact.*, 1998, **111**, 113–119.
43. G. Marest, C. Skoutarides, Th. Barnavon, J. Tousset, S. Fayeulle and M. Robelet: *Nucl. Instrum. Methods*, 1983, **209–210**, 259–265.
44. N. Moncoffre, G. Marest, S. Hiadsi and J. Tousset: *Nucl. Instrum. Methods B: Beam Interact. Mater. Atoms*, 1986, **15**, 620–624.
45. V. N. Koinkar, S. M. Chaudhari, S. M. Kanetkar and S. B. Ogale: *Thin Solid Films*, 1989, **15**, 335–342.
46. M. A. El Khakani, H. Jaffrezic, G. Marest, N. Moncoffre and J. Tousset: *Mater. Sci. Eng.*, 1989, **115**, 37–42.
47. S. M. M. Ramos, L. Amaral, M. Behar, G. Marest, A. Vasquez and F. C. Zawislak: *Mater. Sci. Eng. A*, 1989, **115**, 31–36.
48. T. R. Jervis, D. L. Williamson, J. P. Hirvonen and T. G. Zocco: *Mater. Lett.*, 1990, **9**, 379–383.
49. M. A. El Khakani, G. Marest, N. Moncoffre and J. Tousset: *Surf. Coat. Technol.*, 1992, **51**, 87–92.
50. V. V. Uglov, J. A. Fedotova, A. K. Kuleshov, A. L. Danilyuk, N. T. Kvasov, R. Günzel, R. Reuther and E. Richter: *Surf. Coat. Technol.*, 2001, **136**, 226–230.
51. S. J. Choi, S. J. Kwon, S. H. Choo and S. Lee: *Mater. Sci. Eng. A*, 1999, **265**, 208–216.
52. A. L. Kholmetskii, V. M. Anischik, V. V. Uglov, D. P. Rusalsky, A. K. Kuleshov and J. A. Fedotova: *Vacuum*, 2003, **69**, 521–527.
53. V. G. Gavriljuk: *Mater. Sci. Eng. A*, 2003, **345**, 81–89.
54. V. A. Shabashov, L. G. Korshunov, A. G. Mukoseev, V. V. Sagaradze, A. V. Makarov, V. P. Pilyugin, S. I. Novikov and N. F. Vildanova: *Mater. Sci. Eng. A*, 2003, **346**, 196–207.
55. A. I. Deryagin, V. A. Zavalishin and V. V. Sagaradze: *Nanostruct. Mater.*, 1998, **10**, 411–418.
56. J. H. Ladriere and X. J. He: *Mater. Sci. Eng.*, 1986, **77**, 133–138.
57. Z. Fucheng and L. Tingquan: *Wear*, 1997, **212**, 195–198.
58. M. B. Stearns: *Phys. Rev.*, 1966, **147**, 439–453; *J. Appl. Phys.*, 1964, **35**, 1095–1096.
59. L. Cser, J. Ostanevich and L. Pal: *Phys. Status Solidi*, 1967, **20**, 581–589.
60. L. Cser, J. Ostanevich and L. Pal: *Phys. Status Solidi*, 1967, **20**, 591–596.
61. M. R. Lesoille and P. M. Gielen: *Phys. Status Solidi*, 1970, **37**, 127–139.
62. R. Hergt, E. Wieser, H. Gengnagel and A. Gladun: *Phys. Status Solidi*, 1970, **41**, 255–263.
63. I. Vincze and L. Cser: *Phys. Status Solidi B*, 1972, **50**, 709–715.
64. G. A. Perez Alcazar and E. Galvao da Silva: *J. Phys. F Metal Phys.*, 1987, **17**, 2323–2335.
65. E. P. Yelusov, E. V. Voronia and V. A. Barinov: *J. Magn. Magn. Mater.*, 1992, **115**, 271–280.
66. D. Bandyopadhyay, S. Suwas, R. M. Singru and S. Bhargava: *J. Mater. Sci.*, 1998, **33**, 109–116.
67. C. E. Johnson, M. S. Ridout and T. E. Cranshaw: *Proc. Phys. Soc.*, 1963, **81**, 1079–1090.
68. T. E. Cranshaw: *J. Phys. F Metal Phys.*, 1972, **2**, 615–624.
69. C. E. Guillaume: *C. R. Acad. Sci.*, 1897, **125**, 235.
70. D. C. Price and G. Hembree: *Solid State Commun.*, 1973, **12**, 925–929.
71. Z. Eliezer, S. Nadiv (Niedzwiedz), M. Ron and B. Z. Weiss: *Mater. Sci. Eng.*, 1973, **11**, 269–273.
72. J. Hesse and J. B. Müller: *Solid State Commun.*, 1977, **22**, 637–642.
73. T. Sohmura and F. E. Fujita: *J. Magn. Magn. Mater.*, 1979, **10**, 255–256.
74. U. Gonser, S. Nasu and W. Kappes: *J. Magn. Magn. Mater.*, 1979, **10**, 244–251.
75. D. G. Rancourt, P. Hargraves, G. Lamarche and R. A. Dunlap: *J. Magn. Magn. Mater.*, 1990, **87**, 71–82.
76. B. N. Goshchitskii, V. V. Sagaradze, A. G. Mukoseev and V. A. Shabashov: *Mater. Sci. Eng. A*, 1999, **273–275**, 453–456.
77. Y. A. Abdu, H. Annersten, T. Ericsson and P. Nordblad: *J. Magn. Magn. Mater.*, 2004, **280**, 243–250.
78. J. Chappert and R. B. Frankel: *Phys. Rev. Lett.*, 1967, **19**, 570–572.
79. R. J. Pollard: *J. Phys. Condens. Matter*, 1990, **2**, 983–991.
80. Q. A. Pankhurst and R. J. Pollard: 'Mössbauer spectroscopy applied to magnetism and materials science', Vol. 1, (ed. G. J. Long and F. Grandjean), 77–113; 1993, New York, Plenum Press.
81. J. M. D. Coey and P. W. Readman: *Nature*, 1973, **246**, 476–478.
82. G. Ferey, F. Varret and J. M. D. Coey: *J. Phys. C Solid State Phys.*, 1979, **12**, L531–L537.
83. R. J. Pollard and Q. A. Pankhurst: *J. Phys. Condens. Matter*, 1992, **4**, L317–L323.
84. J. M. Greneche, J. Linares, F. Varret, Y. Lalignant and G. Ferey: *J. Magn. Magn. Mater.*, 1988, **73**, 115–122.
85. C. Meyer, F. Hartmann-Boutron and Y. Gros: *J. Magn. Magn. Mater.*, 1986, **46**, 254–266.
86. M. Reissner, W. Steiner, J. P. Kappler, P. Bauer and M. J. Besnus: *J. Phys. F Metal Phys.*, 1984, **14**, 1249.
87. A. Pösinger, H. Winkler and W. Steiner: *J. Phys. Condens. Matter*, 1993, **5**, 3653–3662.
88. T. Bauermann, M. M. Abd-Elmeguid, J. P. Sanchez, T. Takabatake and H. Micklitz: *J. Phys. C Solid State Phys.*, 1983, **16**, 6435–6442.
89. A. K. Majumdar and P. von Blanckenhagen: *Phys. Rev. B*, 1984, **29**, 4079–4085.
90. B. Huck and J. Hesse: *J. Magn. Magn. Mater.*, 1989, **78**, 247–254.
91. D. Bandyopadhyay: *J. Phys. Condens. Matter*, 1999, **11**, 1199–1209.
92. D. Bandyopadhyay: *Z. Metallkd.*, 2000, **91**, 171–174.
93. D. Bandyopadhyay: Int. Conf. on 'Advances in materials and materials processing' (ICAMMP), (ed. N. Chakraborti and U. K. Chatterjee), 754–757; 2002, Tata McGraw-Hill.
94. D. Bandyopadhyay, R. M. Singru and A. K. Majumdar: *Z. Metallkd.*, 2001, **92**, 367–369.
95. D. Bandyopadhyay, R. M. Singru and A. K. Majumdar: *Hyperfine Interact.*, 1999, **122**, 239–252.
96. R. J. Weiss: *Proc. Phys. Soc.*, 1963, **82**, 281–288.
97. W. Klement, R. H. Willens and P. Duwez: *Nature*, 1960, **187**, 869.
98. Y. Yoshizawa, S. Oguma and K. Yamauchi: *J. Appl. Phys.*, 1988, **64**, 6044–6049.
99. J. M. Greneche, M. Henry and F. Varret: *J. Magn. Magn. Mater.*, 1982, **26**, 153–156.
100. J. M. Greneche and F. Varret: *J. Phys. C Solid State Phys.*, 1982, **15**, 5333–5344.
101. G. Barault, L. Rohr and J. M. Greneche: *J. Magn. Magn. Mater.*, 1993, **128**, 258–266.
102. M. Bourrous, M. Henry, J. M. Greneche and F. Varret: 'Rapidly quenched metals', (ed. S. Steeb and H. Warlimont), 1231; 1985, Amsterdam, North Holland.
103. D. Bandyopadhyay: *Hyperfine Interact.*, 2000, **131**, 111–120.
104. D. Bandyopadhyay: *Mater. Res. Bull.*, 2000, **34**, 2369–2374.
105. D. Bandyopadhyay: *Solid State Commun.*, 1999, **109**, 611–614.

106. D. Bandyopadhyay: 'Mössbauer spectroscopic studies of some iron-based alloys, metallic glasses and minerals', PhD thesis, Indian Institute of Technology, Kanpur, India, 1996.
107. A. Samanta and D. Bandyopadhyay: *Z. Metallkd.*, 1999, **90**, 335–337.
108. D. Bandyopadhyay and R. M. Singru: *J. Mater. Sci. Lett.*, 1998, **17**, 2025–2027.
109. N. Banerjee, U. C. Jouri, V. N. Kulkarni and R. M. Singru: *J. Mater. Sci.*, 1995, **30**, 417.
110. T. Nagarajan, U. C. Ansari, S. Srinivasan, V. Sridharan and A. Narayanasamy: *Mater. Sci. Eng.*, 1988, **97**, 355–359.
111. A. K. Bhatnagar and N. Ravi: *Phys. Rev. B*, 1983, **28**, 359–367.
112. M. Kosimura and M. Takahashi: Proc. Int. Conf. on 'Rapidly quenched metals', Sendai, 1981.
113. M. Kosimura, A. Abe, M. Takahashi, S. Inawashiro and S. Katsura: Proc. Int. Conf. on 'Rapidly quenched metals', Sendai, 1981.
114. M. Kosimura, S. Ishio and T. Miyazaki: *Sci. Rep. Tohoku Univ.*, 1980, **28A**, 299.
115. M. Sagawa, S. Fujimura, N. Togawa, H. Yamamoto and Y. Matsuura: *J. Appl. Phys.*, 1984, **55**, 2083–2087.
116. J. J. Croat, J. F. Herbst, R. W. Lee and F. E. Pinkerton: *Appl. Phys. Lett.*, 1984, **44**, 148–149.
117. G. C. Hadjipanayis, R. C. Hazelton and K. R. Lawless: *J. Appl. Phys.*, 1984, **55**, 2073–2077; *Hyperfine Interact.*, 1984, **72**, 111.
118. J. M. D. Coey and H. Sun: *J. Magn. Magn. Mater.*, 1990, **87**, L251–L254.
119. J. M. D. Coey and D. P. E. Hurley: *J. Magn. Magn. Mater.*, 1992, **104–107**, 1098–1101.
120. R. Fruchart, P. L'Heritier, P. Dalmas, D. Fruchart, P. Wolfers, J. M. D. Coey, L. P. Ferreira, P. Guillen, P. Vulliet and A. Yaouanc: *J. Phys. F Metal Phys.*, 1987, **17**, 483–501.
121. H. Onodera, Y. Yamaguchi, H. Yamamoto, M. Sagawa, Y. Matsuura and H. Yamomoto: *J. Magn. Magn. Mater.*, 1984, **46**, 151–156.
122. F. E. Pinkerton and W. R. Dunham: *Appl. Phys. Lett.*, 1984, **45**, 1248–1250.
123. M. Rosenberg, P. Deppe, M. Wojcik and H. Stadelmeir: *J. Appl. Phys.*, 1985, **57**, 4124–4126.
124. L. R. K. Rosenberg, R. F. Oliveira, H. R. Rechenberg and F. P. Missell: *J. Appl. Phys.*, 1985, **57**, 4127–4129.
125. J. M. D. Coey, J. M. Cadogan and D. H. Ryan: 'Nd–Fe permanent magnets – their present and future applications', (ed. I. V. Mitchell), 143; 1985, Amsterdam, Elsevier.
126. R. Eibler, R. Grössinger, G. Hilscher, H. R. Kirchmayr, O. Mayerhofer, H. Sassik, X. K. Sun and G. Wiesinger: in 'Nd–Fe permanent magnets – their present and future applications', (ed. I. V. Mitchell), 167; 1985, Amsterdam, Elsevier.
127. D. Givord, S. H. Li and J. M. Moreau: *Solid State Commun.*, 1984, **50**, 497–499.
128. C. B. Shoemaker, D. P. Shoemaker and R. Fruchart: *Acta Crystallogr. C*, 1984, **40**, 1665–1668.
129. J. F. Herbst, J. J. Croat and W. B. Yelon: *J. Appl. Phys.*, 1985, **57**, 4086–4090.
130. D. Givord, J. M. Moreau and P. Tenaud: *Solid State Commun.*, 1985, **55**, 303–306.
131. W. Kümmerle and U. Gradmann: *Solid State Commun.*, 1977, **24**, 33–35.
132. K. H. J. Buschow, A. M. van Dipen, N. M. Beekmans and J. W. M. Biesterbos: *Solid State Commun.*, 1978, **28**, 181–185.
133. M. Boge, G. Czjzek, D. Givord, C. Jeandey, H. S. Li and J. L. Oddou: *J. Appl. Phys.* F Metal Phys., 1986, **16**, L67–L72.
134. R. Coehoorn and J. H. K. Buschow: *J. Magn. Magn. Mater.*, 1993, **118**, 175–181.
135. J. M. D. Coey and Q. Qi: *Hyperfine Interact.*, 1994, **90**, 265–284.
136. Q. Qi, H. Sun and J. M. D. Coey: *Hyperfine Interact.*, 1991, **68**, 27–38.
137. A. I. C. Persiano, J. D. Ardisson, R. A. Mansur, C. C. Colucci and S. Gama: *Hyperfine Interact.*, 1994, **83**, 209–215.
138. A. I. C. Persiano, J. D. Ardisson, F. A. Batista, C. C. Colucci and S. Gama: *J. Magn. Magn. Mater.*, 1994, **136**, 149–157.
139. A. H. Morrish, Z. W. Li, X. Z. Zhou and S. Dai: *J. Phys. D Appl. Phys.*, 1996, **29**, 2290–2296 and references therein.
140. Z. Zeng, D. R. Sanchez, D. Guenzburger, D. E. Ellis, E. M. Baggio-Saitovitch and H. Micklit: *Phys. Rev. B*, 1997, **55**, 3087–3092.
141. R. Nakayama and T. Takeshita: *J. Alloys Comp.*, 2003, **193**, 259–261.
142. P. J. McGuiness, C. Short, A. F. Wilson and I. R. Harris: *J. Alloys Comp.*, 1992, **184**, 243–255.
143. T. Takeshita: *J. Alloys Comp.*, 1993, **193**, 231–234.
144. F. D. Saccone, F. H. Sanchez, C. Rodrigue Torres, B. Gebel and O. Gutfleisch: *J. Magn. Magn. Mater.*, 2001, **226–230**, 1461–1463.
145. A. Ashfaq, M. Matsuura, N. Ikuta and M. Sakurai: *J. Appl. Phys.*, 1999, **85**, 5681–5683.
146. O. S. Zarechnyuk and P. I. Kripyakevich: *Sov. Phys. Crystallogr.*, 1963, **7**, 436.
147. K. H. J. Buschow and A. M. van der Kraan: *J. Phys. F Metal Phys.*, 1978, **8**, 921–932.
148. I. Felner, I. Nowik, M. She and K. H. J. Buschow: *J. Magn. Magn. Mater.*, 1982, **27**, 61–64.
149. J. A. Paixao, M. Ramos Silva, S. Sa Sorensen, B. Lebech, G. H. Lander, P. J. Brown, S. Langridge, E. Talik and A. P. Gongalves: *Phys. Rev. B*, 2000, **61**, 6176–6188.
150. P. Gaczynski, F. G. Vagizov, W. Suski, B. Kotur, W. Iwasieczko and H. Drulis: *J. Magn. Magn. Mater.*, 2001, **225**, 351–358.
151. P. Gaczynski, F. G. Vagizov, W. Suski, B. Kotur, K. Wochowski and H. Drulis: *J. Magn. Magn. Mater.*, 2000, **214**, 37–43.
152. J. Pszczola, P. Stoch, J. Suwalski and J. Zukrowski: *J. Alloys Comp.*, 2004, **364**, 29–36.
153. H. Chiriac, N. Lupu and J. M. Greneche: *J. Magn. Magn. Mater.*, 2002, **242–245**, 1310–1313.
154. G. J. Long, O. A. Pringle, P. C. Ezekwenna, S. R. Mishra, D. Hautot and F. Grandjean: *J. Magn. Magn. Mater.*, 1998, **186**, L10–L20.
155. Q. Wang, B. Gu and X. Zhang: J. Phys. Condens. Matter, 1990, **2**, 9815–9820.
156. H. B. Haung, W. J. Zheng, Y. D. Dai, Y. He and Y. F. Hsia: *Physica B*, 2003, **328**, 271–275.
157. S. Nasu, T. Kawakami, S. Kawasaki and M. Takano: *Hyperfine Interact.*, 2002, **144–145**, 119–127.
158. A. P. Douvalis, M. Venkatesan, J. M. D. Coey, T. Alamelu and U. V. Varadaraju: *Hyperfine Interact.*, 2002, **144–145**, 267–272.
159. M. N. Baibich, J. M. Broto, A. Fert, F. Nguyen van Dau, F. Petroff, P. Eitenne, G. Creuzet, A. Friederich and J. Chazelas: *Phys. Rev. Lett.*, 1988, **61**, 2472–2475.
160. E. E. Fullerton, J. S. Jiang and S. D. Bader: *J. Magn. Magn. Mater.*, 1999, **200**, 392–404.
161. E. E. Fullerton, J. S. Jiang, M. Grimsditch, C. H. Sowers and S. D. Bader: *Phys. Rev. B*, 1998, **58**, 12193–12200.
162. R. Skomski and J. M. D. Coey: *Phys. Rev. B*, 1993, **48**, 15812–15816.
163. E. Goto, N. Hayashi, T. Miyashita and K. Nakagawa: *J. Appl. Phys.*, 1965, **36**, 2951–2958.
164. G. J. Bowden, J. M. L. Beaujour, S. Gordeev, P. A. J. de Groot, B. D. Rainford and M. Sawicki: *J. Phys. Condens. Matter*, 2000, **12**, 9335–9346.
165. P. Grünberg, R. Schreiber, Y. Pang, M. B. Brodsky and H. Sower: *Phys. Rev. Lett.*, 1986, **57**, 2442–2445.
166. T. Shinjo: in 'Advances in condensed matter science', (ed. S. Maekawa and T. Shinijo), vol. 3; 2002, Taylor & Francis.
167. N. Hosoito, K. Kawaguchi, T. Shinjo, T. Takada and Y. Endoh: *J. Phys. Soc. Jpn*, 1984, **53**, 2659–2667.
168. E. Nordström, B. Kalska, L. Häggström, P. Blomqvist and R. Wäppling: *Hyperfine Interact.*, 2002, **141–142**, 465–469.
169. A. P. Kuprin, L. Cheng, Z. Altounian and D. H. Ryan: *Hyperfine Interact.*, 2002, **144/145**, 141–149.
170. V. Uzdina, W. Keuneb and M. Walterfangb: *J. Magn. Magn. Mater.*, 2002, **240**, 504–507.
171. J. Balogh, D. Kaptas, T. Kemeny, L. F. Kiss, T. Pusztai and I. Vincze: *Hyperfine Interact.*, 2002, **141–142**, 13–20.
172. R. Gupta, A. Gupta, D. K. Avasthi, G. Principi and C. Tosello: *Nucl. Instrum. Methods B: Beam Interact. Mater. Atoms*, 1999, **156**, 153–157.
173. E. Kuzmann, G. Principi, C. Tosello, K. Havancsak, S. Stichleutner, I. Gerócs, Z. Homonnay and A. Vertes: *Nucl. Instrum. Methods B: Beam Interact. Mater. Atoms*, 2001, **183**, 425–431.
174. T. Shinjo: *Surf. Sci. Rep.*, 1991, **12**, 51–98.
175. J. Bland: 'A Mössbauer spectroscopy and magnetometry study of magnetic multilayers and oxides', PhD thesis, Department of Physics, University of Liverpool, 2002, 79.
176. M. F. Thomas, J. Bland, G. S. Case, J. A. Hutchings and O. Nikolov: *Hyperfine Interact.*, 2000, **126**, 377–386.
177. Y. Kobayashi, S. Nasu, T. Emoto and T. Shinjo: *J. Magn. Magn. Mater.*, 1996, **156**, 45–46.
178. T. Emoto, N. Hosoito and T. Shinjo: *J. Magn. Magn. Mater.*, 1996, **156**, 47–48.
179. A. Gupta, A. Paul, R. Gupta, D. K. Avasthi and G. Principi: *J. Phys. Condens. Matter*, 1998, **10**, 9669–9680.
180. Third Int. Conf. on 'Nanostructured materials', Koma, Hawaii, July 1961.
181. Fourth Int. Conf. on 'Nanostructured materials', Stockholm, Sweden, June 1998.
182. Fifth Int. Conf. on 'Nanostructured materials', Sendai, Japan 2000.
183. Proc. Workshop on 'Russian research activities on nanoparticles and nanostructured materials', St. Petersburg, Russia, August 1997.

184. Proc. workshop on 'R & D status and trends in nanoparticles, nano materials and nanodevices in the United States', Arlington, VA, May 1997.
185. D. Herr, M. Meyyappan and V. Zhirnov (eds.): Workshop Report: 'SRC/NASA Ames workshop on emerging opportunities and issue in nanotubes and nanoelectronics', November 1998.
186. 'Nanostructured science and technology', NSTC Report: Worldwide status and trends; 1999, Kluwer Academic Publishers.
187. 'Physics of nanostructures', (ed. J. H. Davies and A. R. Long); 1992, Bristol and Philadelphia, Institute of Physics Publishing.
188. N. J. De Nardo: 'Nanophase characterization of surfaces and interfaces'; 1994, Weinheim, New York, VCH.
189. J. H. Fendler (ed.): 'Nanoparticles and nanostructured films: preparation, characterization and applications'; 1998, Weinheim, Wiley-VCH.
190. L. V. Interrante and M. J. Hampden Smith (ed.): 'Chemistry of advanced materials: an overview'; 1998, New York: Wiley-VCH.
191. B. C. Crandall (ed.): 'Nanotechnology: molecular speculations on global abundance'; 1996, Cambridge, MA, MIT Press.
192. Y. Yoshizawa and K. Yamauchi: *Mater. Trans. JIM*, 1990, **31**, 307–314.
193. G. Herzer: *IEEE Trans. Magn.*, 1994, **30**, 4800–4802.
194. A. Hernando and T. Kulik: *Phys. Rev. B*, 1994, **49**, 7064–7067.
195. J. M. Greneche: *Hyperfine Interact.*, 2003, **148–149**, 79–89.
196. Y. L. Huang, D. S. Xue, P. H. Zhou, Y. Maa and F. S. Li: *Mater. Sci. Eng. A*, 2003, **359**, 332–337.
197. M. Vasquez-Mansilla, R. D. Zysler, C. Arciprete, M. Dimitrijewits, D. Rodriguez-Sierra and C. Saragovi: *J. Magn. Magn. Mater.*, 2001, **226–230**, 1907–1909.
198. Y. Yoshizawa, S. Ogama and K. Yamuchi: *J. Appl. Phys.*, 1988, **84**, 6044–6046.
199. M. E. McHenry, M. A. Willard and D. E. Laughlin: *Prog. Mater. Sci.*, 1999, **44**, 291–433.
200. J. Hesse, T. Graf, M. Kopecwicz, A. Afanas'ev and M. A. Chuev: *Hyperfine Interact.*, 1998, **113**, 499–506.
201. O. Hupe, H. Bremers, J. Hesse, A. Afnas'ev and M. Chuev: *Nanostruct. Mater.*, 1999, **12**, 581–584.
202. T. Girchardt, B. Friedrichs, E. Woldt, J. Hesse, K. G. Efthimiadis and S. C. Chadjivasilisou: *Nanostruct. Mater.*, 1999, **12**, 585–588.
203. O. Hupe, M. Chuev, H. Bremers, J. Hesse and A. Afnas'ev: *J. Phys. Condens. Matter*, 1999, **11**, 10545–10556.
204. A. Afnas'ev, M. Chuev and J. Hesse: *Phys. Rev. B*, 1997, **56**, 5489–5499.
205. N. Popandian, A. Narayanasamy, K. Chattopadhyay, M. Manivl Raja, K. Ganesan, C. N. Chinnasamy and B. Jeyadevan: *J. Appl. Phys.*, 2003, **93**, 6182–6187.
206. M. Manivl Raja, N. Popandian, B. Majumdar, A. Narayanasamy and K. Chattopadhyay: *Mater. Sci. Eng. A*, 2001, **304–306**, 1062–1065.
207. M. Manivl Raja, K. Chattopadhyay, B. Majumdar and A. Narayanasamy: *J. Alloys Comp.*, 2000, **297**, 199–205.
208. T. Szumiata, K. Brzozka, M. Gawronski, B. Gorka, K. Jezuita, J. S. Blazquez-Gamez, T. Kulik, R. Zuberek, A. Slawska-Waniewska and J. M. Greneche: *J. Magn. Magn. Mater.*, 2002, **250**, 83–91.
209. A. Zorkovska, J. Kova, P. Sova, P. Petrovic and M. Konc: *J. Magn. Magn. Mater.*, 215–2000, **216**, 492–494.
210. N. V. Dmitrieva, N. M. Kleinerman, V. A. Lukshina, V. V. Serikov and A. P. Potapov: *J. Magn. Magn. Mater.*, 2000, **215–216**, 453–454.
211. N. Randrianantoandro, A. Slawska-Waniewska and J. M. Greneche: *Phys. Rev. B*, 1997, **56**, 10797–10800.
212. M. Miglierini, M. Seberini, I. Toth and K. Vitazek: *J. Magn. Magn. Mater.*, 2003, **265**, 243–247.
213. Y. Il Kim, D. Kim and C. Sub Lee: *Physica B Condens. Matter*, 2003, **337**, 42–51.
214. N. Hayashi, I. Sakamoto, T. Toriyama, H. Wakabayashi, T. Okada and K. Kuriyama: *Surf. Coat. Technol.*, 2003, **169–170**, 540–543.
215. A. S. Lileev, Yu. D. Yagodkin, M. Reissner and W. Steiner: *J. Magn. Magn. Mater.*, 2003, **258–259**, 504–506.
216. M. Hasiaka, M. Miglierini, Y. Yamashiro, W. H. Ciurzynska and H. Fukunaga: *J. Magn. Magn. Mater.*, 2002, **239**, 506–508.
217. A. D. Barra-Barrera, R. K. Murakami, C. S. M. Partiti and V. Villas-Boas: *J. Magn. Magn. Mater.*, 2001, **226–230**, 1426–1427.
218. D. R. de Jesus and C. S. M. Partiti: *J. Magn. Magn. Mater.*, 2001, **226–230**, 1527–1529.
219. L. Wang and F. S. Li: *J. Magn. Magn. Mater.*, 2001, **223**, 233–237.
220. S. N. Kane, A. Gupta, L. Kraus and P. Duhaj: *J. Magn. Magn. Mater.*, 2000, **215–216**, 375–377.
221. A. Blachowicz, J. Zbroszczyk, J. Olszewski, W. H. Ciurzynska, H. Fukunaga, K. Narita, B. Wyslocki and M. Hasiak: *J. Magn. Magn. Mater.*, 2000, **215–216**, 422–424.
222. C. E. M. Campos, V. Drago, J. C. de Lima, T. A. Grandi, K. D. Machado and M. R. Silva: *J. Magn. Magn. Mater.*, 2004, **269**, 6–14.
223. G. A. Prinz: *Science*, 1990, **250**, 1092–1097.
224. G. A. Prinz: in 'Ultrathin magnetic structures II', (ed. B. Heinrich and J. A. C. Bland), 1; 1994, Berlin, Springer-Verlag.
225. F. Monteverde, A. Michel, A. Kherici and J. P. Eymery: *Thin Solid Films*, 2000, **379**, 114–121.
226. H. P. Gunnlaugsson, G. Weyer, M. Dietrich, M. Fanciulli, K. Bharuth-Ram and R. Sielemann: *Appl. Phys. Lett.*, 2002, **80**, 2657–2659.
227. Yu. L. Mikhlin, A. V. Kuklinskiy, N. I. Pavlenko, V. A. Varnek, I. P. Asanov, A. V. Okotrub, G. E. Selyutin and L. A. Solovyev: *Geochim. Cosmochim. Acta*, 2002, **66**, 4057–4067.
228. A. Roy, D. Das and J. Ghose: *Mater. Res. Bull.*, 2002, **37**, 2383–2392.
229. L. Ehm, S. Vogel, K. Knorr, P. Schmid-Beurmann and W. Depmeier: *J. Alloys Comp.*, 2002, **339**, 30–34.
230. T. Becze-Deák, L. Bottyán, P. Bonville, D. L. Nagy, B. Molnár, U. W. Pohl and H. Spiering: *J. Phys. Chem. Solids*, 2001, **62**, 987–997.
231. C. S. Kim, S. I. Park and Y. J. Oh: *J. Magn. Magn. Mater.*, 2000, **215–216**, 40–42.
232. T. Takeda, R. Kanno, Y. Kawamoto, M. Takano, S. Kawasaki, T. Kamiyama and F. Izumi: *Solid State Sci.*, 2000, **2**, 673–687.
233. I. Felner, I. Nowik and E. R. Buminger: *Hyperfine Interact.*, 1990, **61**, 1035.
234. P. Boolchand and D. McDaniel: 'Studies of high temperature superconductors', vol. 4, (ed. A. V. Narlikar); 1990, New York, Nova Science.
235. I. Felner and I. Nowik: *Superconducting Sci. Technol.*, 1955, **8**, 121–142.
236. L. Bauernfeind, W. Widder and H. F. Braun: *Physica C*, 1995, **254**, 151–158.
237. J. W. Lynn, B. Keimer, C. Ulrich, C. Bernhard and J. L. Tallon: *Phys. Rev. B*, 2000, **61**, R14964–R14967.
238. R. Kruk, R. Kmiec, P. W. Klamut, B. Dabrowski, D. E. Brown, M. Maxwell and C. W. Kimball: *Physica C*, 2002, **370**, 71–78.
239. M. E. Lines and M. Eibschutz: *Physica C*, 1990, **166**, 235–247.
240. F. Gao, D. Li, J. He, Y. Tian, D. Yu and S. Zhang: *Physica C*, 2002, **371**, 151–155.
241. R. Escamilla, T. Akachi, R. Gomez, V. Marquina, M. L. Marquina and R. Ridaura: *Physica C*, 2003, **385**, 373–382.
242. Y. Li, E. Baggio-Saitovitch, Y. B. Wang, G. H. Cao, N. Chen, Z. X. Zhao and L. Wei: *Physica C*, 1999, **315**, 129–144.
243. E. Kuzmann, M. Mair, Z. Klencsar, A. Vertes, Z. Homonnay and G. Gritzner: *Physica C*, 1999, **319**, 12–20.
244. Y. Li, J. A. Larrea, E. Baggio-Saitovitch, G. C. Che, Z. X. Zhao, G. H. Cao and Z. X. Xu: *Physica C*, 1999, **312**, 283–288.
245. E. Kuzmann, M. Mair and G. Gritzner: *Physica C*, 1999, **312**, 45–54.
246. S. V. Korostin, Yu. V. Permyakov and E. F. Makarov: *Physica C*, 2000, **336**, 137–142.
247. I. Solomon: *Compt. Rend.*, 1960, **250**, 3828.
248. J. G. Stevens, A. Khasanov, J. W. Miller, H. Pollak and Z. Li: *Hyperfine Interact.*, 1998, **117**, 71–81.
249. A. Prasad, R. M. Singru and A. K. Biswas: *Phys. Status Solidi (a)*, 1985, **87**, 267.
250. D. Bandyopadhyay, R. M. Singru and A. K. Biswas: *Miner. Eng.*, 2000, **13**, 973–978.
251. F. Habashi: 'Chalcopyrite, its chemistry and metallurgy'; 1978, New York, McGraw-Hill.
252. S. Prasad and B. D. Pandey: *Miner. Eng.*, 1998, **11**, 763–781.
253. J. Lipka, M. Miglierini, J. Sitek, P. Baláz and K. Tkácová: *Nucl. Instrum. Methods B: Beam Interact. Mater. Atoms*, 1993, **76**, 183–184.
254. R. I. Razouk: *J. Appl. Chem. (Lond.)*, 1965, **15**, 191.
255. S. P. Taneja and C. H. W. Jones: *Fuel*, 1984, **63**, 675–701.
256. H. J. Shyu, P. P. Vaishnava and P. A. Montano: *Fuel*, 1981, **60**, 1022–1026.
257. G. Klingelhöfer, S. J. Campbell, G. M. Wang, P. Held, B. Stahl and E. Kankeleit: *Hyperfine Interact.*, 1998, **111**, 335–339.
258. J. Mazo-Zuluaga, C. A. Barrero, J. Diaz-Teran and A. Jerez: *Hyperfine Interact.*, 2003, **148–149**, 153–161.
259. M. Mohapatra, S. Anand, R. P. Das, C. Upadhyay and H. C. Verma: *Int. J. Miner. Process.*, 2003, **69**, 75–86.
260. M. Mohapatra, S. Anand, R. P. Das, C. Upadhyay and H. C. Verma: *Hydrometallurgy*, 2002, **66**, 125–134.
261. M. Mohapatra, S. Anand, R. P. Das, C. Upadhyay and H. C. Verma: *Hydrometallurgy*, 2002, **65**, 227–235.
262. J. D. Betancur, J. Restrepo, C. A. Palacio, A. L. Morales, J. Mazo-Zuluaga, J. J. Fernandez, O. Perez, J. F. Valderruten and A. Bohorquez: *Hyperfine Interact.*, 2003, **148–149**, 163–175.
263. S. J. Stewart, R. A. Borzi, E. D. Cabanillas, G. Punte and R. C. Mercader: *J. Magn. Magn. Mater.*, 2003, **260**, 447–454.

264. C. J. Warris and P. G. McCormic: *Miner. Eng.,* 1997, **10**, 1119–1125.
265. A. F. Mulaba-Bafubianandi, H. Pollak, M. Mashlan, D. Jancik and A. Kholmetskii: *Miner. Eng.*, 2001, **14**, 445–448.
266. H. Dong, J. K. Fredrickson, D. W. Kennedy, J. M. Zachara, R. K. Kukkadapu and T. C. Onstott: *Chem. Geol.*, 2000, **169**, 299–318.
267. D. A. Brown, B. L. Sherriff, J. A. Sawicki and R. Sparling: *Geochim. Cosmochim. Acta*, 1999, **63**, 2163–2169.
268. G. Klingelhöfer, B. Bernhardt, J. Foh, U. Bonnes, D. Rodionov, P. A. Dd Souza, Ch. Schröder, R. Gellert, S. Kane, P. Gütlich and E. Kankeleit: *Hyperfine Interact.*, 2002, **144–145**, 371–379.
269. G. Klingelhöfer, P. Held, R. Teucher, F. Schlichting, J. Foh and E. Kankeleit: *Hyperfine Interact.*, 1995, **95**, 305–339.
270. http://iacgu7.chemie.uni-mainz.de/klingelhoefer/mer.html
271. M. D. Dyar and M. W. Schaefer: *Earth Planet. Sci. Lett.*, 2004, **218**, 243–259.
272. R. V. Morris, G. Klingelhöfer, R. L. Korotev and E. D. Shelfer: *Hyperfine Interact.*, 1998, **117**, 405–432.
273. P. Gay, G. M. Bancroft and M. G. Brown: Proc. '1st Lunar Planet. Sci. Conf.', 1970, 481.
274. R. M. Housley, R. W. Grant, A. H. Muir Jr, M. Blander and M. Abdel-Gawad: Proc. '2nd Lunar Planet. Sci. Conf.', 1971, 2125.
275. C. L. Herzenberg and D. L. Riley: Proc. '1st Lunar Planet. Sci. Conf.', 1970, 2221.
276. T. C. Gibb, R. Greatrex, N. N. Greenwood and M. H. Battey: Proc. '3rd Lunar Planet. Sci. Conf.', 1972, 2479.
277. R. M. Housley, M. Blander, M. Abdel-Gawad, R. W. Grant and A. H. Muir Jr: Proc. '1st Lunar Planet. Sci. Conf.', 1970, 2251.
278. S. Mitra: 'Applied Mössbauer spectroscopy, theory and practice for geochemists and archaeologists'; 1992, New York, Pergamon.
279. P. A. Bland, F. J. Berry, A. J. T. Jull, T. B. Smith, A. W. R. Bevan, J. M. Cadogan, A. S. Sexton, L. A. Franchi and C. T. Pillinger: *Hyperfine Interact.*, 2002, **142**, 481–494.
280. G. P. Huffman and F. E. Huggins: *Fuel*, 1978, **57**, 592–604.
281. S. P. Taneja and C. H. W. Jones: *Fuel*, 1984, **63**, 695–701.
282. K. Asami, P. Sears, E. Furimsky and Y. Ohtsuka: *Fuel Process. Technol.*, 1996, **47**, 139–151.
283. J. C. Medina, S. J. Butala, C. H. Bartholomew and M. L. Lee: *Fuel*, 2000, **79**, 89–93.
284. J. C. Medina, S. J. Butala, C. H. Bartholomew and M. L. Lee: *Geochim. Cosmochim. Acta*, 2000, **64**, 643–649.
285. J. Ozaki, Y. Nishiyama, J. D. Cashion and L. J. Brown: *Fuel*, 1999, **78**, 489–499.
286. M. A. Ahmed, R. E. Vandenberghe, E. De Grave, N. A. Eissa and J. V. Ibarra: *Fuel*, 1999, **78**, 453–457.
287. S. V. Pysh'yev, V. I. Gayvanovych, A. Pattek-Janczyk and J. Stanek: *Fuel,* 2004, **83**, 1117–1122.
288. A. G. Anshits, E. V. Kondratenko, E. V. Fomenko, A. M. Kovalev, N. N. Anshits, O. A. Bajukov, E. V. Sokol and A. N. Salanov: *Catal. Today*, 2001, **64**, 59–67.
289. F. B. Waanders, E. Vinken, A. Mans and A. F. Mulaba-Bafublandi: *Hyperfine Interact.*, 2003, **148–149**, 21–29.
290. C. Renfrew and P. G. Bahn: 'Archaeology: theory, methods and practice', 3rd edn; 2000, New York, Thames and Hudson.
291. R. Gebhard: in 'Prehistoric gold in Europe: mines, metallurgy and manufacture', (ed. G. Morteani and J. P. Northover), Vol. 280 of NATO ISI Series E: Applied Sciences, 261–272; 1995, Dordrecht, Kluwer Academic Publishers.
292. L. Stievano, M. Bertelle and S. Calogero: *Hyperfine Interact.*, 2003, **150**, 13–31.
293. C. Janot and P. Delcroix: *J. Phys. Coll.*, 1974, **35–C6**, 557–561.
294. A. Simopoulos, A. Kostikas and N. H. J. Gangas: Proc. Fifth Int. Conf. on 'Mössbauer spectroscopy', vol. 3, (ed. M. Hucl and T. Zemcik), 759–762; 1975, Nuclear Information Centre.
295. L. Lazzarini, R. Falcone, F. Burragato, G. Galetti and S. Calogero: 1st European Workshop on 'Archaeological ceramics', (ed. F. Burragato, O. Grubessi and L. Lazzarini), 269–280; 1994, Universita degli Studi di Roma 'La Sapienza'.
296. I. Ortalli, A. Vera, A. Antonini and L. B. Ponzi: *Hyperfine Interact.,* 1986, **29**, 1133–1136.
297. R. Gebhard, J. Riederer, R. Schwabe, U. Wagner and G. Kossack: Proc. 25th Int. Symp. on 'Archaeometry', (ed. Y. Maniatis), 207–215; 1989, Amsterdam, Elsevier.
298. L. Stievano, M. Bertelle, S. Calogero and F. E. Wagner: in 'Mössbauer spectroscopy in archaeology', (ed. U. Wagner), *Hyperfine Interact.*, 2004, **154**, 83–94.
299. R. Rüffler: *Hyperfine Interact.*, 1996, **99**, 401–407.
300. U. Wagner, F. E. Wagner, W. Häusler and I. Shimada: in 'Radiation in art and archaeometry', (ed. D. E. Creagh and D. A. Bradley); 2000, Amsterdam, Elsevier.
301. U. Wagner, R. Gebhard, E. Murad, I. Shimada and F. E. Wagner: Proc. Int. Workshop on 'Studies of magnetic properties of fine particles and their relevance to materials science', (ed. J. L. Dorman and D. Fiorani), Rome, Italy, November 1991; 1992, Rome, Elsevier Science Publishers.
302. R. E. M. Hedges: *Nature,* 1975, **254**, 501–503.
303. Z. Y. Gao, S. H. Chen and X. Chen: *Hyperfine Interact.*, 1994, **91**, 663–668.
304. S. H. Chen, Z. Y. Gao, G. Hu and X. Chen: *Hyperfine Interact.*, 1994, **91**, 651–656.
305. G. Qin and S. Li: *Hyperfine Interact.*, 1992, **70**, 1041–1044.
306. Y. F. Zheng and Y. F. Hsia: *Hyperfine Interact.*, 1991, **68**, 131–142.
307. Y. H. Wu, X. Y. Duan and L. Ding: *Hejishu*, 1988, **11**, 39–42 (in Chinese).
308. T. J. Zhang, G. Q. Ji and H. H. Li: *Hejishu*, 1986, **2**, 7–10.
309. S. Calogero, L. Lazzarini, M. Oddone and L. Diamandescu: *Sci. Tech. Cul. Heri.* 1994, **3**, 63–73.
310. N. Jiang: *J. Nanjing Museum*, 1983, 1.
311. F. Gauzzi, B. Verdini, G. Principi, R. Gupta, A. Raccanelli and U. Russo: Proc. Int. Conf. on 'Applications of the Mössbauer effect, Part II', vol. 50, (ed. I. Ortalli), 777–780; 1996, Società Italiana di Fisica.
312. R. Hong, Y. Zheng, J. Lu, J. Fan, C. Zhang and J. T. Wu: *Zhongshan Daxue Xuebao, Ziran Kexueban (J. Zhongshan University (Nat. Sci.))*, 1982, **2**, 95.
313. M. I. Oshtrakh: *J. Mol. Struct.*, 1999, **480–481**, 109–120.
314. R. Banerjee: *Life Chem. Rep.*, 1983, **1**, 209.
315. M. F. Perutz, G. Fermi, B. Luisi, B. Shaanan and R. C. Liddington: *Cold Spring Harb. Symp. Quant. Biol.*, 1987, **52**, 555–565.
316. D. P. E. Dickson: in 'Mössbauer spectroscopy applied to inorganic chemistry', (ed. G. J. Long), vol. 1, 339–389; 1984, Plenum.
317. D. P. E. Dickson and C. E. Johnson: in 'Structural and resonance techniques in biological research', (ed. D. L. Rousseau), 245–293; 1984, Academic Press.
318. K. Spartalian and G. Lang: in 'Applications of Mössbauer spectroscopy', (ed. R. L. Cohen), vol. 2, 249–279; 1980, Academic Press.
319. A. Vertes, L. Korecz and K. Burger: 'Mössbauer spectroscopy', 352–359; 1979, Academia Kiada.
320. M. I. Oshtrakh: *Spectrochim. Acta, Part A,* 2004, **60**, 217–234.
321. M. I. Oshtrakh and V. A. Semionkin: *Mol. Biol. (Moscow)*, 1985, **19**, 1310.
322. S. H. Bell, M. P. Weir, D. P. E. Dickson, J. F. Gibson, G. A. Sharp and T. J. Peters: *Biochim. Biophys. Acta Protein Struct. Mol. Enzymol.*, 1984, **787**, 227–236.
323. E. Bill, E. E. Di Iorio, A. Trautwien and K. Winterhalter: Proc. Int. Conf. on 'Application of Mössbauer effect', 648; 1982, Indian National Science Academy.
324. X. S. Zeng and Y. Lian: *Hyperfine Interact.*, 1992, **71**, 1327.
325. L. F. Bernini and P. C. Giordano: *Biochim. Biophys. Acta Protein Struct. Mol. Enzymol.*, 1988, **957**, 281–285.
326. D. P. E. Dickson, N. M. K. Reid, S. Mann, V. J. Wade, R. J. Ward and T. J. Peters: *Biochim. Biophys. Acta Protein Struct. Mol. Enzymol.*, 1988, **957**, 81–90.
327. T. G. St. Pierre, K. C. Tran, J. Webb, D. J. Macey, P. Pootrakul and D. P .E. Dickson: *Hyperfine Interact.*, 1992, **71**, 1279.
328. T. G. St. Pierre, D. P. E. Dickson and D. H. Jones: *Hyperfine Interact.*, 1988, **42**, 917.
329. D. P. E. Dickson, N. M. K. Reid, S. Mann, V. J. Wade, R. J. Ward and T. J. Peters: *Hyperfine Interact.*, 1989, **45**, 225.
330. E. R. Bauminger and I. Nowik: *Hyperfine Interact.*, 1998, **111**, 159–170.
331. E. R. Bauminger: in 'Applications of the Mössbauer effect', (ed. E. Baggio-Saitovitch, E. Galvao da Silva and H. R. Rechenberg), 110; 1990, Singapore, World Scientific.
332. A. Yayon, E. R. Bauminger, S. Ofer and H. Ginsburg: *J. Biol. Chem.*, 1984, **259**, 8163–8167.
333. D. Ben-Shachar and M. B. H. Youdium: in 'Iron and human disease', (ed. R. B. Lauffer), 349; 1992, London, CRC Press.
334. E. R. Bauminger and P. M. Harrison: *Hyperfine Interact.*, 2003, **151–152**, 3–19.
335. D. M. Lawson, P. J. Artymiuk, S. J. Yewdall, J. M. A. Smith, J. C. Livingstone, A. Treffry, A. Luzzago, S. Levy, P. Arosio, C. Cesareni, C. D. Thomas, W. V. Shaw and P. M. Harrison: *Nature*, 1991, **349**, 541.
336. E. R. Bauminger, P. M. Harrison, D. Hechel, I. Nowik and A. Treffry: *Biochim. Biophys. Acta Protein Struct. Mol. Enzymol.*, 1991, **1118**, 48–58.
337. P. Santambrogio, S. Levi, A. Cozzi, B. Corsi and P. Arosio: *Biochem. J.*, 1996, **314**, 139–144.
338. B. Window: *J. Phys. E: Sci. Instrum.*, 1971, **4**, 401–402.